PNNL-17162

Pacific Northwest
National Laboratory
Operated by Battelle for the
U.S. Department of Energy

Characterization of Direct-Push Vadose Zone Sediments from the 241-B and 241-BX Tank Farms

CF Brown
JP Icenhower
W Um
BN Bjornstad
MM Valenta
C Iovin
DC Lanigan
RE Clayton
KN Geiszler
ET Clayton
IV Kutnyakov
SR Baum
M J Lindberg
RD Orr

December 2007

Prepared for the U.S. Department of Energy
under Contract DE-AC05-76RL01830

DISCLAIMER

PACIFIC NORTHWEST NATIONAL LABORATORY
operated by
BATTELLE
for the
UNITED STATES DEPARTMENT OF ENERGY
under Contract DE-AC05-76RL01830

Printed in the United States of America

Available to DOE and DOE contractors from the
Office of Scientific and Technical Information,
P.O. Box 62, Oak Ridge, TN 37831-0062;
ph: (865) 576-8401
fax: (865) 576-5728
email: reports@adonis.osti.gov

Available to the public from the National Technical Information Service,
U.S. Department of Commerce, 5285 Port Royal Rd., Springfield, VA 22161
ph: (800) 553-6847
fax: (703) 605-6900
email: orders@ntis.fedworld.gov
online ordering: http://www.ntis.gov/ordering.htm


This report was printed on recycled paper.

PNNL-17162

Characterization of Direct-Push Vadose Zone Sediments from the 241-B and 241-BX Tank Farms

C. F. Brown
J. P. Icenhower
W. Um
B. N. Bjornstad
M. M. Valenta
C. Iovin
D. C. Lanigan
R. E. Clayton
K. N. Geiszler
E. T. Clayton
I. V. Kutnyakov
S. R. Baum
M. J. Lindberg
R. D. Orr

December 2007

Prepared for
CH2M HILL Hanford Group, Inc. and
the U.S. Department of Energy
under Contract DE-AC05-76RL01830

Pacific Northwest National Laboratory
Richland, Washington 99354

Executive Summary

Geochemical tests provide evidence for the transit of a plume of caustic waste solution through the sediment column at the Hanford 241-B and -BX Tank Farms. Direct-push samples recovered from boreholes surrounding Tanks 241-B-110 and 241-BX-102 and related waste transfer lines and diversion boxes included sediments typical of those previously recovered from other localities on the Hanford Site. The Hanford formation sediments are dominantly quartzo-feldspathic sands containing lithic fragments, displaying a range of particle size distributions and sorting characteristics. Some moderately well-sorted, fine-grained lithologies are interpreted as lenticular bodies irregularly dispersed in coarser-grained, more poorly sorted sediments. Tier I tests conducted on the vadose zone sediments revealed an inverse correlation between moisture content and sediment size fraction (i.e., there is greater moisture content in finer-grained sediments). The Tier I tests also showed that the pore water solutions were likely sodium-rich, moderately saline, and possessed higher pH values than background (uncontaminated) sediments. These data are characteristic of sediments that have encountered sodium-rich, saline, caustic waste solution, as documented in other reports at other suspect contamination sites around Hanford. Analyses of solutions from 1:1 water extracts reveal relatively balanced cation and anion concentrations, indicating that most of the geochemical species have been accounted for. The water extract data for affected sediments also indicate unusually high concentrations of aluminum, iron, and phosphorus. The relatively high concentrations of aluminum and iron may be the result of dissolution of secondary amorphous phases that precipitated after a reactive plume partially dissolved aluminum- and iron-bearing phases as it migrated through the sediment column. On the other hand, the presence of elevated concentrations of phosphorous may be the tell-tale signature of wastes derived from the bismuth phosphate separation process. Elements typically mobile in the subsurface, such as technetium-99, are present at either low concentrations or are below the analytical detection limit. However, we expect that the mobile elements would be present mainly along a narrow plume front, and if this front had passed deeper into the sediment profile than depths sampled, the retention of these elements would be minor. Alternatively, uranium-238 was detected in nearly all the direct-push sediments (by acid extract experiments) from around the BX Tank Farm at concentrations above the natural crustal average (0.76 pCi/g), and we also detected the presence of several anthropogenic radioisotopes, such as cobalt-60, cesium-137, europium-154, and europium-155 (by gamma energy analysis). These data confirm contamination of the sediments.

We selected a pair of lithologies from a single direct-push hole from near BX-102 that we anticipated would reveal details of the mechanism of radionuclide binding in the sediments and subjected them to a series of Tier II tests. These samples, coarse- and fine-grained specimens subdivided from a single lithologic entity, are labeled B1JWW6C fine and coarse. The positioning of fine- and coarse-grained materials provided a good opportunity to probe the controls that mineralogy, sediment size fraction, and hydraulic properties exert on the distribution of radionuclide elements. To determine the total concentration of uranium in the sediments, we completely dissolved aliquots of sediment using an acid mixture and a specially designed microwave apparatus. The fine-grained sample contained nearly four times the concentration of uranium as the coarse-grained sample (390 versus 108 μg/g U). Another set of tests was performed on the coarse-grained sample that was subdivided by dry sieving into its various size fractions, which revealed that most of the uranium resides in the finer size fractions. It is not yet evident, however, if this preference for the finer particle fraction is a reflection of mineralogical, hydraulic, or kinetic factors. A pair of tests was carried out in an attempt to distinguish between mobile or “labile” and immobile (sequestered) uranium. The first test consisted of exposing the sediment to a bicarbonate-

carbonate leach solution. The solution was designed to remove weakly sorbed uranium from mineral grains by forming strong uranyl-carbonate aqueous complexes without liberating sequestered uranium by dissolving solid reservoirs. The second test consisted of equilibrating the uranium-contaminated sediment with a synthetic groundwater solution and then spiking the solution with a uranium isotope that can easily be distinguished analytically from common uranium. The dopant in this case was uranium-233, which can be conveniently detected using liquid scintillation counting. This test relies on the supposition that weakly sorbed common uranium (from contamination) can exchange with the doped uranium-233 such that the uptake of the tracer isotope can be quantified. Therefore, the extent of uptake of uranium-233 correlates with the amount of labile uranium in the system.

From both the Tier I and Tier II tests, we calculated an estimated uranium partitioning value, or K_d (concentration of uranium attached to the solid divided by the concentration of uranium in solution), for the B1JWW6C fine and coarse sediments. Based on the concentration of uranium recovered in the bicarbonate-carbonate solution and the concentration of uranium from the 1:1 water extract solution, we obtained K_d values of 983 and 1.56 mL/g for the fine- and coarse-grained specimens, respectively. The concentration of uranium extracted by the bicarbonate-carbonate solution represents the uranium that desorbs from the mineral surfaces and is therefore regarded as the amount of uranium attached to the solid in the K_d computation. These K_d values are numerically similar to those obtained from the acid extract and 1:1 water extract data, in which values of 927 and 1.27 mL/g were obtained for the fine- and coarse-grained specimens, respectively. The concentrations of uranium determined from isotope exchange experiments are lower than those obtained by the acid or bicarbonate-carbonate extracts, so the resulting K_d values are smaller (832 and 1.19 mL/g for the fine- and coarse-grained, respectively), yet are similar to the other K_d values quoted above. The values of K_d determined by the bicarbonate-carbonate and the isotope exchange experiments are the same within 10% relative, indicating that the values are indistinguishable statistically. The quantities of labile uranium in the coarse- and fine-grained sediments are, by the two test methods, similar and make up 51 to 67% and 63 to 75% of the total uranium, respectively. These data indicate that a sizeable fraction of uranium is sequestered in a phase that is resistant to dissolution.

The search for the identity of the uranium-sequestering phase was aided by microscopic techniques. Specimens from the B1JWW6C fine and coarse fractions were subjected to micro-X-ray fluorescence (μ–XRF) and micro-X-ray absorption near-edge spectroscopy (μ-XANES). Small areas (400 × 400 μm) were analyzed, and X-ray maps from μ-XRF showed a strong correlation between the spatial proximity of uranium and calcium. Evaluation of the oxidation state of uranium in these spots indicated that the majority of uranium is in the hexavalent state [U(VI)]. These data support the supposition that the uranium sequestering phase is the calcium uranyl silicate, uranophane [$Ca(UO_2)_2(SiO_3OH)_2(H_2O)_5$]. Further analysis using time-resolved laser induced fluorescence (TRLIF) bolstered the hypothesis that uranophane is the main uranyl phase present in the sample. Measurement of the fluorescent signal by TRLIF at cryogenic temperatures (6±1K) and a delay of 1.2 ms yields data that are consistent with the spectrum of uranophane in both the fine- and coarse-grained samples.

The data provided in this report add more information to the large body of data that has been developed regarding the contamination history of Hanford sediments. While the sediments in this report are not the most contaminated materials recovered from boreholes at Hanford, this investigation further delineates the extent of contamination from wastes that escaped either from storage or during transit between waste storage tanks. It is likely that the plume front migrated down past the level of sediment

sampling from the direct-push boreholes, so a detailed estimate of the extent that contaminants migrated after release to the subsurface cannot be made with this study alone. On the other hand, this study lends considerable weight to the notion that simple geochemical tests, such as the 1:1 water extract, can quickly supply evidence to show that pollution has occurred. Further, the data show that uranium sequestration occurs by formation of micro-precipitates within small pore volumes in the sediment, and that an unusual amount is present in the finer-grained fractions that are interspersed throughout the Hanford formation. Thus, this study shifts the focus of where contaminant uranium resides from the lithic fragments to fine sand- and silt-sized grains that are present in the majority of the sediments. Therefore, although more data are needed, this report provides a vital link to understanding the migration of contaminants that encounter different lithologies possessing different hydraulic qualities. Modeling the migration of contaminants and the movement of pore waters may thus depend on understanding the effects of capillary barriers that form when fine- and coarse-grained sediments are coincident.

A final recommendation is to use the pore water composition data from the shallow direct-push sediments near the B Tank Farm diversion boxes and BX Tank Farm in the on-going efforts to "ground truth" the field resistivity data collected by hydroGEOPHYSICS, Inc.

Acknowledgments

This work was conducted as part of the Tank Farm Vadose Zone Project led by CH2M HILL Hanford Group, Inc., in support of the U.S. Department of Energy (DOE)'s Office of River Protection. The authors wish to thank John G. Kristofzski, Fredrick M. Mann, David A. Myers, Michael P. Connelly, and Harold A. Sydnor of CH2M HILL Hanford Group, Inc. and Dwayne Crumpler of Columbia Energy and Environmental Services for their planning support and technical review of this work, and R. Jeff Serne of Pacific Northwest National Laboratory (PNNL) for his technical review of the report. We would also like to express our gratitude to Robert Lober of the DOE Office of River Protection for his support and interest.

We would especially like to thank Kent D. Reynolds, Dave Skoglie, Kelly Olson, and Mark Repko of Duratek Federal Services, Inc. for their efforts in selecting depths to sample and executing the field work that obtained the samples.

Finally, the authors would also like to thank Sheila Bennett (PNNL) for the editorial review and final formatting of this technical report.

Acronyms and Abbreviations

ASA	American Society of Agronomy
ASTM	American Society for Testing and Materials
bgs	below ground surface
DOE	U.S. Department of Energy
EC	electrical conductivity
EPA	U.S. Environmental Protection Agency
GEA	gamma energy analysis
H1	Hanford formation – H1 unit
H2	Hanford formation – H2 unit
HCl	hydrochloric acid
HF	hydrofluoric acid
HNO_3	nitric acid
IC	ion chromatography or ion chromatograph
ICP-MS	inductively coupled plasma-mass spectrometer
ICP-OES	inductively coupled plasma-optical emission spectroscopy
K_d	distribution coefficient, or sorption partition coefficient, in units of mL/g
NDIR	non-dispersive infrared
Nd:YAG	neodymium-doped yttrium aluminum garnet
NMR	nuclear magnetic resonance
PNNL	Pacific Northwest National Laboratory
TRLIF	time-resolved laser-induced fluorescence
USGS	U.S. Geological Survey
WMA	waste management area
XANES	X-ray absorption near edge structure
XRD	X-ray diffraction
XRF	X-ray fluorescence

Units of Measure

ºC	temperature in degrees Celsius [T(ºC) = T(K) – 273.15)]
Ci	curie
cm	centimeter
ft	foot
g	gram
g	acceleration due to gravity
in.	inch
K	degrees Kelvin
µ	micro
µCi	microcurie
µeq	microequivalent
µg	microgram
µm	micrometer
m	meter
M	molarity, mol/L
meq/L	milli-equivalent per liter
mg	milligram
mL	milliliter
mm	millimeter
mM	millimolar
mN	millinormal
mol	mole
mS	milliSiemen
ms	millisecond
N	normal
nCi	nanocurie
ng	nanogram
pCi	picocurie
s	second
wt%	weight percent

Contents

Figures

Tables

1.0 Introduction

The overall goals of the Tank Farm Vadose Zone Project, led by CH2M HILL Hanford Group, Inc., are to define risks from past and future single-shell tank farm activities; identify and evaluate the efficacy of interim measures; and aid, via collection of geochemical information and data, the future decisions that must be made by the U.S. Department of Energy (DOE) regarding the near-term operations, future waste retrieval, and final closure activities for the single-shell tank waste management areas (WMAs). A more complete discussion of the goals of the Tank Farm Vadose Zone Project is available in the overall work plan, *Phase 1 RCRA Facility Investigation/Corrective Measures Study Work Plan for the Single-Shell Tank Waste Management Areas* (DOE 1999). Specific details of the rationale for activities performed at WMA B-BX-BY are found in Rogers and Knepp (2000). To help facilitate these activities, CH2M HILL Hanford Group, Inc., previously petitioned scientists from Pacific Northwest National Laboratory (PNNL) to perform detailed analyses of vadose zone sediment collected near Tanks 241-B-110 and 241-BX-102 within the 241-B and 241-BX Tank Farms, respectively (Serne et al. 2002e,f). Upon completion of those activities, additional near-surface sampling (data reported in this report) was performed in the B and BX Tank Farms to further investigate potential leak events. Included in Rogers and Knepp (2000) and Knepp (2002) are discussions on shallow sediment sampling and characterization activities needed to better determine the status of potential leaks from tanks BX-101 and BX-110 and from around diversions boxes south of the B Tank Farm. The locations requiring additional study and sediment characterization were designated in Figure ES.2 of the B-BX-BY Field Investigation Report (FIR); Knepp (2002). The B-BX-BY FIR also called for more study of uranium mobility to refine solid phase solubility and transport conditions related to bismuth phosphate wastes that were accidentally released from several single-shell tanks, including BX-102. Such uranium studies using several of the sediment samples obtained in the recent direct-push campaign near the BX Tank Farm were performed and documented herein.

This report contains all the geochemical and selected physical characterization data collected on vadose zone sediment recovered from two sampling campaigns, one south of the B Tank Farm and one within the BX Tank Farm. In the first sampling campaign four direct-push characterization holes were emplaced to investigate vadose zone contamination associated with potential leaks from the 241-B Tank Farm diversion boxes (241-B-151, 241-B-152, and 241-B-153). The 241-B diversion boxes were reported to have leaked metal waste in 1951 (Wood et al. 2000). Metal waste is considered to be the most contaminated waste stream leaked in WMA B-BX-BY and could have contaminated the vadose zone with tank waste contaminants, including uranium and technetium-99. Uranium and technetium-99 were two of the primary contaminants of interest in sediments retrieved from near the diversion boxes because their presence could necessitate additional characterization activities in the area. A map highlighting the area of study is presented in Section 2 (Figure 2.2).

This report also contains all the geochemical and selected physical characterization data collected on vadose zone sediment recovered from three direct-push characterization holes emplaced to investigate vadose zone contamination south and east of Tank 241-BX-102. Wood et al. (2000) postulated that a transfer line connecting Tanks 241-BX-102 and 241-BX-103 plugged in 1951, causing the release of metal waste from an inlet port in Tank 241-BX-102. It has been estimated that much as 4 curies of technetium-99 was released to the vadose zone as a result of this leak event (Wood et al. 2000). Although an extensive characterization study involving sediments from this locale has been completed (Serne et al.

2002e), additional near-surface sediment samples were collected to better define the lateral extent of the waste plume-sediment interaction. A location map highlighting the area of interest is presented in Section 2 (Figure 2.3).

This report is divided into sections that describe the geochemical characterization methods employed and the results of analysis of the 241-B and 241-BX Tank Farm direct-push samples. English units are used for descriptions and discussions of drilling activities and samples because that is the system of units used by drillers to measure and report depths. To convert feet to meters, multiply by 0.3048; to convert inches to centimeters, multiply by 2.54. The metric system is used in this report for all other purposes.

2.0 Geology

The 241-B-BX Tank Farms were constructed within Pleistocene Hanford formation and Holocene eolian deposits that mantle the giant Cold Creek flood bar (Wood et al. 2000). The geology beneath the B-BX-BY WMA has been the subject of numerous reports, including those by Wood et al. (2000), Narbutovskih (1998), Caggiano (1996), and Price and Fecht (1976). Sediments overlying basalt bedrock consist of predominantly Ice Age flood deposits of the Hanford formation. Locally, erosional remnants of the Cold Creek unit (formerly referred to as the Plio-Pleistocene unit) and/or the Ringold Formation may lie between the Hanford formation and the basalt. The upper 10.7 m (35 ft) of the Hanford formation was removed during construction of the tank farms and the stockpiled sediments were later used as backfill around the underground storage tanks (Wood et al. 2000). The stratigraphy is shown in Figure 2.1, while the terminology used for the B-BX-BY WMA is summarized in Table 2.1.

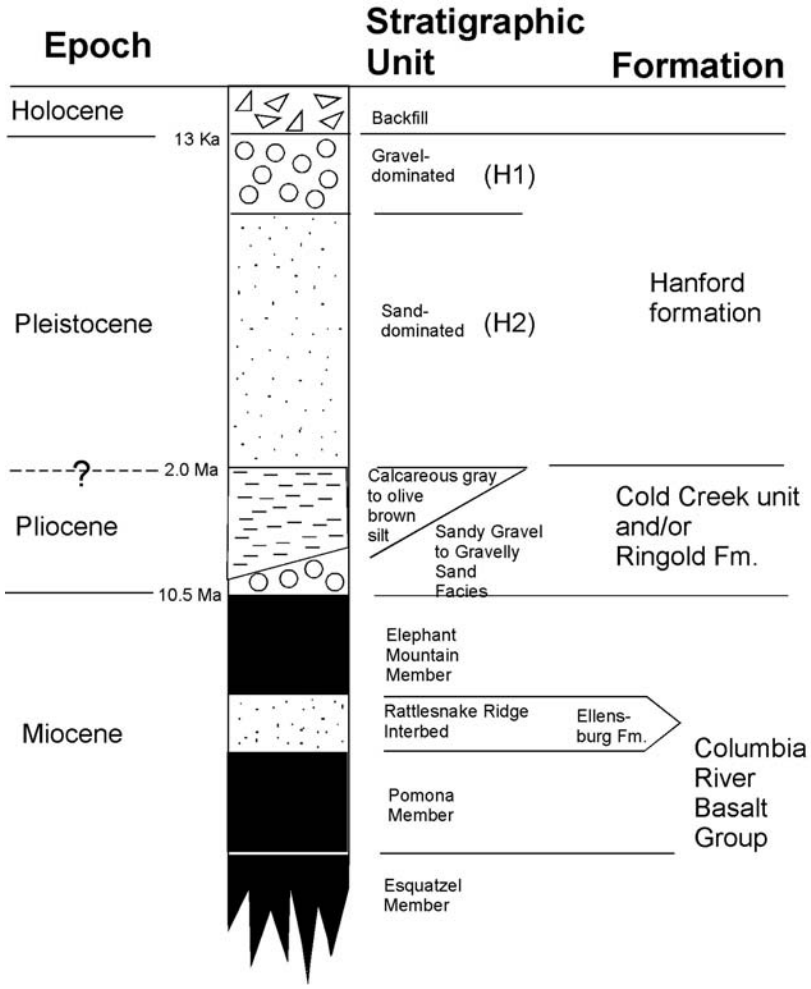

Figure 2.1. Generalized, Composite Stratigraphy for the Late Cenozoic Sediments in the Vicinity of the B-BX-BY WMA (modified after Wood et al. 2000)

Table 2.1. Stratigraphic Terminology Used for the B-BX-BY WMA (modified after Wood et al. 2000)

Stratigraphic Symbol	Formation	Facies/Subunit	Description	Genesis
Holocene/Fill	NA	Backfill	**Poorly sorted cobbles, pebbles, and coarse to medium sand with some silt** derived from the Hanford formation (Price and Fecht 1976)	Anthropogenic
H1	Hanford formation	Unit H1	**An upper gravel sequence consisting of high-energy, gravel-dominated facies interbedded with lenticular and discontinuous layers of sand-dominated facies**. Equivalent to the upper gravel sequence discussed by Last et al. (1989) and Lindsey et al. (1992), to the H1 sequence discussed by Lindsey et al. (1994) and the Qfg (Quaternary Flood Gravel-dominated) documented by Reidel and Fecht (1994).	Cataclysmic flood deposits
H2		Unit H2	**Sand sequence** consisting predominantly of sand-dominated facies, with multiple graded beds of plane to foreset-bedded sand or gravelly sand, which sometimes grade upward to silty sand or silt. Equivalent to the sandy sequence discussed in Last et al. (1989) and Lindsey et al. (1992), to the H2 sequence discussed by Lindsey et al. (1994) and to Qfs (Quaternary Flood Sand-dominated) documented by Reidel and Fecht (1994).	
CCU	Cold Creek unit (formerly Plio-Pleistocene unit)	Silt Facies	**Silt sequence consisting of interstratified well sorted calcareous silt and fine sand**. At least partially correlative with the "early Palouse soil" described by Tallman et al. (1979) and DOE (1988) and included with the Plio-Pleistocene unit by Lindsey et al. 1994, and Slate 1996, 2000; now referred to as the Cold Creek unit (DOE 2002)	Fluvial overbank and/or eolian deposits (with some weakly developed paleosols)
CCU and/or Ringold Formation		Sandy Gravel to Gravelly Sand Facies	**Sandy gravel to gravelly sand sequence consisting predominantly of unconsolidated basaltic sands and gravels.**	Pre-Pleistocene alluvium

2.1 Characterization and Sampling Methods

This document reports on seven recent vadose zone cone-penetrometer (direct-push) boreholes drilled in the vicinity of the 241-B-BX Tank Farms. Four of the holes were drilled within the 241-B Tank Farm (Figure 2.2), and the other three were drilled within the 241-BX Tank Farm (Figure 2.3).

Direct-push holes were drilled in two stages. First, direct-push holes were advanced to collect down-hole geophysical logs (i.e., spectral gamma) information and to identify radioactively contaminated zones. Next, contaminated zones of interest were sampled with a second direct-push hole drilled immediately adjacent to the first. A small-diameter sediment core was collected from a single target interval in each hole for geological and geochemical characterization.

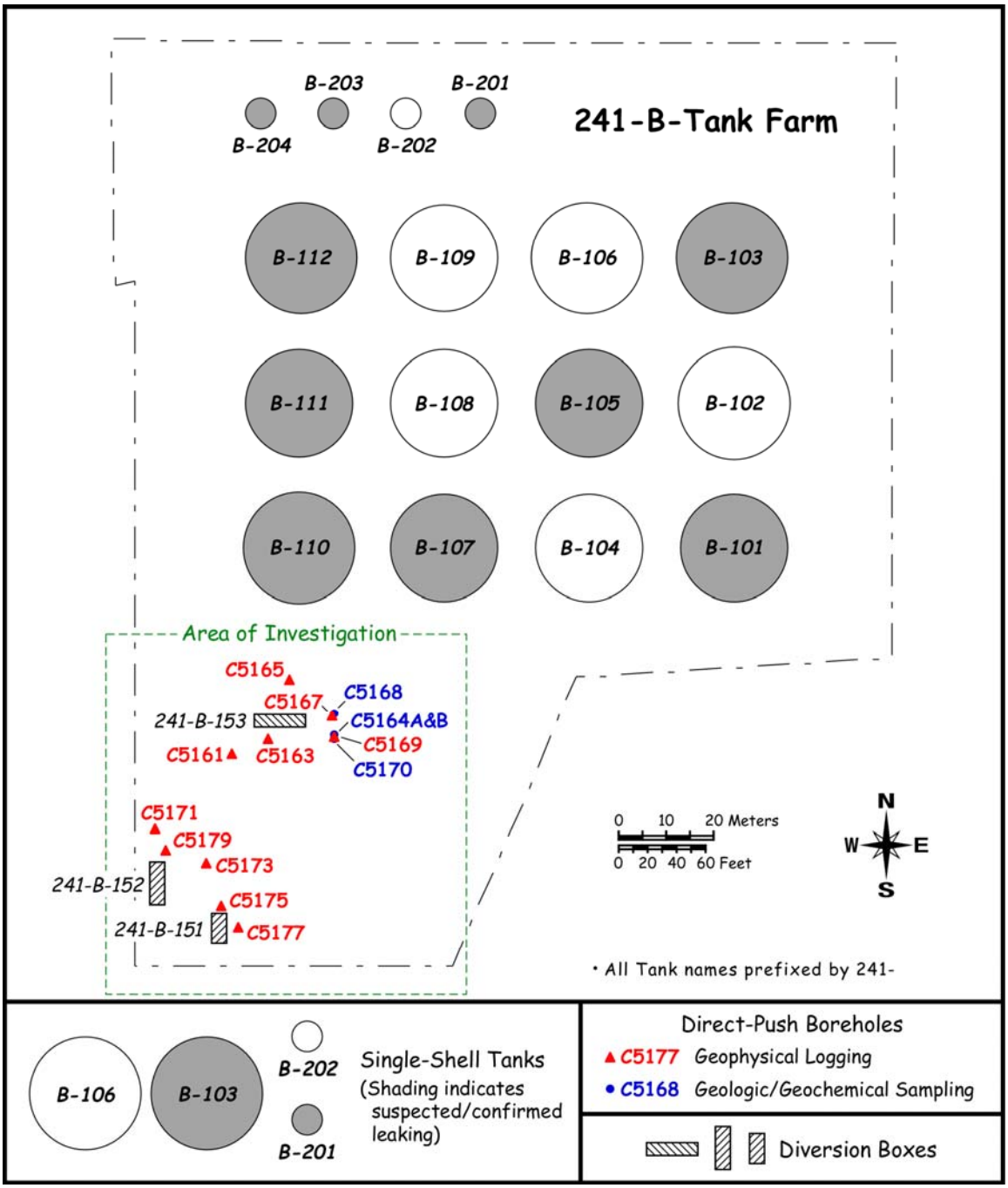

Figure 2.2. Locations of New Direct-Push Boreholes in Vicinity of the 241-B Tank Farm

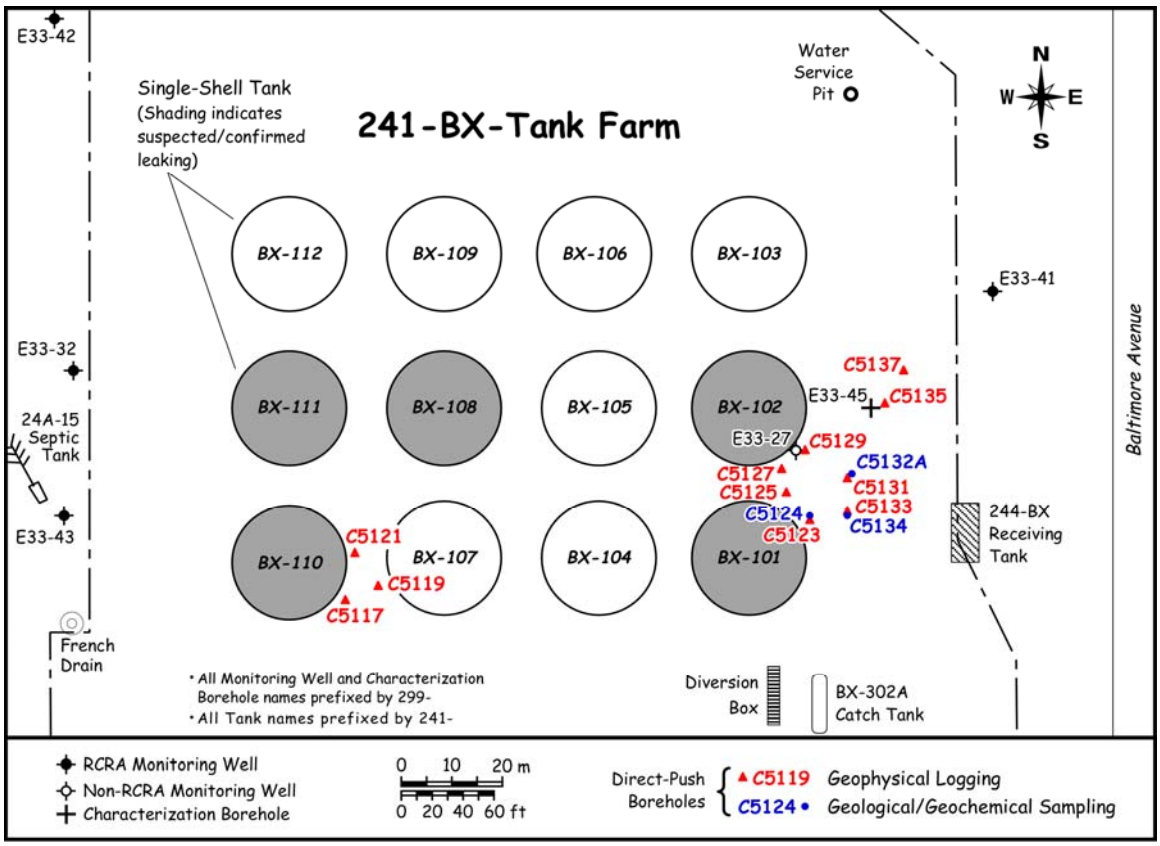

Figure 2.3. Locations of New Direct-Push Boreholes in Vicinity of the 241-BX Tank Farm

In each of the sampled push holes, an attempt was made to push a 2-ft-long core barrel down into the sediment. The core barrel was lined with three 1.5-inch outer diameter (OD), 6-inch-long stainless steel liners. A fourth sample was collected as a grab sample from the shoe on the core barrel. Only four of the seven pushes produced a full core barrel; three of the pushes recovered <1.5 ft of core (Tables 2.2 and 2.3). One of the holes (C5164) was pushed twice after the first attempt (C5164A) was unsuccessful at recovering a complete 2-ft core.

In the laboratory, immediately upon extruding the cores from their liners, moisture samples were collected and high-resolution color photographs were obtained for each core or grab sample (see Appendices A and C). Next, standard descriptions of grain size, sorting, color, structure, consolidation, moisture content, mineralogy, and reaction with hydrochloric acid were entered into geologic core logs (see Appendices B and D). Cores were also sub-sampled for laboratory characterization of physical and chemical properties at that time.

All of the direct-push samples collected within the B-BX Tank Farms came from the upper portion of the Hanford formation. A general discussion of the Hanford formation in B-BX-BY WMA follows.

Table 2.2. Direct-Push Samples from the 241-B Tank Farm

Lab Sample #	Sample Type	Upper depth (ft)	Lower depth (ft)	Mid-depth (ft)	Date Received	Date Processed	Lithology	Stratigraphic Unit	Companion Geophysically Logged Hole	% Moisture	Comments
B1M564C	core	17.00	17.50	17.25	1/9/2007	2/15/2007	sandy gravel	Hanford fm., H1 unit	C5169	3.08	
B1M564B	core	17.50	18.00	17.75	1/9/2007	2/15/2007	sandy gravel	Hanford fm., H1 unit		3.08	
B1M564A	core	18.00	18.50	18.25	1/9/2007	2/15/2007	sandy gravel	Hanford fm., H1 unit		3.79	
B1LTY5C	core	21.00	21.50	21.25	1/9/2007	2/15/2007	gravelly sand	Hanford fm., H2 unit	C5169	8.05	
B1LTY5B	core	21.50	22.00	21.75	1/9/2007	2/15/2007	fn-med sand	Hanford fm., H2 unit		10.14	
B1LTY5A	core	22.00	22.50	22.25	1/9/2007	2/15/2007	fn-med sand	Hanford fm., H2 unit		16.83	
B1LTY5	grab	22.50	23.00	22.75	1/9/2007	2/15/2007	fn-med sand	Hanford fm., H2 unit		15.38	
B1LTY4	grab	19.50	21.50	20.50	1/9/2007	2/15/2007	silt	Hanford fm., H2 unit	C5169	3.61	Note: samplers-only got drill in 1 inch before it got stuck (collected sample)
B1M565C	core	17.00	17.50	17.25	1/16/2007	2/15/2007	fine sand	Hanford fm., H2 unit	C5167	9.68	Split into two subsamples; upper sample from fn-md sand, lower sample from very fine sand lens
							very fn sand lens	Hanford fm., H2 unit		14.09	
B1M565B	core	17.50	18.00	17.75	1/16/2007	2/15/2007	fn-med sand	Hanford fm., H2 unit		9.83	
B1M565A	core	18.00	18.50	18.25	1/16/2007	2/15/2007	very fn/fn sand	Hanford fm., H2 unit		9.38	
B1M565	grab	18.50	19.00	18.75	1/16/2007	2/15/2007	fn-med sand	Hanford fm., H2 unit		12.00	

Table 2.3. Direct-Push Samples from the 241-BX Tank Farm

Borehole	Sample #	Sample Type	Upper depth (ft)	Lower depth (ft)	Mid-depth (ft)	Date Received	Date Processed	Lithology	Stratigraphic Unit	Companion Geophysically Logged Hole	% Moisture	Comments
C5134	B1JWW6C	core	76.8	77.2	77.0	6/30/2006	9/11/2006	silty fine sand, calcareous	Hanford fm., H2 unit	C5133	12.79	Split in two subsamples; upper sample from silty sand and lower sample from coarse sand
								med-coarse sand	Hanford fm., H2 unit		3.82	
	B1JWW6B	core	77.2	77.8	77.5	6/30/2006	9/11/2006	med-coarse sand	Hanford fm., H2 unit		3.22	
	B1JWW6A	core	77.8	78.2	78.0	6/30/2006	9/11/2006	med-coarse sand	Hanford fm., H2 unit		2.07	
C5132	B1JWW7C	core	63.0	63.5	63.3	7/6/2006	9/11/2006	med-coarse sand	Hanford fm.	C5131	6.41	
	B1JWW7B	core	63.5	64.0	63.8	7/6/2006	9/11/2006	med-coarse sand	Hanford fm., H2 unit		7.86	
	B1JWW7A	core	64.0	64.5	64.3	7/6/2006	9/11/2006	sl. pebbly coarse sand	Hanford fm., H2 unit		3.14	
	B1JWW7	grab	64.5	65.0	64.8	7/6/2006	9/11/2006	med-very coarse sand	Hanford fm., H2 unit		1.99	
C5124	B1JWW8B	core	44.0	44.5	44.3	7/21/2006	9/11/2006	coarse-very coarse sand	Hanford fm., H2 unit	C5123	4.99	
	B1JWW8A	core	44.5	45.0	44.8	7/21/2006	9/11/2006	Coarse-very coarse sand	Hanford fm., H2 unit		4.94	

2.2 Hanford Formation

The Hanford formation is an informal name assigned to Pleistocene cataclysmic flood deposits within the Pasco Basin (Tallman et al. 1979; DOE 1988, 2002). Ice-Age floods originated from periodic failures of ice dams that bottled up glacial Lake Missoula and other Pleistocene water bodies (Bjornstad 2006). The Hanford formation may include some minor fluvial, colluvial, and/or eolian deposits interbedded with flood deposits.

The Hanford formation consists predominantly of unconsolidated sediments that cover a wide range in grain size and sorting, from poorly sorted boulder-bearing to better-sorted sand, silty sand, and silt. In general, the Hanford formation is subdivided into three principal facies: 1) gravel-dominated, 2) sand-dominated, and 3) interbedded sand- and silt-dominated. Gravel-dominated flood deposits formed toward the center of the basin where currents and energy were the strongest. Here smaller particles were kept in suspension by the fast moving, highly turbulent flood waters. As flood energy decreased toward the margins of the basin, flood deposits transitioned to the sand-dominated and interbedded sand- and silt-dominated facies. Because of the widely different and complex flow dynamics during Ice Age flooding, Hanford formation strata are extremely heterogeneous and their physical properties anisotropic (DOE 2002, Bjornstad 2006). The bulk of the vadose zone within the Pasco Basin and the Hanford Site, including the B-BX WMA, lies within sediments of the Hanford formation.

During Ice Age flooding, sediments accumulated onto the huge Cold Creek Bar, which makes up the 200 Area Plateau. Cold Creek Bar grew as sediments were episodically laid down in series of perhaps hundreds of floods spanning a million years or more (Pluhar et al. 2006). A network of braided flood channels sweeping across the bar locally scoured into the pre-existing deposits and backfilled with coarse sand and gravel. Elsewhere, thick blankets of sand were laid down at higher elevations within and between these channels. Cold Creek Bar is a prominent land form, up to 12 miles long and several miles wide, that grew during repeated Ice Age floods at the east end of Umtanum Ridge as floods expanded into the basin and dropped their sedimentary load.

Gravel-dominated flood facies of the Hanford formation predominate in the northern 200 East and 200 West Areas, which were closer to high-energy flood channels. These coarse-grained deposits transition laterally into finer-grained deposits of sand and eventually sand interbedded with silt to the south.

2.2.1 Gravel-Dominated Sequence (H1 Unit)

A gravel-dominated sequence referred to as the H1 unit forms the top of the Hanford formation within the B-BX-BY WMA (see Figure 2.4). Based on observations of outcrop and intact core samples, the Hanford formation upper gravel sequence is interpreted to consist of the high-energy gravel-dominated facies interbedded with lenticular and discontinuous layers of the sand-dominated facies. Interbedded sand- and silt-dominated facies are occasionally present but constitute a relatively small percentage of the total. Moisture content in the gravel-dominated samples is only about 3 to 4 wt% (Table 2.2). The maximum thickness of the H1 unit reflects a north-south trending trough (i.e., channel) that trends beneath BX and BY Tank Farms; maximum thickness of the H1 unit in this trough is about 20 m (60 ft) (Wood et al. 2000).

Figure 2.4. Gravel-Dominated Sediment Sample from the Hanford Formation, H1 Unit. Sample collected from push hole C5164A (B Tank Farm), 17.5 to 18.0 ft depth.

2.2.2 Sand-Dominated Sequence (H2 Unit)

A thick sand-dominated sequence, the H2 unit, dominates the lower portion of the Hanford formation (see Figure 2.5). Internally, this sequence probably contains multiple graded beds of plane- to foreset-bedded sand or gravelly sand several meters or more thick, which sometimes grade upward into silty sand or silt. Cementation is very minor or absent, and total $CaCO_3$ content is generally only a few weight percent or less. Finer-grained materials present in the H2 unit, especially fine sand beds, produce higher moisture retention (10 to 15 wt%) due to naturally higher capillary forces present in these types of sediment (Table 2.2).

The top of the H2 unit sand sequence rises to the south beneath the B-BX-BY WMA. The Hanford formation sand sequence is thickest [60 m (200 ft)] in the central and southern portion of WMA B-BX-BY and thins to as little as 30 m (110 ft) to the north (Wood et al. 2000).

Figure 2.5. Sand-Dominated Sediment Sample from the Hanford Formation H2 Unit. Two medium to coarse sand layers are separated by a thin bed of pale brown very fine sand. Sample collected from push hole C5168 (B Tank Farm), 17.5 to 18.0 ft depth.

3.0 Geochemical Methods and Materials

This chapter discusses the methods and philosophy used to characterize the 241-B and 241-BX Tank Farm direct-push samples and the parameters that were measured and analyzed in the laboratory. It also describes the materials and methods used to conduct analyses of the physical, geochemical, and radio-analytical properties of the sediments.

3.1 Sample Inventory

3.1.1 241-B Tank Farm Direct-Push Samples

At the 241-B Tank Farm, sediment samples were collected from four direct-push holes (Figure 2.2). Each direct-push sampling campaign resulted in up to three depth-discrete cores (1.25 inches in diameter by 6 inches long) and one grab sample consisting of the material captured in the drive shoe. Each sample interval collected within the 241-B Tank Farm was numbered using Hanford Environmental Information System specific sample names. The core samples from each sample interval were further identified by the letters A, B, or C, where the A Liner was always in the deeper position closest to the drive shoe. One laboratory duplicate sample was collected during core opening and is designated by the nomenclature DUP. Additionally, sample B1M565C from push hole C5164A was split into two samples, B1M565C fine and B1M565C sand, based on the presence on a fine-grained lens of sediment in the sample liner. Recovery of samples was fairly good in most of the push holes. The one exception was push hole C5170, which only had material recovered from the shoe. Details about the 241-B Farm direct-push samples are presented in Table 3.1.

Table 3.1. Sample Inventory from the 241-B Farm Direct-Push Holes[a,b]

Sample Number	Push Hole Number	Sample Recovery (%)	Sample Number	Push Hole Number	Sample Recovery (%)
B1LTY5C	C5164B	90	B1M564A	C5164A	100
B1LTY5B	C5164B	65	B1LTY4	C5170	NA
B1LTY5A	C5164B	50	B1M565C	C5168	70
B1LTY5	C5164B	NA	B1M565B	C5168	50
B1M564C	C5164A	85	B1M565A	C5168	55
B1M564B	C5164A	100	B1M565	C5168	NA

(a) Shaded cells indicate grab samples.
(b) NA indicates not applicable.

3.1.2 241-BX Tank Farm Direct-Push Samples

At the 241-BX Tank Farm, sediment samples were collected from three direct-push holes, as shown in Figure 2.3. Each direct-push sampling campaign resulted in up to three depth-discrete cores (1.25 inches in diameter by 6 inches long) and one grab sample consisting of the material captured in the

drive shoe. Like the samples from the 241-B Tank Farm, each sample interval collected within the 241-BX Tank Farm was numbered using a Hanford Environmental Information System[(a)] specific sample name. The core samples from each sample interval were further identified by the letters A, B, or C, where the A liner was always closest to the drive shoe. One laboratory duplicate sample was collected during core opening and is designated by the suffix DUP. Additionally, sample B1JWW6C from push hole C5134 was split into two samples, B1JWW6C fine and B1JWW6C coarse, based on the presence of a fine-grained lens of sediment in the sample liner. Recovery of samples was fairly good in most of the push holes. Sediment was not recovered from the shoe in push holes C5324 and C5134. Details about the 241-BX Farm direct-push samples are listed in Table 3.2.

Table 3.2. Sample Inventory from the 241-BX Farm Direct-Push Holes[(a,b)]

Sample Number	Push Hole Number	Sample Recovery (%)	Sample Number	Push Hole Number	Sample Recovery (%)
B1JWW6C	C5134	100	B1JWW7A	C5132	95
B1JWW6B	C5134	95	B1JWW7	C5132	NA
B1JWW6A	C5134	60	B1JWW8B	C5124	60
B1JWW7C	C5132	100	B1JWW8A	C5124	80
B1JWW7B	C5132	95			

(a) Shaded cells indicate grab samples.
(b) NA indicates not applicable.

3.2 Approach

During a past investigation at WMA SX, investigators reported that changes in sediment type and contaminant concentrations typically occurred within a few inches in a given liner (Serne et al. 2002b). It was concluded that a more methodical scoping approach would be necessary to provide the technical justification for selecting samples for detailed characterization as defined in the data quality objectives process (DOE 1999). Subsequently, a method was developed to select samples that considered depth, geology (e.g., lithology, grain-size composition, and carbonate content), individual liner contaminant concentration (e.g., radionuclides, nitrate), moisture content, and overall sample quality. Extraction/ leaching procedures were performed, and certain key parameters (moisture content and gamma energy analysis [GEA]) were measured on sediment from each liner. Grab samples were used in this study only if insufficient sample material for characterization and analysis was available in the core samples.

During the geologic examination of the core samples, the liner contents were subsampled for moisture content, gamma-emission radiocounting, 1:1 water extracts (which provide soil pH, electrical conductivity [EC], cation, and anion data), total carbon and inorganic carbon content, and 8 M nitric acid extracts (which provide a measure of the total leachable concentration of contaminants within the sediment). Sampling preference was always biased toward the finer-grained and/or wetter material contained in each liner. The remaining sediment from each liner was then sealed and placed in cold storage.

(a) The Hanford Environmental Information System is a consolidated set of electronic systems that manage data collected during environmental monitoring of the Hanford Site.

3.3 Materials and Methods

During subsampling of each core liner or grab sample, every effort was made to minimize moisture loss and prevent cross contamination between samples. Depending on the sample matrix, very coarse pebbles and larger material (i.e., >32 mm) were avoided during sub-sampling. Larger lithic fragments (cobbles) were excluded to provide moisture contents representative of GEA and 1:1 sediment:water extract samples. Therefore, the results from the sub-sample measurements may contain a possible bias toward higher concentrations for some analytes that would be preferentially associated with the smaller-sized sediment fractions. As an example of this potential bias, we acknowledge previous investigations that reported that contaminant uranium is manifested as micro-precipitates in fractures within granitic lithic fragments that make up only 4% by volume of the Hanford sediments (Liu et al. 2004, 2006; McKinley et al. 2006). It is our contention that the contaminant uranium is not solely harbored by crevasses in lithic fragments, and our study aims to identify these additional reservoirs of uranium.

Both Pacific Northwest National Laboratory (PNNL) and American Society for Testing and Materials (ASTM) procedures were followed for visual descriptions and geological descriptions of all direct-push samples (ASTM 1993). The sediment classification scheme used for geologic identification of the sediment types (used solely for graphing purposes in this report) was based on the modified Folk/ Wentworth classification scheme (Folk 1968, Wentworth 1922).

3.3.1 Moisture Content

Gravimetric water contents of the sediment samples from each liner and shoe grab sample were determined using appropriate PNNL procedures based on *Test Method for Laboratory Determination of Water (Moisture) Content of Soil and Rock by Mass* (ASTM 1998). One representative subsample of at least 15 to 70 g was used. Sediment aliquots were placed in tared containers, weighed, and dried in an oven at 105°C until constant weight was achieved, which took at least 24 hours. The containers were removed from the oven, sealed, cooled, and weighed. At least two mass measurements, each after a 24-hour heating period, were performed to ensure that all moisture was removed. All mass measurements were performed using a calibrated balance. A calibrated weight set was used to verify balance performance before weighing the samples. The gravimetric water content was computed as the percentage change in soil weight before and after oven drying.

3.3.2 1:1 Sediment:Water Extracts

Water-soluble inorganic constituents were determined using a 1:1 sediment:deionized-water extract method chosen because the sediment was too dry to easily extract vadose zone pore water. The extracts were prepared by adding an exact weight of deionized water to approximately 60 to 80 g of sediment sub-sampled from each liner or drive shoe grab sample. The weight of deionized water needed was calculated using the weight of the field-moist samples and their previously determined moisture contents. The sum of the existing moisture (pore water) and the deionized water was fixed at the mass of the dry sediment. An appropriate amount of deionized water was added to screw cap jars containing the sediment samples. The jars were sealed and briefly shaken by hand, then placed on a mechanical orbital shaker for one hour. The samples were allowed to settle, usually overnight, until the supernatant liquid was fairly clear.

The supernatant was carefully decanted, filtered, and analyzed for pH, conductivity, and anion, cation, alkalinity, and radionuclide analyses. More details can be found in Rhoades (1996) and ASA (1996).

3.3.2.1 pH and Conductivity

Two approximately 3-mL aliquots of the 1:1 sediment:water extract supernatants were used for pH and conductivity measurements. The pH of the extracts was measured with a solid-state pH electrode and a pH meter calibrated with buffers 4, 7, and 10. Electrical conductivity was measured and compared to potassium chloride standards with a range of 0.001 to 1.0 M.

3.3.2.2 Anions

The 1:1 sediment:water extracts were analyzed for anions using ion chromatography (IC). Fluoride, chloride, nitrite, bromide, nitrate, carbonate, phosphate, and sulfate were separated on a Dionex AS17 column with a gradient elution of 1- to 35-mM sodium hydroxide and measured using a conductivity detector. This methodology is based on U.S. Environmental Protection Agency (EPA) Method 300.0A (EPA 1984) with the exception of using sodium hydroxide as the elutant. Water extract chromatograms were visually scanned to check for unidentified peaks caused by the presence of other constituents.

3.3.2.3 Cations and Trace Metals

Major cation analysis was performed using an inductively coupled plasma-optical emission spectroscopy (ICP-OES) unit using high-purity calibration standards to generate calibration curves and verify continuing calibration during the analytical run. Multiple dilutions of each 1:1 water extract were prepared and analyzed to investigate and correct for matrix interferences. Details of this method are found in EPA Method 6010B (EPA 2000b). The second instrument, which was used to analyze trace metals, including technetium-99 and uranium-238, was an inductively coupled plasma-mass spectrometer (ICP-MS) using PNNL procedures based on EPA Method 6020 (EPA 2000c).

3.3.2.4 Alkalinity

The alkalinity of several of the 1:1 sediment:water extracts was measured using standard titration. The procedure is equivalent to the U.S. Geological Survey National Field Manual (USGS 2001) method.

3.3.2.5 8 M Nitric Acid Extract

Approximately 20 g of oven-dried sediment was contacted with 8 M nitric acid at a ratio of approximately 5 parts acid to 1 part sediment. The slurries were heated to about 80°C for several hours, after which the fluid was separated by filtration through 0.45-µm membranes. The acid extracts were analyzed for major cations and trace metals using ICP-OES and ICP-MS techniques, respectively. The acid digestion procedure is based on EPA Method 3050B (EPA 2000a).

3.3.2.6 Gamma Energy Analysis

GEA was performed on sediment from the direct-push liners. All samples were analyzed using 60% efficient intrinsic germanium gamma detectors. All germanium counters were efficiency calibrated for

distinct geometries using mixed gamma standards traceable to the National Institute of Standards and Technology (NIST). Field-moist samples were placed in 150-cm^3 counting containers and analyzed for 100 minutes in a fixed geometry. All spectra were background subtracted. Spectral analysis was conducted using libraries containing most mixed fission products, activation products, and natural decay products. Control samples were run throughout the analysis to ensure correct operation of the detectors. The controls contained isotopes with photo peaks spanning the full detector range and were monitored for peak position, counting rate, and full-width half-maximum. Details are listed in PNNL procedure *Gamma Energy Analysis, Operation, and Instrument Verification using Genie2000™ Support Software*.

3.3.2.7 Carbon Content of Sediment

The total carbon concentration in aliquots of sediment from the core liners was measured by combustion at approximately 900°C with a Shimadzu TOC-V CSN instrument with a SSM-5000A total organic carbon analyzer, based on ASTM *Standard Test Methods for Analysis of Metal Bearing Ores and Related Materials by Combustion Infrared Absorption Spectrometry* (ASTM 2001). Samples were placed into pre-combusted and tared ceramic combustion sample holders and weighed on a calibrated balance. After the combustion sample holders were placed into the furnace introduction tube, an approximately 2-minute waiting period was allowed for the ultrapure oxygen carrier gas to remove any carbon dioxide introduced to the system from the atmosphere during sample placement. After this sparging process, the sample was moved into the combustion furnace and the combustion was begun. The carrier gas then delivered the sample combustion products to the cell of a non-dispersive infrared gas analyzer where the carbon dioxide was detected and measured. The amount of CO_2 measured is proportional to the total carbon content of the sample. Adequate system performance was confirmed by analyzing known quantities of a calcium carbonate standard.

Sediment samples were analyzed for inorganic carbon content by placing the sediment aliquot into a ceramic combustion boat. The combustion boat was placed into the sample introduction tube where it was sparged with ultrapure oxygen for two minutes to remove atmospheric carbon dioxide. A small amount (usually 0.6 mL) of 3 M phosphoric acid was then added to the sample in the combustion boat. The boat was moved into the combustion furnace where it was heated to 200°C. Samples were completely covered by the acid to allow full reaction to occur. Ultrapure oxygen swept the resulting carbon dioxide through a dehumidifier and scrubber into the cell of a non-dispersive infrared gas analyzer where the carbon dioxide was detected and measured. The amount of CO_2 measured is proportional to the inorganic carbon content of the sample. Organic carbon content was determined by the difference between the inorganic carbon and total carbon concentrations.

3.3.3 Tier II Testing of Sediments from the 241-BX Tank Farm

Data obtained from the Tier I tests, discussed in this section, showed evidence for the transit of waste solution through sediments of the Hanford formation. One manifestation of the trek of the waste plume is uranium contamination. Concentrations of uranium in the sediments are above those of typical crustal abundances (2.7 μg/g) (Taylor 1964), and a large fraction of the mass of uranium is present as a weakly sorbed complex, indicated by leaching experiments. Weakly sorbed uranium is not how uranium is typically manifested in pristine sediments. In most cases, "natural" uranium is locked up as a substituted cation in solid heavy mineral phases such as apatite [$Ca_5(PO_4)_3(OH,F,Cl)$], sphene [$CaTi(SiO_4)(O,OH,F)$],

zircon [$Zr(SiO_4)$], or baddeleyite (ZrO_2). Thus, the presence of weakly sorbed uranium, which is easily solubilized from sediments using water or acid extracts, is generally an indication of contamination.

The processes that control uranium migration in the subsurface are a point of some ambiguity. Previous investigators have shown that complete removal of uranium from contaminated sediments is difficult. This may be attributed to the presence of a uranium-sequestering solid phase that is resistant to dissolution (Qafoku et al. 2005). Such phases are different than the heavy mineral solids mentioned above. Typically, the heavy minerals have a detrital origin, or may be a phase completely enclosed within a lithic fragment. Contaminant uranium, on the other hand, is typically present in phases in which uranium is an essential component, and not as substituted cation. An example of a phase containing essential uranium is micro-precipitates of uranyl phosphates or silicates that precipitate in tiny cracks or void spaces within the sediments. Evidence for the existence of micro-precipitates of uranium that form in small cracks within lithic fragments has been reported in Liu et al. (2004, 2006) and McKinley et al. (2006). These precipitates appear to be mainly uranyl [i.e., U(VI)] silicates such as boltwoodite and uranophane (Ilton et al. 2006) and, by virtue of their presence in small cracks and pits, are not typically in communication with pore waters. When aqueous solutions come into contact with these reservoirs of uranium, liberation of uranium to the bulk solution is dependent on the kinetics of dissolution and diffusion of uranium. However, the results of this study indicate that uranium microprecipitates exist in cracks and crevices of materials other than granitic lithic fragments. Our hypothesis is that micro-precipitates can form in narrow spaces within the sediments and are not confined solely to crevasses within lithic fragments. Powerful microscopic techniques were used to test this hypothesis and to identify the phase or phases that harbor uranium.

One coarse- and one fine-grained specimen from push hole C5134 (at 77 ft bgs) were selected for more detailed analysis. These specimens, labeled B1JWW6C coarse and B1JWW6C fine, respectively, were selected because the positioning of coarse- and fine-grained samples gave us a good opportunity to investigate the heterogeneous distribution of uranium over a limited spatial scale. The Tier II characterization consisted of particle size distribution, microwave-assisted digestion, X-ray diffraction (XRD) analyses, various leaching and isotope-exchange procedures, and micro-analysis methods, all of which are described below, to determine the residence of uranium. A third sample, B1JWW6A (from borehole C5134 at 78 ft bgs), was used only for time-resolved laser-induced fluorescence (TRLIF) spectroscopy as an internal comparison to the B1JWW6C fine and B1JWW6C coarse samples.

3.3.3.1 Particle-Size Analysis

The dry sieving method was used to determine the particle-size distribution for selected bulk sediment samples (B1JWW6C fine and B1JWW6C coarse). The method is based on the procedure *Standard Test Method for Particle-Size Analysis of Soils* (ASTM 1986). The silt/clay (<0.0625 mm), very fine sand (0.0625 mm <size <0.125 mm), fine sand (0.125 mm <size <0.250 mm), medium sand (0.250 mm <size <0.500 mm), coarse sand (0.5 mm <size <1.0 mm), very coarse sand (1.0 mm <size <2.0 mm), and gravel (>2.0 mm) size fractions for each sediment sample were separated by dry sieving. The silt and clay size fractions were determined using the hydrometer method.

3.3.3.2 Microwave-Assisted Digestion

The concentration of uranium was determined in each size fraction by complete dissolution in a strong acid mixture. The rate of dissolution of the sediment material was accelerated using a special microwave procedure. The microwave digestion solution consisted of 16 M HNO_3 (17%), 12 M HCl (7%), 32 M HF (3.3%), 0.5 g of H_3BO_3 (1.5%), and deionized water. The digestion solution to sediment ratio used in this total digestion method was 30 mL to 0.35 g. The reactors that enclosed the acid solution and the soil specimen were specially designed Teflon containers for microwave-assisted digestion. Typically, the digestion required only 30 minutes to realize complete dissolution. The resulting solutions were filtered (0.45-μm syringe filters) and analyzed for dissolved uranium using ICP-MS.

3.3.3.3 X-Ray Diffraction

The mineralogy of each bulk sediment sample was determined using powder XRD analysis. The bulk sediment was prepared by grinding about 2 g of homogenized sample in an agate mortar and pestle. All sediment samples were analyzed on a Scintag XRD unit using monochromatic Cu Kα radiation (λ = 1.5418 Å). Randomly oriented bulk samples were scanned from 2° to 65° 2θ with a dwell time of 2 seconds. Scans were collected automatically and processed using commercial software (JADE® XRD pattern processing software).[(a)] Mineral identification was based on powder diffraction files published by the Joint Committee for Powder Diffraction Standards.

3.3.3.4 Labile Uranium Leaching Using (Bi)carbonate Solution

The concentration of labile (easily removable fraction) uranium in the sediment bulk sample was determined using a sodium bicarbonate/carbonate mixed solution (1.44×10^{-2} M in $NaHCO_3$ and 2.8×10^{-3} M in Na_2CO_3). The notion of "labile" uranium rests on the supposition that uranium weakly sorbed onto sediment grains will be vulnerable to re-uptake into solution due to formation of strong uranium bicarbonate and carbonate complexes. The relatively mild bicarbonate-carbonate solution is unlikely to liberate much uranium locked up in mineral matrices (Kohler et al. 2004) and is, therefore, considered to be a good index of easily-removed uranium. The reagent pH was ~9.1, and the solid-to-solution ratio was 10 g/L. Leachate aliquots were collected into two separate containers for further analysis, one aliquot for measurement of U and Ca concentration and the second for pH determination. Solutions were filtered using 0.45-μm syringe filters and analyzed for uranium and calcium using ICP-MS and ICP-OES, respectively. The leached uranium concentration was determined as a function of time ranging from 1 to 30 days. The mass of uranium and calcium were corrected for the small volume change after each small aliquot (2 mL) was removed at each sample collection time.

3.3.3.5 Isotope Exchange for Labile Uranium

A suite of isotope exchange experiments was also conducted to determine labile uranium concentrations in the sediment samples. This method assumes that the concentration of labile uranium is subject to equilibrium requirements and that the number of sites onto which uranium can sorb is relatively fixed. Therefore, a solution of synthetic groundwater in contact with the sediment would result in an equilibrium amount of labile uranium to desorb. If the solution were then spiked with a uranium isotope that could be

(a) JADE® XRD pattern processing software is manufactured by Materials Data, Inc., Livermore, California.

differentiated analytically from the resident uranium isotopes, equilibrium between the uranium isotopes, solution, and the solids should be established. The ability to measure the concentrations of different uranium isotopes will result in the quantification of the easily removed fraction of uranium in the specimen. The interested reader should consult Kohler et al. (2004) for further details.

Accordingly, each sediment sample was contacted with a synthetic groundwater at a solid-to-solution ratio of 10 g/L for 1 day, and then the slurry was spiked with 32.7 pCi/mL of uranium-233 isotope. The uranium-233 isotope was selected because it can easily be distinguished from resident uranium (uranium-238) by liquid scintillation counting methods. Synthesized groundwater was previously equilibrated with excess $CaCO_3$ solid for 7 days and used after filtration. The chemical composition of synthesized groundwater is shown in Table 3.3. Duplicate tests were run to check for reproducibility. The spiked slurries were mixed gently on a platform shaker, and effluent samples were collected periodically (1, 3, 5, 7, 10, 14, 21, and 30 days). Effluent aliquots were filtered using a 0.45-μm filter at each collection time and analyzed for uranium-233 and total uranium with a liquid scintillation counter and ICP-MS, respectively. The pH was also measured at each collection time. The labile uranium concentration on sediment was calculated using the following equation:

$$C_{labile} = (^{233}U_{total} / {}^{233}U_{dissolved}) \times C_{total} \quad (3.1)$$

Where

C_{labile} = labile uranium concentration in solution
$^{233}U_{total}$ = initially spiked total ^{233}U activity
$^{233}U_{dissolved}$ = dissolved ^{233}U activity in solution at each collection time
C_{total} = total uranium concentration in solution.

C_{labile} concentration can be converted to labile uranium concentration per gram of sediment by dividing C_{labile} by the solid concentration used.

Table 3.3. Composition of Synthesized Groundwater[(a)]

Constituents	Concentration (M)
Na^+	1.53×10^{-3}
K^+	4.30×10^{-4}
Ca^{2+}	4.97×10^{-4}
Mg^{2+}	5.29×10^{-4}
HCO_3^-	1.03×10^{-3}
CO_3^{2-}	1.11×10^{-5}
SO_4^{2-}	9.81×10^{-4}
NO_3^-	1.19×10^{-3}
(a) pH ~ 8.1 (measured).	

3.3.3.6 Synchrotron-Based Micro-XRF and Micro-XANES

High-energy micro-X-ray fluorescence (μ-XRF) was used to examine the elemental composition as well as the spatial association of selected metals in the sediment samples. Each sample was prepared in two configurations: 1) as a monolayer on Kapton tape and as a 1/16-inch-thick sample. Two spots

containing uranium were analyzed for each sample. The soil samples were placed in aluminum sample holders, the holders were sealed with Kapton tape, and analysis was performed on beamline X27A at the National Synchrotron Light Source at Brookhaven National Laboratory. Micro-synchrotron XRF data were collected on the samples at an incident X-ray energy of 17.4 keV using a 13-element germanium (Ge) detector. Elemental mapping was obtained on a 400 × 400-μm area using a focused beam of approximately 5 to 10 μm. Two-dimensional image maps were obtained for 10 elements, including Ca, Cr, Cu, Fe, Mn, Pb, Sr, Ti, U, and Zn.

Specific areas in the sample that contained elevated uranium concentrations were identified prior to micro-X-ray absorption near edge structure (μ-XANES) analysis. The objective of XANES is to subject the specimen to a high-energy monochromatic beam that scans just above and below the binding energy of core-shell electrons of the target element. The specimen absorbs the energy of the incident beam until the X-ray energy matches that of the electron binding energy. At this point, the spectrum is manifested as a sharply increasing trace known as the absorption edge. At energies above the binding energy of the target element, the spectra display an oscillating trace, and the position of the peak can be used to identify the oxidation state of the element. The oxidation state of uranium in the sediment was determined using μ-XANES analysis on a 10 × 15-μm spot at the uranium L_{III} edge (17.166 keV). Bulk XANES analysis on a 1 × 15-mm spot was also conducted on beamline X11A to obtain an average oxidation state for uranium in the sediments. Calibration standards, namely, uranyl nitrate [$UO_2(NO_3)_2$] and uranium dioxide (UO_2) were used to establish the absorption edge positions for U(VI) and U(IV), respectively. Spectra were normalized to the edge-jump using ATHENA software.[(a)] Data were analyzed to determine the spatial and chemical distribution of uranium with the metals.

3.3.3.7 Time-Resolved Laser-Induced Fluorescence (TRLIF) Spectroscopy

TRLIF spectroscopy was performed in a Cryo Industries RC-152 cryostat at liquid helium (He) temperature (6 ± 1K) on three sediment samples (B1JWW6C fine, B1JWW6C coarse, and B1JWW6A). The advantage afforded by TRLIF spectroscopy is that a very small sample volume is excited by a pulsed laser at a specified wavelength, and the energy causes fluorescence in the target uranium phase. Solid uranium-bearing phases as well as dissolved uranium species (Wang et al. 2004, 2005b) can be analyzed at detection levels that cannot be achieved by Raman, nuclear magnetic resonance (NMR), or other spectroscopic techniques. Because the fluorescence spectra emitted depend on the nature of the bonding relationship between uranium and the surrounding atoms, the spectral signature of each uranium species is unique and allows for confident identification and assignment. At room temperature, the fluorescent spectra for many species are quenched by electron transitions (among other things), but at cryogenic temperatures, the lack of such quenching results in a sharp, intense spectrum. A further complication arises from the duration of fluorescence; the spectra are time-sensitive, and the sharpness of the spectra depends on the time interval selected for data acquisition. The duration of the spectral signal also depends on the nature of the bonds between uranium and its surrounding shell of atoms, and obtaining the optimal signal must be determined experimentally.

Three sediment samples were analyzed after the samples were mounted onto a copper sample holder with a sapphire window. The sample cell was exposed directly to the vapor flow of liquid He, and the sample temperature was controlled by tuning both the liquid He flow rate and the electric current applied

(a) Naval Research Laboratory, Washington, D.C.

to the internal heater of the cryostat. The normal fluorescence emission spectra of samples were obtained at 415 nm using a neodymium-doped yttrium aluminum garnet (Nd:YAG) laser with the frequency-doubled output of a MOPO-730 pulsed laser after the spectrograph wavelength was calibrated with a xenon lamp (Spectra Physics model 6033). Time-resolved fluorescence emission spectra were collected with a thermoelectrically cooled Princeton Instrument PIMAX time-gated intensified charge-coupled camera at the exit port of an Acton SpectroPro 300i double monochromator spectrograph. The data record was controlled by WinSpec data acquisition software and analyzed using IGOR[(a)] software.

3.3.3.8 Strontium-90 Separation and Determination

The acid extractions from Tier 1 activities were further characterized to provide us with more information on the degree of contamination within the sediments. The acid leach solution was assayed for gross α- and β-radiation emitting isotopes and the results confirmed the presence, but did not identify the specific isotope(s), that emitted β-radiation. There is a wide range of suspect β-emitters that could give rise to the radiation signal (for example technetium-99 and strontium-90), so in order to identify the source(s), we employed special separation procedures. In essence, these procedures relied on ion-exchange columns containing an exchange resin specifically designed to capture a particular cation complex. Previous experience with Hanford borehole sediments collected within the 241-B Tank Farm (see Serne et al. 2002f for additional details) led us to suspect strontium-90 as the primary candidate β-emitter. The procedure for Sr separation, based on document AGG-RRL-003.2, 2000, is described below.

Aliquots of filtered acid extracts were diluted in 8 M HNO_3 and submitted for Sr separation and analysis. We employed a tracer method, in which an isotope of strontium, in this case, ^{85}Sr, could be easily differentiated from ^{90}Sr analytically and used to assess the total recovery of the separation process. A 0.1-5 mL aliquot of sample was spiked with ^{85}Sr tracer and passed through a SrSpec® column [Eichrom Technologies, Chicago]. The purpose of the ^{85}Sr tracer is to ensure that all strontium was removed from the column by elution with nitric acid. The columns were washed with 10 column volumes (20 mL) of 8M nitric acid. Strontium (^{85}Sr and ^{90}Sr) was eluted from the SrSpec column into glass liquid scintillation vials using 15 mL of deionized water. The vials were placed under a heat lamp overnight to evaporate the water to dryness. 15 mL of Optifluor® scintillation cocktail was added to each vial. Gamma spectroscopy was used to determine the chemical yield from the added ^{85}Sr tracer. The samples were then analyzed by liquid scintillation counting (LSC) to determine the amount of ^{90}Sr originally present in the sediment sample. A matrix spike, a blank spike, a duplicate, and blanks were run with each sample set to determine the efficiency of the separation procedure as well as the purity of reagents.

(a) IGOR is a product of WaveMetrics, Inc., Lake Oswego, Oregon.

4.0 Results and Discussion

This section presents the geochemical and physical characterization data collected on sediment from the direct-push holes emplaced within the 241-B and 241-BX Tank Farms. The primary goals of these tests were to provide basic characterization data and to form the basis on which the nature and extent of mobile contaminants in the vadose zone sediments could be determined. This fundamental information included moisture content, total and inorganic carbon content, pH, EC, and measurements of major cations, anions, and trace metals (including technetium-99 and uranium-238) in 1:1 sediment:water extracts. In addition, concentrations of major cations and trace metals (including technetium-99 and uranium-238) were measured from 8 M nitric acid extracts. GEA of the sediments was also performed to probe for any detectable anthropogenic gamma emitting radionuclides.

4.1 Vadose Zone Sediment from 241-B Farm Direct-Push Samples

All of the sediment samples obtained from the 241-B Tank Farm were collected east of the 241-B-153 diversion box; thus, all of the discussion that follows in Section 4.1 is focused on this locale.

4.1.1 Moisture Content

The moisture content of the 10 core liners (one liner sample split into two discrete samples) and 3 grab samples collected from the 241-B Farm direct-push holes are presented as a function of depth in Table 4.1 and Figure 4.1. Several of the samples displayed elevated moisture contents: the shoe material

Table 4.1. Gravimetric Moisture Content of Samples Obtained from the 241-B Farm Direct-Push Holes[(a)]

Sample ID	Probe Hole ID	Mid-Depth (ft bgs)	Moisture (%)
B1LTY5C	C5164B	21.25	8.05%
B1LTY5B	C5164B	21.75	10.1%
B1LTY5A	C5164B	22.25	16.8%
B1LTY5	C5164B	22.75	15.4%
B1M564C	C5164A	17.25	3.08%
B1M564B	C5164A	17.75	3.08%
B1M564A	C5164A	18.25	3.79%
B1LTY4	C5170	20.50	3.61%
B1M565C sand	C5168	17.25	9.68%
B1M565C fine	C5168	17.25	14.1%
B1M565B	C5168	17.75	9.83%
B1M565A	C5168	18.25	9.38%
B1M565	C5168	18.75	12.0%

(a) Shaded cells indicate grab samples.

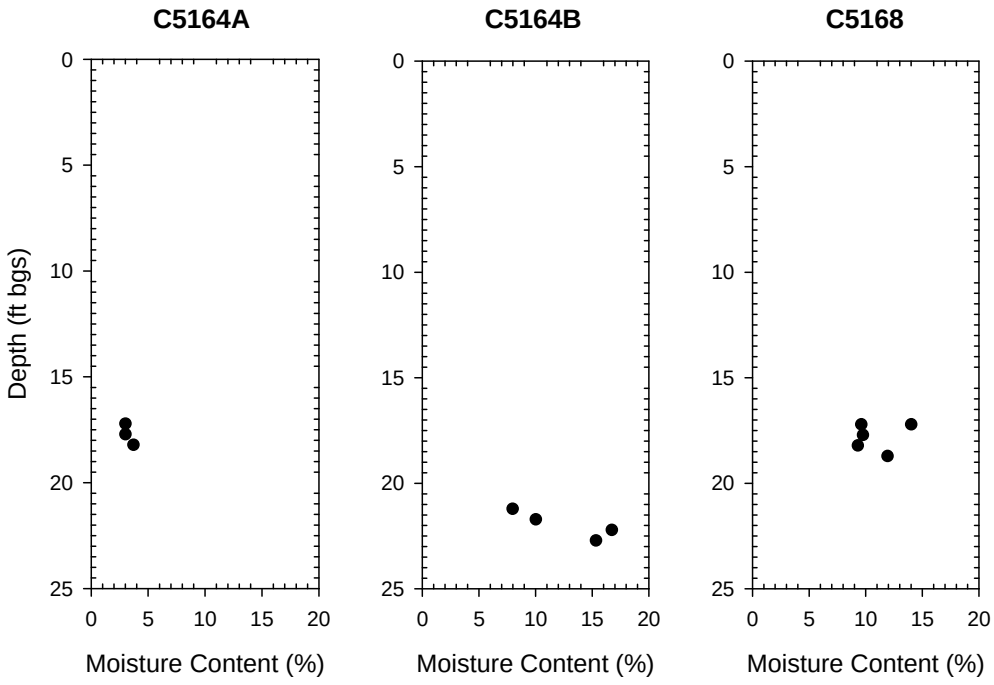

Figure 4.1. Moisture Content Data for the 241-B Farm Direct-Push Samples

and A and B liner material from push hole C5164B all had gravimetric moisture contents in excess of 10%, and all of the samples collected from push hole C5168 had gravimetric moisture contents of 10% or more. It is obvious that a fine-grained lens was encountered between 18 and 21 ft bgs at push holes C5164A and C5164B. Direct-push hole C5164A was placed between 17 and 18.5 ft bgs and had an average gravimetric moisture content of 3.39%, while direct-push hole C5134B, which was between 21.5 and 23 ft bgs, had an average gravimetric moisture content of 12.6%. The moisture contents measured in these samples compare well with those measured from similar lithologies in the background borehole (C3391), which was emplaced southeast of the 241-B Tank Farm (Lindenmeier et al. 2003). Moisture contents measured in borehole C3391 within the Hanford formation H1 unit ranged from approximately 2% to over 12% depending on the amount of gravel, sand, and silt/clay contained in the sample. These moisture contents for uncontaminated sediments from the borehole correlate well with the range measured in the 241-B Farm direct-push samples (3.08 to 16.8%) and imply that elevated moisture measured in several of the direct-push samples is likely controlled by sample lithology rather than an indication of past liquid releases in the environs.

4.1.2 1:1 Sediment:Water Extracts

The samples from the 241-B Tank Farm direct-push campaign were characterized by performing 1:1 sediment:water extracts. The following tables present the mass of a given constituent leached per gram of sediment as measured in the water extracts. Other tables show dilution-corrected values that represent concentrations in vadose zone pore water. As discussed in several other Vadose Zone Characterization Project reports, the dilution-corrected 1:1 sediment:water extracts are a reasonable estimate of the actual vadose zone pore water in most contaminated sediments and slightly over-predict actual pore water concentrations in uncontaminated sediments (see Serne et al. 2002a–f).

4.1.2.1 pH and Electrical Conductivity

The 1:1 sediment:water extract pH and EC data for the 241-B Farm core samples are shown in Table 4.2 and Figure 4.2. The pH is tabulated as measured in the 1:1 sediment:water extracts, but the EC is corrected for dilution and tabulated as if it was actual pore water. Due to sample mass limitations, no analyses could be performed on material recovered from the shoe in push hole C5170.

Table 4.2. pH for 1:1 Sediment:Water Extracts and Dilution-Corrected EC Values from 241-B Farm Core Samples

Sample ID	Probe Hole ID	Mid-Depth (ft bgs)	pH[(a)]	Pore Water Conductivity[(b)] (mS/cm)
B1LTY5C	C5164B	21.25	**9.05**	5.22
B1LTY5B	C5164B	21.75	**9.33**	5.14
B1LTY5B DUP	C5164B	21.75	**9.10**	5.28
B1LTY5A	C5164B	22.25	**9.41**	4.76
B1M564C	C5164A	17.25	**8.76**	5.22
B1M564B	C5164A	17.75	**8.34**	5.40
B1M564A	C5164A	18.25	7.76	3.73
B1M565C sand	C5168	17.25	**9.40**	8.42
B1M565C fine	C5168	17.25	**9.38**	6.54
B1M565B	C5168	17.75	**9.67**	8.52
B1M565A	C5168	18.25	**9.69**	9.06

(a) Bold numbers denote elevated values.
(b) EC values are dilution corrected and represent pore water concentrations, not 1:1 extract values.

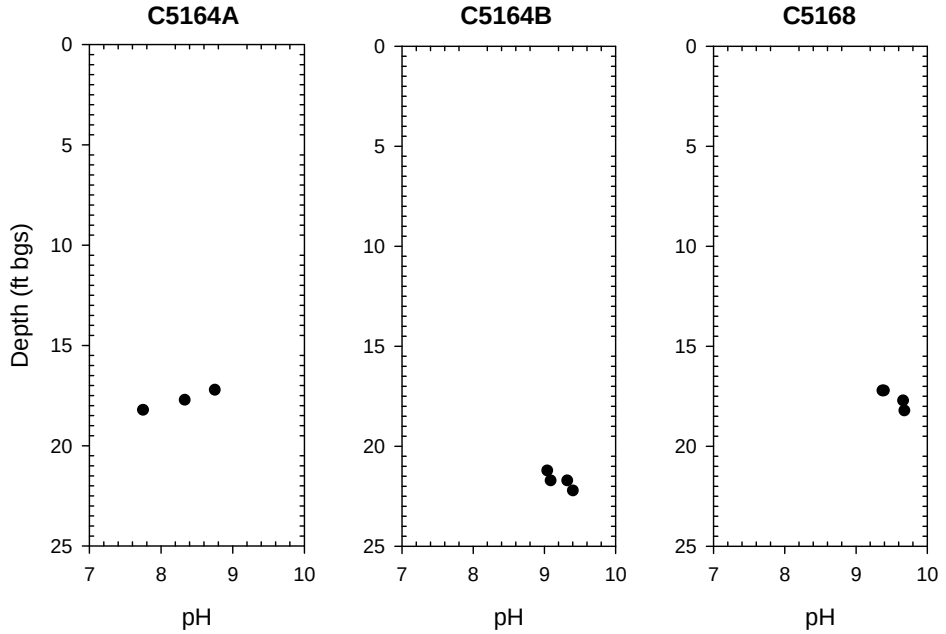

Figure 4.2. pH for 1:1 Sediment:Water Extracts from the 241-B Farm

It has been well documented in several borehole reports that uncontaminated Hanford sediments have soil pH values ranging from 7.0 to 8.0 (Serne et al 2002a, 2004b; Lindenmeier et al. 2003; Brown et al. 2006). Sediment pH values are considered slightly elevated between 8.0 and 8.5 and are significantly elevated above 8.5. Previous characterization activities have shown that soil pH is typically significantly elevated in locations where tank waste has entered the vadose zone (Serne et al. 2002b,c, 2004a,b; Brown et al. 2006, 2007). Natural minerals in the sediment eventually buffer the alkaline waste solution as it migrates through the vadose zone, resulting in normal soil pH values down gradient from waste source discharge points. Elevated soil pH values were measured in sediments retrieved from push holes C5164B, C5164A, and C5168. In fact, only one sample analyzed as part of this study did not contain an elevated soil pH. This sample (B1M564A), which was collected from push hole C5164A, had a soil pH of 7.76. Interestingly, the other two core samples retrieved from this push hole both had elevated soil pH values, at 8.34 and 8.76, respectively. While elevated, these were still considerably lower than the pH values measured in core samples from the remaining two push holes. Sediments from push hole C5164B had pH values that ranged from 9.05 to 9.41, while those retrieved from push hole C5138 ranged from 9.38 to 9.69. These data clearly indicate that tank waste fluids did enter the vadose zone near the 241-B-153 diversion box.

The pore water-corrected EC data (Table 4.2 and Figure 4.3) for the samples from the 241-B Farm ranged from dilute (3.73 mS/cm) to slightly elevated (9.06 mS/cm). The only samples that had elevated pore water-corrected conductivities were those collected from push hole C5168. The average conductivity of these samples was 8.14 mS/cm; average conductivity for the remaining core samples was 4.96 mS/cm. For comparison, the average pore water-corrected conductivity of the background borehole was 2.63 mS/cm (Lindenmeier et al. 2003). Serne et al. (2002e,f) calculated pore water conductivities as high as 15.1 and 55.9 mS/cm in the boreholes northeast of Tank 241-B-110 and east of Tank 241-BX-102, respectively. Therefore, the pore water in the sediment samples collected near the 241-B-153 diversion

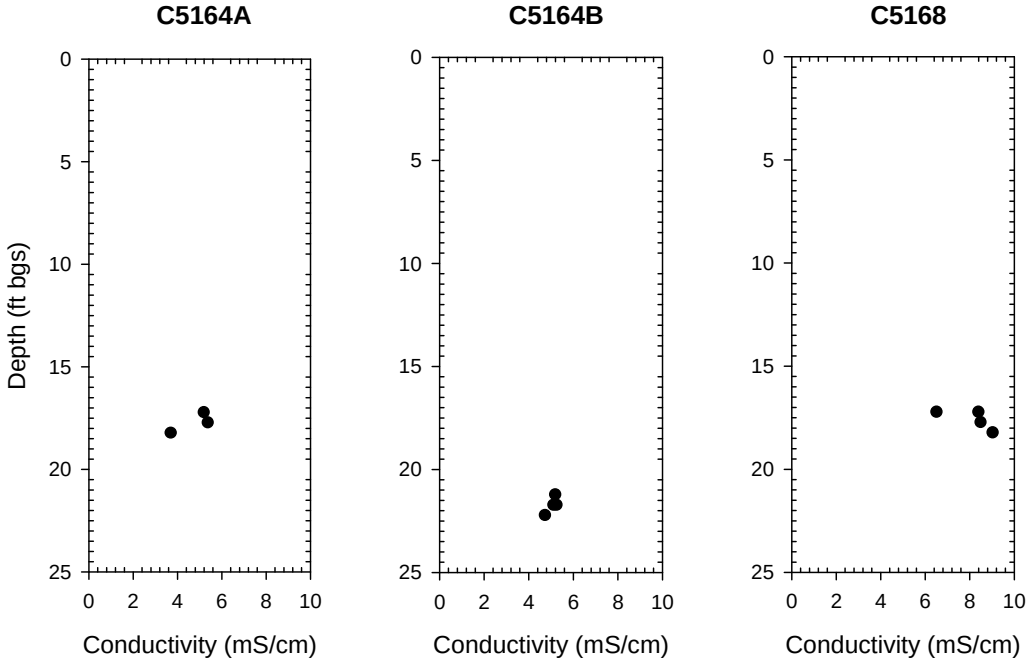

Figure 4.3. Pore Water-Corrected EC for 1:1 Sediment:Water Extracts from 241-B Farm

box appeared to have slightly elevated dissolved salt content compared with core samples collected from the background borehole (C3391) and were more dilute than contaminated core samples from boreholes S01052 (near 241-B-110) and S01014 (near 241-BX-102).

4.1.2.2 Composition of the 1:1 Sediment:Water Extracts from the 241-B Tank Farm Direct-Push Core Samples

The concentrations of the major anions, cations, and several trace constituents obtained by the water extract procedure are discussed in this subsection. The anion data are tabulated in Table 4.3 in units of mass per gram of dry sediment. Three of the 1:1 sediment:water extracts contained slightly elevated concentrations of fluoride (greater than 1 μg/g) compared to the average fluoride concentration measured in the background borehole (C3391); 0.39 μg/g. The push holes containing the samples with elevated fluoride concentrations were C5164B (C liner) and C5168 (C liner). The C liner is the liner the farthest distally from the drive shoe and represents the shallowest sample collected within the sample string. Several of the 1:1 sediment:water extracts contained elevated phosphate concentrations (1.0 to 3 μg/g) compared to the average phosphate concentration of 0.40 μg/g found in the background borehole (C3391). These samples were collected from push holes C5164B (A and B liners) and C5168 (C liner). It is believed that metal waste from the bismuth phosphate extraction process, which contained 1.4 M phosphate, was lost to the vadose zone near the 241-B diversion boxes (Wood et al. 2000); therefore, we were not alarmed to find elevated concentrations of phosphate in these sediments. Although the chloride, nitrate, and sulfate concentrations ranged between 0.60 and 6.2 μg/g, 1.22 and 12.5 μg/g, and 2.30 and 12.6 μg/g, respectively, none of these analytes were significantly elevated in concentration above those measured in the background borehole (C3391).

Table 4.3. Water-Extractable Anions in the 241-B Farm Core Samples (μg/g dry sediment)[a,b,c]

Sample ID	Probe Hole ID	Mid-Depth (ft bgs)	Fluoride (μg/g)	Chloride (μg/g)	Nitrate (μg/g)	Sulfate (μg/g)	Phosphate (μg/g)
B1LTY5C	C5164B	21.25	**2.15E+00**	8.02E-01	2.76E+00	1.26E+01	<1.50E+00
B1LTY5B	C5164B	21.75	N/R	<5.01E-01	2.80E+00	4.18E+00	**1.79E+00**
B1LTY5B DUP	C5164B	21.75	N/R	6.21E-01	4.15E+00	6.85E+00	**2.23E+00**
B1LTY5A	C5164B	22.25	N/R	8.44E-01	1.25E+01	4.49E+00	**3.19E+00**
B1M564C	C5164A	17.25	5.02E-01	<5.02E-01	1.75E+00	3.53E+00	<1.51E+00
B1M564B	C5164A	17.75	6.85E-01	<5.23E-01	1.22E+00	9.22E+00	<1.57E+00
B1M564A	C5164A	18.25	7.46E-01	5.99E-01	1.27E+00	5.12E+00	<1.50E+00
B1M565C sand	C5168	17.25	**1.13E+00**	6.22E+00	1.55E+00	1.23E+01	**1.77E+00**
B1M565C fine	C5168	17.25	**1.33E+00**	6.60E+00	6.83E+00	9.68E+00	**1.77E+00**
B1M565B	C5168	17.75	7.73E-01	7.95E-01	4.48E+00	2.72E+00	<1.51E+00
B1M565A	C5168	18.25	N/R	1.26E+00	3.22E+00	2.30E+00	**1.65E+00**

(a) Bold values denote concentrations elevated above background.
(b) Less than values indicate the instrument returned a negative value.
(c) N/R indicates that the value was not reported due to a peak interference.

The water-extractable major cations in the 241-B Tank Farm push-hole sediments are tabulated in Table 4.4 and illustrated in Figure 4.4 in units of mass per gram of sediment on a dry weight basis. Bismuth phosphate neutralized metal waste contained between 3.8 and 4.8 M sodium (Serne et al. 2007; Jones et al. 2001), so it is not surprising that all the direct-push core samples analyzed contained elevated concentrations of water-extractable sodium. In fact, sodium was the dominant water-extractable cation in all of the sediments analyzed. Water-extractable sodium concentrations ranged from a low of 17.7 μg/g in push hole C5164A to a high of 201 μg/g in push hole C5168. Although the total water-extractable sodium varied in these samples by more than an order of magnitude, the fact that it was always the dominant water-extractable cation indicates that all of these sediments have likely been contaminated by tank waste. Sodium from waste fluids displaces divalent cations, such as calcium and magnesium, as the contaminant plume migrates through the sediments. Because of the lack of additional samples from deeper in the vadose zone, it is impossible to estimate how deep the cation exchange front exits in the vadose zone beneath the 241-B diversion boxes.

Table 4.4. Water-Extractable Major Cations in the 241-B Farm Core Samples (μg/g dry sediment)[(a,b,c)]

Sample ID	Probe Hole ID	Mid-Depth (ft bgs)	Calcium (μg/g)	Potassium (μg/g)	Magnesium (μg/g)	Strontium (μg/g)	Sodium (μg/g)
B1LTY5C	C5164B	21.25	*1.65E+00*	(1.73E+00)	*9.83E-01*	(9.86E-03)	**8.40E+01**
B1LTY5B	C5164B	21.75	*(6.31E-01)*	(1.94E+00)	(1.85E-01)	(3.05E-03)	**1.03E+02**
B1LTY5B DUP	C5164B	21.75	*(8.66E-01)*	(2.28E+00)	*4.08E-01*	(6.45E-03)	**1.26E+02**
B1LTY5A	C5164B	22.25	*(8.31E-01)*	(2.84E+00)	(2.14E-01)	(4.17E-03)	**1.62E+02**
B1M564C	C5164A	17.25	*5.43E+00*	(7.72E+00)	*1.18E+00*	(2.44E-02)	**1.88E+01**
B1M564B	C5164A	17.75	*4.88E+00*	(6.90E+00)	*1.44E+00*	(3.03E-02)	**2.00E+01**
B1M564A	C5164A	18.25	*3.94E+00*	(3.62E+00)	*8.89E-01*	(2.68E-02)	**1.77E+01**
B1M565C-sand	C5168	17.25	*(6.79E-01)*	(1.36E+00)	(2.39E-01)	(2.88E-02)	**1.63E+02**
B1M565C fine	C5168	17.25	*(9.70E-01)*	(3.18E+00)	(1.96E-01)	(5.11E-03)	**2.01E+02**
B1M565B	C5168	17.75	*(9.16E-01)*	(2.62E+00)	*4.54E-01*	(6.86E-03)	**1.70E+02**
B1M565A	C5168	18.25	*(6.47E-01)*	(2.46E+00)	(1.74E-01)	(6.74E-03)	**1.69E+02**

(a) Bold values denote concentrations elevated above background.
(b) Italicized values denote analytically low concentrations.
(c) Parentheses indicate reported value was less than the limit of quantification for the analysis.

The water-extractable aluminum, iron, silicon, and sulfur in the 241-B Farm direct-push sediments are shown in Table 4.5. The sulfur data were converted to water-extractable sulfate so the results could be compared with IC sulfate data in Table 4.3. The agreement between sulfate measured directly in the water extracts using IC and indirectly by converting ICP measurements to sulfate was poor. Typically, these two analytical methods generate sulfate data with a percent difference of ±10, but in these samples, relative percent differences ranged from approximately 25 to 80%. The ICP results, which represent total sulfur in the samples, were always higher than the sulfate data reported via IC, indicating that either there is a non-sulfate source of sulfur in these sediments or that one of the data sets is biased. Based on this, only the data acquired via ion chromatographic analysis of the samples should be used to report sulfate concentrations. The concentration of water-soluble aluminum was elevated (above the detection limit) in samples from all of the direct-push holes and attains concentrations as high as 2.36 μg/g in push hole C5164B. It appears that these elevated concentrations of aluminum result from chemical reactions

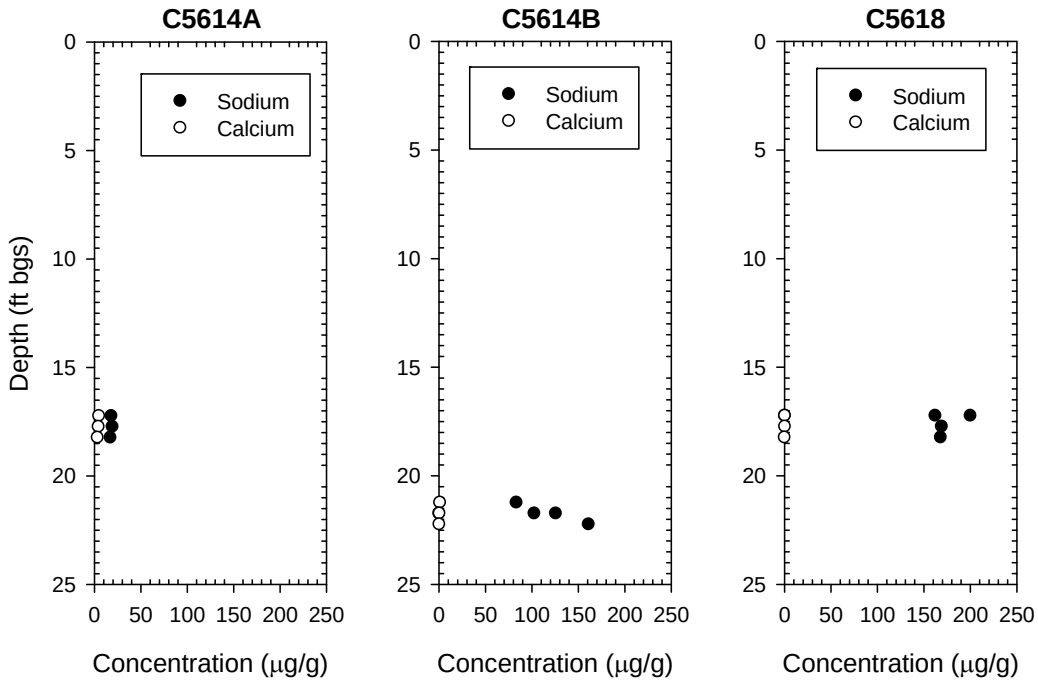

Figure 4.4. 1:1 Sediment:Water Extractable Sodium and Calcium Data from 241-B Direct-Push Samples

(dissolution/precipitation) between alkaline tank fluids and native sediments that formed precipitates of amorphous aluminum phases that are more water soluble than crystalline aluminum-rich mineral phases in the pristine sediments. Likewise, concentrations of water-extractable iron were found in all of the sediments analyzed. Like aluminum, iron is not generally water extractable unless the sediment has been chemically altered (e.g., via a caustic waste stream). Therefore, the water-extractable aluminum and iron concentrations in these samples provide evidence of mineral alteration of the sediment via contact with tank waste.

Table 4.5. Water-Extractable Cations in the 241-B Farm Core Samples (μg/g dry sediment)[(a,b)]

Sample ID	Probe Hole ID	Mid-Depth (ft bgs)	Aluminum (μg/g)	Iron (μg/g)	Sulfur as SO_4^{2-} (μg/g)	Silicon (μg/g)
B1LTY5C	C5164B	21.25	**2.36E+00**	**5.73E+00**	1.99E+01	2.34E+01
B1LTY5B	C5164B	21.75	**4.13E-01**	**7.91E-01**	5.58E+00	1.54E+01
B1LTY5B DUP	C5164B	21.75	**1.02E+00**	**2.33E+00**	9.69E+00	1.89E+01
B1LTY5A	C5164B	22.25	**3.86E-01**	**7.72E-01**	6.80E+00	1.83E+01
B1M564C	C5164A	17.25	**7.65E-01**	**1.70E+00**	5.92E+00	1.09E+01
B1M564B	C5164A	17.75	**1.15E+00**	**2.66E+00**	1.35E+01	1.29E+01
B1M564A	C5164A	18.25	**4.16E-01**	**8.00E-01**	6.72E+00	1.01E+01
B1M565C sand	C5168	17.25	(4.24E-01)	**1.02E+00**	2.14E+01	1.65E+01
B1M565C fine	C5168	17.25	**4.94E-01**	**9.17E-01**	1.39E+01	2.34E+01
B1M565B	C5168	17.75	**1.31E+00**	**2.97E+00**	3.97E+00	2.40E+01
B1M565A	C5168	18.25	**4.08E-01**	**8.42E-01**	5.47E+00	1.93E+01

(a) Bold values denote concentrations elevated above background.
(b) Parentheses indicate reported value was less than the limit of quantification for the analysis.

The water extract data for potentially mobile metals such as technetium-99, uranium-238, chromium, molybdenum, ruthenium, and silver are recorded in Table 4.6. Not one sample collected from the three push holes (nine samples total) contained quantifiable concentrations of water-leachable technetium. Except for uranium, none of the mobile metals were detected at elevated concentrations in water extracts of the sediments. However, we did not expect to find a significant amount of mobile metals in these samples because they were all collected within a few vertical feet of the contaminant source term. Because mobile metals are not retained by the solid matrix, we only expect to find elevated concentrations along a narrow front farther down gradient from the source (see Wan et al. 2004, for an enlightening example). These results agree with previous characterization efforts that revealed a lack of water-extractable mobile tank waste metals in zones exhibiting elevated soil pH values (Serne et al. 2002b,c; Brown et al. 2006).

4.1.3 Vadose Zone Pore Water Chemical Composition

The 1:1 water extract data were processed to estimate the pore water composition of the existing moisture in vadose zone sediments so that electrical balances (anions versus cations) of the pore water could be evaluated. From knowledge of the moisture content of the sediment samples taken from the liners of each direct-push sampler and the grab samples, the amount of deionized water that would be needed to make the water extract exactly one part water (total of native pore water and added deionized water) to one part by weight dry sediment was calculated. The ratio of the total volume of water in the extract to the native mass of pore water is the dilution factor. We assumed that the deionized water acted solely as a diluent of the existing pore water and that the deionized water did not dissolve any of the solids in the sediments. Thus, by correcting for the dilution, an estimate of the actual chemical composition of the native pore-water in the vadose zone sediments could be derived.

However, the assumption that none of the solids are dissolved during the water extraction process is simplistic. Further, the available evidence indicates that the accuracy of this estimate depends on the degree to which sediments are contaminated. Comparison of actual vadose zone sediment pore water that was obtained via ultracentrifugation with the dilution-corrected calculated pore waters from both contaminated and uncontaminated sediments from SX and B-BX Tank Farms (see Serne et al. 2002b–f) for highly contaminated sediments is quite good. However, for slightly contaminated or uncontaminated sediments, the dilution-corrected water extract data are biased high by a factor of 2 to 7 for many constituents in that the true pore water is less saline. For the B Tank Farm direct-push data set, not enough sample material was available to collect actual pore water via ultracentrifugation. Therefore, it is assumed that the derived pore water concentrations for the B direct-push samples are slightly biased toward higher concentrations.

Tables 4.7 and 4.8 show the derived pore water composition of key constituents in meq/L. The samples had a dissolved salt load ranging from 69.2 meq/L for sample B1M564A from push hole C5164A to a high of 169 meq/L for sample B1M565A from push hole C5168. All of the samples analyzed contained sodium as the dominant water-extractable cation and bicarbonate/carbonate as the dominant anion. Sample B1M564A contained 20.3 meq/L sodium, 5.19 meq/L calcium, 2.45 meq/L potassium, and 1.93 meq/L magnesium. The cations in this sample were balanced by the following anions: 2.81 meq/L sulfate, 1.04 meq/L fluoride, and trace amounts of chloride and nitrate. In addition, the alkalinity of the solution was 32.1 meq/L. Sample B1M565A contained 78.1 meq/L sodium with trace amounts of calcium, magnesium, and potassium, and these cations were balanced almost entirely by

Table 4.6. Water-Extractable Mobile Metals in the 241-B Farm Core Samples (μg/g dry sediment)[a,b]

Sample ID	Probe Hole ID	Mid-Depth (ft bgs)	^{99}Tc (pCi/g)	^{238}U (μg/g)	^{52}Cr (μg/g)	^{95}Mo (μg/g)	^{101}Ru (μg/g)	^{107}Ag (μg/g)
B1LTY5C	C5164B	21.25	(3.44E-02)	7.79E-03	(2.49E-03)	1.04E-01	<5.01E-04	(6.06E-05)
B1LTY5B	C5164B	21.75	<1.70E-01	2.03E-02	(1.24E-03)	8.70E-02	(1.45E-05)	(3.20E-05)
B1LTY5B DUP	C5164B	21.75	<1.51E-01	3.02E-02	(1.54E-03)	1.26E-01	(1.47E-05)	(6.28E-05)
B1LTY5A	C5164B	22.25	<1.71E-01	1.47E-01	2.87E-03	6.14E-02	(7.40E-05)	(1.24E-04)
B1M564C	C5164A	17.25	<1.70E-01	1.48E-03	4.75E-03	1.16E-02	<5.02E-04	(5.02E-05)
B1M564B	C5164A	17.75	<1.77E-01	9.38E-04	6.05E-03	1.57E-02	<5.23E-04	(5.85E-05)
B1M564A	C5164A	18.25	<1.70E-01	7.97E-04	(2.08E-03)	1.92E-02	<5.01E-04	(6.52E-06)
B1M565C sand	C5168	17.25	<1.73E-01	4.37E-02	(1.65E-03)	1.12E-01	(1.27E-05)	(4.73E-05)
B1M565C fine	C5168	17.25	<1.78E-01	8.36E-02	(1.35E-03)	9.67E-02	(1.31E-05)	(3.89E-05)
B1M565B	C5168	17.75	<1.70E-01	5.62E-02	2.89E-03	8.67E-02	(3.46E-05)	(2.27E-04)
B1M565A	C5168	18.25	<1.72E-01	7.11E-02	(1.65E-03)	1.00E-01	(3.39E-05)	(4.60E-05)

(a) Parentheses indicate reported value was less than the limit of quantification for the analysis.
(b) Less than values indicate the instrument returned a negative value.

Table 4.7. Calculated Pore Water Anion Concentrations in the 241-B Tank Farm Core Samples[a,b]

Sample ID	Probe Hole ID	Mid-Depth (ft bgs)	Fluoride (meq/L)	Chloride (meq/L)	Nitrate (meq/L)	Sulfate (meq/L)	Phosphate (meq/L)	Alkalinity (meq/L)
B1LTY5C	C5164B	21.25	1.41E+00	2.81E-01	5.53E-01	3.27E+00	<5.89E-01	5.86E+01
B1LTY5B	C5164B	21.75	N/R	<1.39E-01	4.46E-01	8.59E-01	5.57E-01	5.07E+01
B1LTY5B DUP	C5164B	21.75	N/R	1.73E-01	6.60E-01	1.41E+00	6.96E-01	5.35E+01
B1LTY5A	C5164B	22.25	N/R	1.42E-01	1.20E+00	5.56E-01	5.99E-01	4.64E+01
B1M564C	C5164A	17.25	8.58E-01	<4.60E-01	9.17E-01	2.39E+00	<1.55E+00	6.32E+01
B1M564B	C5164A	17.75	1.17E+00	<4.79E-01	6.37E-01	6.24E+00	<1.61E+00	4.44E+01
B1M564A	C5164A	18.25	1.04E+00	4.45E-01	5.42E-01	2.81E+00	<1.25E+00	3.21E+01
B1M565C sand	C5168	17.25	6.17E-01	1.81E+00	2.58E-01	2.64E+00	5.78E-01	8.15E+01
B1M565C fine	C5168	17.25	4.98E-01	1.32E+00	7.82E-01	1.43E+00	3.96E-01	6.41E+01
B1M565B	C5168	17.75	4.14E-01	2.28E-01	7.35E-01	5.75E-01	<4.84E-01	8.26E+01
B1M565A	C5168	18.25	N/R	3.80E-01	5.53E-01	5.10E-01	5.54E-01	8.73E+01

(a) Less than values indicate the instrument returned a negative value.
(b) N/R indicates that the value was not reported due to a peak interference.

Table 4.8. Calculated Pore Water Cation Concentrations in 241-B Tank Farm Direct-Push Core Samples

Sample ID	Probe Hole ID	Mid-Depth (ft bgs)	Calcium (meq/L)	Potassium[a] (meq/L)	Magnesium (meq/L)	Sodium (meq/L)
B1LTY5C	C5164B	21.25	1.02E+00	(5.52E-01)	1.00E+00	4.53E+01
B1LTY5B	C5164B	21.75	3.11E-01	(4.91E-01)	(1.50E-01)	4.42E+01
B1LTY5B DUP	C5164B	21.75	4.27E-01	(5.76E-01)	3.31E-01	5.41E+01
B1LTY5A	C5164B	22.25	2.47E-01	(4.33E-01)	(1.05E-01)	4.17E+01
B1M564C	C5164A	17.25	8.81E+00	(6.43E+00)	3.14E+00	2.65E+01
B1M564B	C5164A	17.75	7.93E+00	(5.75E+00)	3.84E+00	2.82E+01
B1M564A	C5164A	18.25	5.19E+00	(2.45E+00)	1.93E+00	2.03E+01
B1M565C sand	C5168	17.25	3.51E-01	(3.60E-01)	(2.03E-01)	7.31E+01
B1M565C fine	C5168	17.25	3.44E-01	(5.79E-01)	(1.14E-01)	6.19E+01
B1M565B	C5168	17.75	4.66E-01	(6.83E-01)	3.80E-01	7.51E+01
B1M565A	C5168	18.25	3.45E-01	(6.72E-01)	(1.53E-01)	7.81E+01

(a) Parentheses indicate reported value was less than the limit of quantification for the analysis.

alkalinity of 87.3 meq/L. Overall, these concentrations are very dilute compared to vadose zone pore water found at the SX and BX Tank Farms, where the total dissolved salt loads were as high as 7,000 to 17,000 and 1,000 meq/L, respectively (Serne et al. 2002c,d,e). At borehole E33-46 near Tank B-110, the maximum total dissolved salt load was ~320 meq/L (Serne et al. 2002f). Figure 4.5 shows pore water-corrected sodium and alkalinity data for the B direct-push sediments.

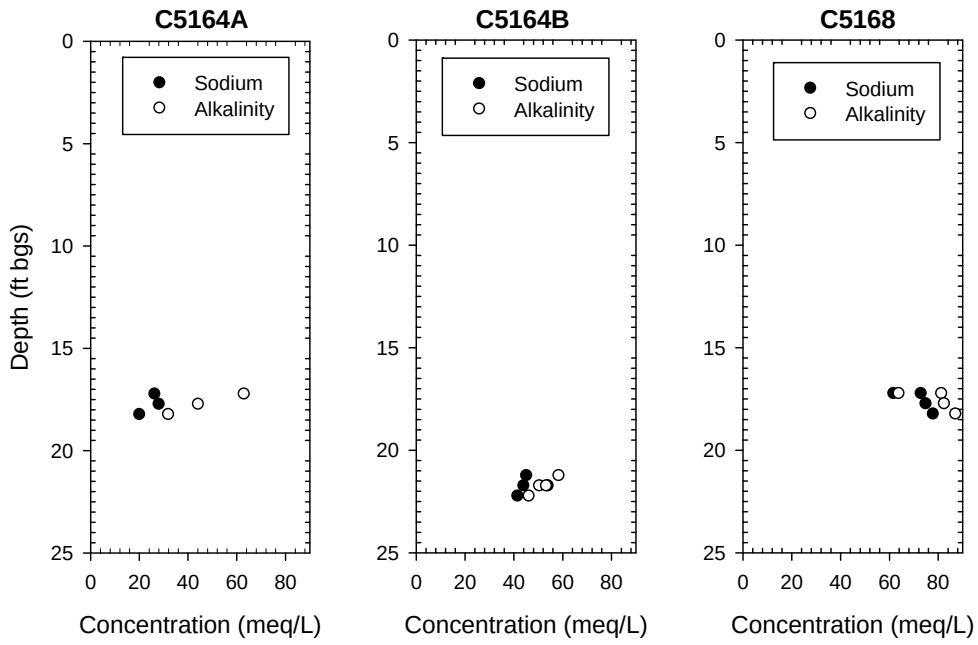

Figure 4.5. Pore Water Corrected Sodium and Alkalinity Data from 241-B Farm Direct-Push Samples

Overall, the calculated charge balance between cations and anions for all of the samples was quite good (less than 15% difference in all samples analyzed except sample B1M564C). Sample B1M564C contained approximately 30% less dissolved cations than anions. Comparing these data, it appears that either the alkalinity measurement for this sample was biased high or analyses have not accounted for a dissolved cation that is present in sufficient quantity to properly balance the electrical charge of these samples.

The notable lack of calcium-dominant samples indicates that the sediments in this region have been affected by a sodium-bearing waste fluid. The source(s) appears to be a moderately concentrated sodium-bearing waste solution that has displaced the natural divalent cations (such as Ca^{2+} and Mg^{2+}) from the cation exchange sites in the sediments. The total vertical extent of the ion exchange front is unknown due to the lack of sediment samples from deeper in the vadose zone.

4.1.4 8-M Nitric Acid-Extractable Amounts of Selected Elements in 241-B Tank Farm Direct-Push Sediments

The same core samples that were characterized for water-leachable constituents were also characterized to see how much of the various constituents could be extracted with hot 8 M nitric acid. A comparison of the quantities that were acid extractable with those that are water extractable typically indicates the relative mobility of a given constituent and can aid in differentiating anthropogenic from naturally occurring constituents. The acid-extractable concentrations are shown in Tables 4.9 and 4.10.

For all of the constituents except sodium and perhaps molybdenum, there were no significantly elevated acid-extractable values in the 241-B Tank Farm direct-push sediments compared with metals

Table 4.9. Acid-Extractable Cations in 241-B Tank Farm Direct-Push Samples (µg/g dry sediment)[a,b]

Sample ID	Probe Hole ID	Mid-Depth (ft bgs)	Calcium (µg/g)	Potassium (µg/g)	Magnesium (µg/g)	Sodium (µg/g)
B1LTY5C	C5164B	21.25	9.70E+03	1.11E+03	5.01E+03	**1.46E+03**
B1LTY5B	C5164B	21.75	9.57E+03	1.32E+03	5.24E+03	**2.54E+03**
B1LTY5B DUP	C5164B	21.75	8.02E+03	1.00E+03	4.59E+03	**1.88E+03**
B1LTY5A	C5164B	22.25	9.07E+03	1.15E+03	5.02E+03	**2.05E+03**
B1M564C	C5164A	17.25	1.00E+04	9.03E+02	4.58E+03	6.50E+02
B1M564B	C5164A	17.75	6.35E+03	7.07E+02	3.47E+03	5.19E+02
B1M564A	C5164A	18.25	7.40E+03	6.67E+02	3.78E+03	4.34E+02
B1M565C sand	C5168	17.25	8.14E+03	9.30E+02	4.54E+03	**2.69E+03**
B1M565C fine	C5168	17.25	9.66E+03	1.56E+03	5.57E+03	**2.90E+03**
B1M565B	C5168	17.75	6.95E+03	9.90E+02	4.45E+03	**2.59E+03**
B1M565A	C5168	18.25	7.47E+03	1.01E+03	4.70E+03	**2.43E+03**

(a) Sodium values were blank corrected due to contamination resulting from filtration of the samples.
(b) Bold values denote concentrations elevated above background.

Table 4.10. Acid-Leachable Cations in the 241-B Farm Core Samples (µg/g dry sediment)[a]

Sample ID	Probe Hole ID	Mid-Depth (ft bgs)	Aluminum (µg/g)	Iron (µg/g)	Phosphorus (µg/g)	Sulfur (µg/g)
B1LTY5C	C5164B	21.25	9.56E+03	3.03E+04	1.24E+03	<5.55E+02
B1LTY5B	C5164B	21.75	1.11E+04	3.25E+04	9.13E+02	<5.99E+02
B1LTY5B DUP	C5164B	21.75	8.09E+03	2.56E+04	9.03E+02	<5.72E+02
B1LTY5A	C5164B	22.25	8.73E+03	2.65E+04	8.84E+02	<5.96E+02
B1M564C	C5164A	17.25	6.20E+03	2.38E+04	1.23E+03	<5.63E+02
B1M564B	C5164A	17.75	4.78E+03	2.01E+04	1.25E+03	<5.25E+02
B1M564A	C5164A	18.25	5.04E+03	2.08E+04	1.24E+03	<5.51E+02
B1M565C sand	C5168	17.25	8.86E+03	3.54E+04	1.05E+03	<5.84E+02
B1M565C fine	C5168	17.25	1.18E+04	3.00E+04	8.86E+02	<6.73E+02
B1M565B	C5168	17.75	8.34E+03	2.68E+04	8.72E+02	<5.77E+02
B1M565A	C5168	18.25	8.67E+03	2.74E+04	8.62E+02	<5.55E+02

(a) Less than values indicate the instrument returned a negative value.

leached from the uncontaminated sediments from borehole 299-E33-338 (Lindenmeier et al. 2003). The sodium data reported in Table 4.11 have been bank corrected to compensate for sodium contamination found in the preparation blank samples.

Table 4.11. Acid-Leachable Mobile Metals in the 241-B Farm Core Samples (μg/g dry sediment)[a,b]

Sample ID	Probe Hole ID	Mid-Depth (ft bgs)	^{99}Tc (pCi/g)	^{238}U (μg/g)	^{95}Mo (μg/g)	^{109}Ag (μg/g)	^{208}Pb (μg/g)
B1LTY5C	C5164B	21.25	<4.71E+01	5.15E-01	**1.49E+00**	6.20E-02	2.64E+00
B1LTY5B	C5164B	21.75	<5.08E+01	6.10E-01	4.92E-01	2.80E-02	2.97E+00
B1LTY5B DUP	C5164B	21.75	<4.85E+01	5.20E-01	3.88E-01	2.69E-02	2.98E+00
B1LTY5A	C5164B	22.25	<5.05E+01	7.06E-01	3.19E-01	3.24E-02	3.38E+00
B1M564C	C5164A	17.25	<4.77E+01	4.11E-01	**1.11E+00**	3.54E-02	1.84E+00
B1M564B	C5164A	17.75	<4.45E+01	3.65E-01	4.95E-01	2.96E-02	1.89E+00
B1M564A	C5164A	18.25	<4.67E+01	4.39E-01	**1.09E+00**	2.43E-02	2.11E+00
B1M565C sand	C5168	17.25	<4.95E+01	6.12E-01	**1.60E+00**	4.92E-02	2.88E+00
B1M565C fine	C5168	17.25	<5.71E+01	7.20E-01	7.20E-01	6.14E-02	4.73E+00
B1M565B	C5168	17.75	<4.90E+01	5.79E-01	4.37E-01	3.43E-02	3.05E+00
B1M565A	C5168	18.25	<4.71E+01	6.81E-01	5.02E-01	3.08E-02	2.97E+00

(a) Bold values denote concentrations elevated above background.
(b) Less than symbol indicates the instrument returned a negative value.

Comparison of the water to acid-extractable concentrations of each constituent was performed by taking the water extract data (Tables 4.4 through 4.6) and dividing them by the acid extract data (Tables 4.9 and 4.10). The data are not presented in this report, but show that less than 0.1% of the acid-extractable quantities of the following elements were water leachable: aluminum, barium, calcium, iron, lead, magnesium, manganese, titanium, and zirconium. Less than 0.5% of the acid-extractable quantities of the following elements were water leachable: chromium, copper, nickel, phosphorous as phosphate, strontium, and zinc. Less than 1% of the acid-extractable cobalt and potassium and less than 10% of the acid-extractable sodium was water-extractable.

4.1.5 Radionuclide Content in Vadose Zone Sediment from the 241-B Tank Farm Direct-Push Holes

Data from the GEA of the samples are shown in Table 4.12. The direct measurement of sediment for gamma-emitting radionuclides showed that the sediments contained natural potassium-40 in all of the direct-push probe holes. The fission product isotopes antimony-125, europium-154, and europium-155 were found in several of the direct-push samples. The peak activity of antimony-125, at 4.72 pCi/g, was measured in the fine-grained sample collected from the B1M565C liner in push hole C5618. This same sample also contained the highest activities of europium-154 and europium-155 measured in the 241-B Farm direct-push samples, at 20.6 and 12.1 pCi/g, respectively. Based on the presence of these radionuclides, it is clear that the sediments recovered from push hole C5168, especially the fine-grained material encountered in the C-liner, has retained some of the less-mobile contaminants leaked into the vadose zone at this location.

Table 4.12. GEA Data for the 241-B Farm Core Samples[a,b,c]

Sample ID	Probe Hole ID	Mid-Depth (ft bgs)	Potassium-40 (pCi/g)	Antimony-125 (pCi/g)	Europium-154 (pCi/g)	Europium-155 (pCi/g)
B1LTY5C	C5164B	21.25	1.48E+01	<1.92E+00	<1.22E+00	<5.75E+00
B1LTY5B	C5164B	21.75	1.57E+01	<1.11E+00	**2.10E+00**	<2.10E+00
B1LTY5A	C5164B	22.25	1.62E+01	<1.57E+00	**5.82E+00**	<3.15E+00
B1LTY5	C5164B	22.75	1.53E+01	<2.18E+00	**1.05E+01**	**4.95E+00**
B1M564C	C5164A	17.25	1.24E+01	<5.32E-01	<3.93E-01	<5.83E-01
B1M564B	C5164A	17.75	1.41E+01	<7.04E-01	<4.94E-01	<7.62E-01
B1M564A	C5164A	18.25	1.12E+01	<6.30E-01	<4.53E-01	<6.69E-01
B1LTY4	C5170	20.50	1.71E+01	<2.08E+00	<2.23E+00	<3.98E+00
B1M565C sand	C5168	17.25	1.22E+01	**1.65E+00**	**7.05E+00**	**4.31E+00**
B1M565C fine	C5168	17.25	1.36E+01	**4.72E+00**	**2.06E+01**	**1.21E+01**
B1M565B	C5168	17.75	1.49E+01	**3.86E+00**	**1.09E+01**	**5.73E+00**
B1M565A	C5168	18.25	1.46E+01	<2.80E+00	**1.03E+01**	<7.68E+00
B1M565	C5168	18.75	1.66E+01	**1.10E+00**	**3.41E+00**	<2.30E+00

(a) Bold values denote concentrations elevated above background.
(b) < Indicates the analyte was not detected, but the minimum detectable activity for the sample has been reported.
(c) Shaded cells indicate grab samples.

The only sample strings that did not contain measurable activities of anthropogenic gamma emitters were those samples retrieved from push holes C5164A and C5170. Therefore, it appears that the primary region impacted by tank waste contaminants resides between the two depths sampled by push holes C5164A and C5164B.

4.1.6 Total Carbon, Calcium Carbonate, and Organic Carbon Content of Vadose Zone Sediment from the 241-B Tank Farm Direct-Push Holes

Data from the total carbon, inorganic carbon, and organic carbon (calculated by difference) contents of the 241-B Tank Farm direct-push sediments are shown in Table 4.13. The inorganic carbon was converted to the equivalent calcium carbonate content. In general, the sediments were low in organic carbon (<0.15% by weight) which is typical of Hanford Site sediments. The average amount of organic carbon in sediments collected from the background borehole (C33991) was 0.06% by weight (Lindenmeier et al. 2003), while the average for all of the 241-B Tank Farm direct-push samples was 0.08% by weight. Inorganic carbon, as $CaCO_3$, was also present at concentrations that are typical for Hanford formation sediments (0.3 to 1.5 wt% as $CaCO_3$) and compared well with other Hanford formation samples (Lindenmeier et al. 2003; Serne et al. 2004a; Brown et al. 2006).

Table 4.13. Carbon Content of the 241-B Farm Vadose Zone Samples

Sample ID	Probe Hole ID	Mid-Depth (ft bgs)	Total Carbon (%)	Inorganic Carbon (%)	Inorganic Carbon as $CaCO_3$ (%)	Organic Carbon (%)
B1LTY5C	C5164B	21.25	1.21E-01	5.38E-02	4.48E-01	6.69E-02
B1LTY5B	C5164B	21.75	1.50E-01	9.26E-02	7.72E-01	5.75E-02
B1LTY5B DUP	C5164B	21.75	2.20E-01	1.30E-01	1.08E+00	8.99E-02
B1LTY5A	C5164B	22.25	2.42E-01	1.85E-01	1.54E+00	5.69E-02
B1M564C	C5164A	17.25	1.55E-01	3.69E-02	3.08E-01	1.18E-01
B1M564B	C5164A	17.75	1.29E-01	4.83E-02	4.03E-01	8.09E-02
B1M564A	C5164A	18.25	1.42E-01	6.05E-02	5.04E-01	8.17E-02
B1M565C sand	C5168	17.25	1.91E-01	5.28E-02	4.40E-01	1.38E-01
B1M565C fine	C5168	17.25	2.57E-01	1.61E-01	1.34E+00	9.54E-02
B1M565B	C5168	17.75	1.57E-01	6.04E-02	5.03E-01	9.61E-02
B1M565A	C5168	18.25	1.59E-01	9.10E-02	7.59E-01	6.81E-02

4.2 Vadose Zone Sediment from 241-BX Farm Direct-Push Samples

4.2.1 Moisture Content

The moisture contents of the 8 core liners and 1 grab sample collected from the 241-BX Farm direct-push holes are presented as a function of depth in Table 4.14 and Figure 4.6. Only one of the samples had a high (in excess of 10%) soil moisture content: the C liner collected in probe hole C5134 contained part of a fine-grained lenticular body that was subsampled and treated as a discrete sample. The nomenclature for this sample, described in Section 3.1.2, is B1JWW6C fine; the moisture content was 12.8%. Direct-push hole C5134 was emplaced east of Tank 241-BX-101 and was driven to a total depth of 78.2 ft bgs. The C-liner from this sample string, which contained the fine-grained material, was the shallowest sample collected from this push hole. Additionally, the fine-grained material was located in the top portion of the liner, indicating that the sample string was pushed through the fine-grained lenticular body but at least captured a portion of it in the shallowest sample collected. As seen in Table 4.14, the samples collected deeper in push hole C5134 contained progressively less moisture, indicating that the fine-grained material encountered in the C-liner could be acting as a capillary barrier to vertical migration of moisture.

The sample string collected from push hole C5132 contained sediments with moisture contents ranging from 2 to approximately 8%. Given this large range in moisture contents, it is obvious that a zone or lenticular body of finer-grained material was encountered within this sample string. The two samples collected from push hole C5124 both had moisture contents of approximately 5%.

The moisture contents measured in the 241-BX Farm direct-push samples compare well with those measured from similar lithologies in the background borehole (C3391) that was emplaced southeast of the 241-B Tank Farm (Lindenmeier et al. 2003). Moisture contents measured in borehole C3391 within the H1 unit ranged from approximately 2% to over 12% depending on the amount of gravel, sand, and silt/clay contained in the sample. These numbers correlate well with the range measured in the 241-BX Farm direct-push samples (1.99 to 12.8%) and imply that elevated moisture measured in several of the direct-push samples is controlled by sample lithology as opposed to past leak events.

Table 4.14. Gravimetric Moisture Content of Samples Obtained from 241-BX Direct-Push Probe Holes[(a)]

Sample ID	Probe Hole ID	Mid-Depth (ft bgs)	Moisture (%)
B1JWW6A	C5134	78.0	2.07
B1JWW6B	C5134	77.5	3.22
B1JWW6C fine	C5134	77.0	12.8
B1JWW6C coarse	C5134	77.0	3.82
B1JWW7	C5132	64.8	1.99
B1JWW7A	C5132	64.3	3.14
B1JWW7B	C5132	63.8	7.86
B1JWW7C	C5132	63.3	6.41
B1JWW8A	C5124	44.8	4.94
B1JWW8B	C5124	44.3	4.99
(a) Shaded cells indicate grab samples.			

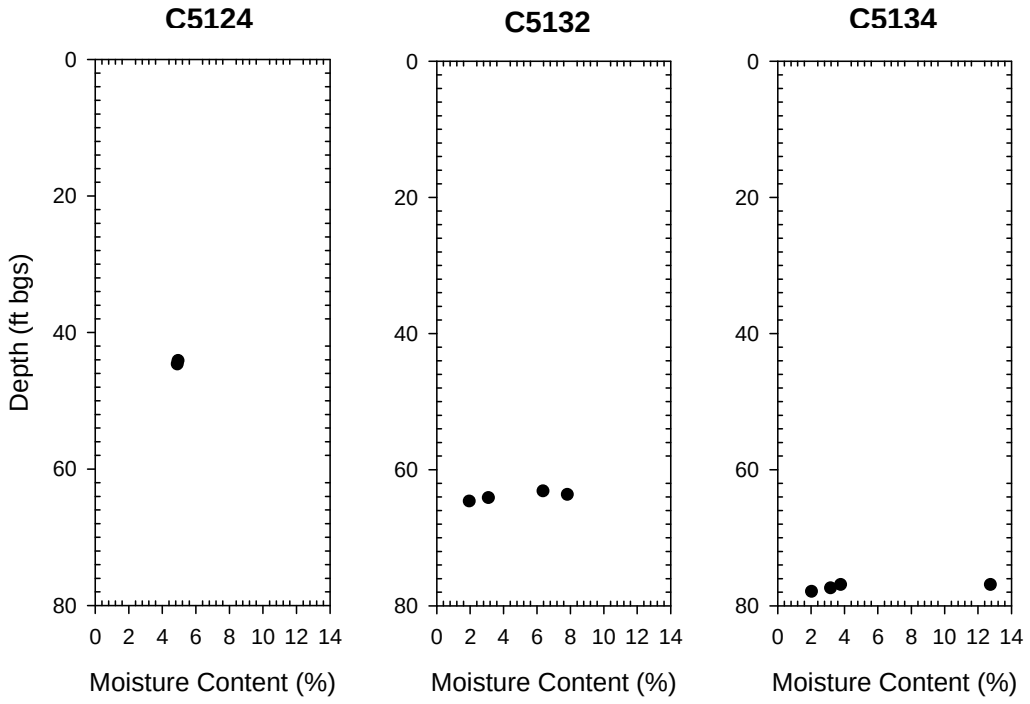

Figure 4.6. Moisture Content Data for the 241-BX Farm Direct-Push Samples

4.2.2 1:1 Sediment:Water Extracts

The samples from the 241-BX Tank Farm direct-push campaign were characterized by performing 1:1 sediment:water extracts. The following subsections present the mass of a given constituent leached per gram of sediment as measured in the water extracts. Other tables show dilution-corrected values that

represent concentrations in vadose zone pore water. As discussed in several other Vadose Zone Characterization Project reports, the dilution-corrected 1:1 sediment:water extracts are a reasonable estimate of the actual vadose zone pore water (see Serne et al. 2002a–f).

4.2.2.1 pH and Electrical Conductivity

The 1:1 sediment:water extract pH and electrical conductivity (EC) data for the BX Farm core and grab samples are shown in Table 4.15 and Figure 4.7. The pH values are tabulated as measured in the 1:1 sediment:water extracts, but EC values are corrected for dilution and tabulated as if it was actual pore water. All of the 1:1 sediment to water extracts were elevated in pH (greater than 8.5). All but one of the samples have sediment:water pH values above 9; the range was from 8.72 in sample B1JWW6B from push hole C5134 to 9.90 in the fine-grained material in sample B1JWW6C (also from push hole C5134). Previous borehole reports have shown that regions of elevated soil pH are considered to be good indicators of the location of the original leak event or very near-field to the initial tank waste entry zone (see Serne et al. 2002a–f). Thus, we can conclude that the elevated pH data indicates the presence of caustic tank-related waste, and the likely source term for the contamination is a leak from Tank BX-101 or -102.

Table 4.15. pH for 1:1 Sediment:Water Extracts and Dilution-Corrected EC Values from 241-BX Farm Core and Grab Samples[(a,b,c)]

Sample ID	Probe Hole ID	Mid-Depth (ft bgs)	pH	Conductivity (mS/cm)
B1JWW6A	C5134	78.0	**9.14**	1.26E+01
B1JWW6B	C5134	77.5	**8.72**	6.23E+00
B1JWW6C fine	C5134	77.0	**9.90**	2.89E+00
B1JWW6C coarse	C5134	77.0	**9.18**	5.18E+00
B1JWW7	C5132	64.8	**9.45**	1.91E+01
B1JWW7A	C5132	64.3	**9.30**	**1.24E+01**
B1JWW7A-DUP	C5132	64.3	**9.52**	**1.09E+01**
B1JWW7B	C5132	63.8	**9.34**	6.93E+00
B1JWW7C	C5132	63.3	**9.37**	8.46E+00
B1JWW8A	C5124	44.8	**9.20**	6.52E+00
B1JWW8B	C5124	44.3	**9.30**	6.52E+00

(a) Bold numbers denote elevated values.
(b) EC values are dilution corrected and represent pore water concentrations not 1:1 extract values.
(c) Shaded cells indicate grab samples.

The pore water-corrected EC data, shown in Figure 4.8, for many of the 241-BX Farm direct-push samples were higher than those measured in the 241-B Farm direct-push water extracts. The 241-BX Farm direct-push samples had calculated pore water conductivities ranging from 2.89 to 19.1 mS/cm, while the background borehole emplaced near the 241-B Tank Farm (Lindenmeier et al. 2003) had pore water-corrected conductivities ranging from 0.883 to 7.81 mS/cm. Therefore, several of the sediments collected as part of the 241-BX Farm direct-push campaign clearly contain elevated concentrations of dissolved salts. The two direct-push holes that contained sediment with elevated pore water conductivities were C5132 and C5134. The peak pore water conductivity, 19.1 mS/cm, was measured in sediment from push hole C5132. Direct-push hole C5132 was the closest sampling location to Tank 241-BX-102;

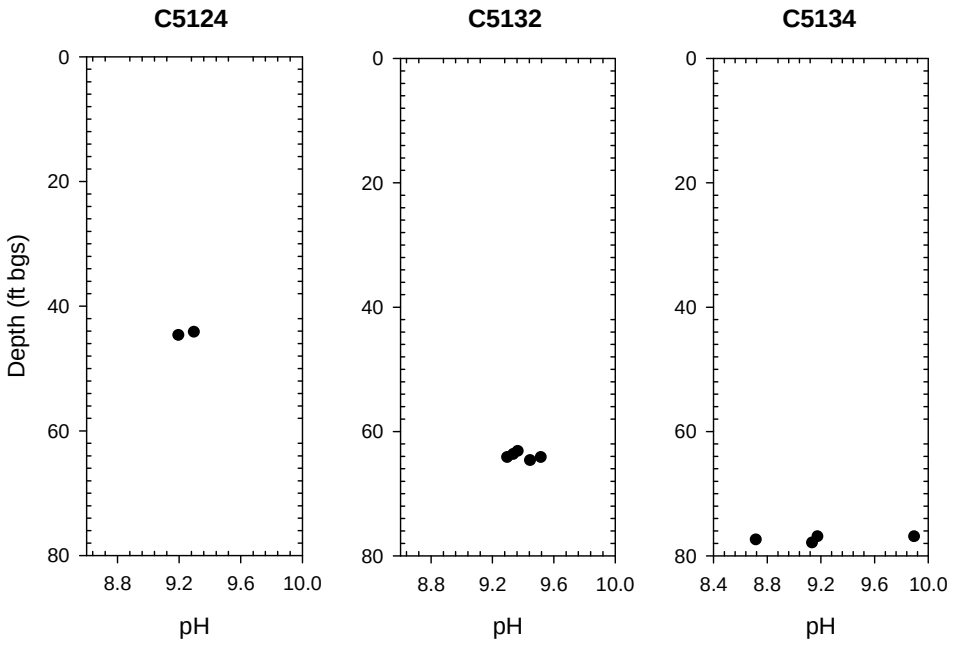

Figure 4.7. 1:1 Sediment:Water Extract pH Data for the 241-BX Farm Direct-Push Samples

thus the elevated EC observed in sediment from this location could be an artifact of a leak from BX-102. These results indicate that the initial impact zone from waste released from BX-102 (and potentially -101) migrated to the southeast of the tank to at least the location and depth intercepted by probe hole C5132. As described in Serne et al. (2002e) and Knepp (2002), most of the 1951 BX-102 overfill fluids have migrated deeper to the northeast of Tank BX-102 perhaps all the way to the water table, based on uranium isotopic signature measurements on vadose zone pore waters and groundwaters (Christensen et al. 2004).

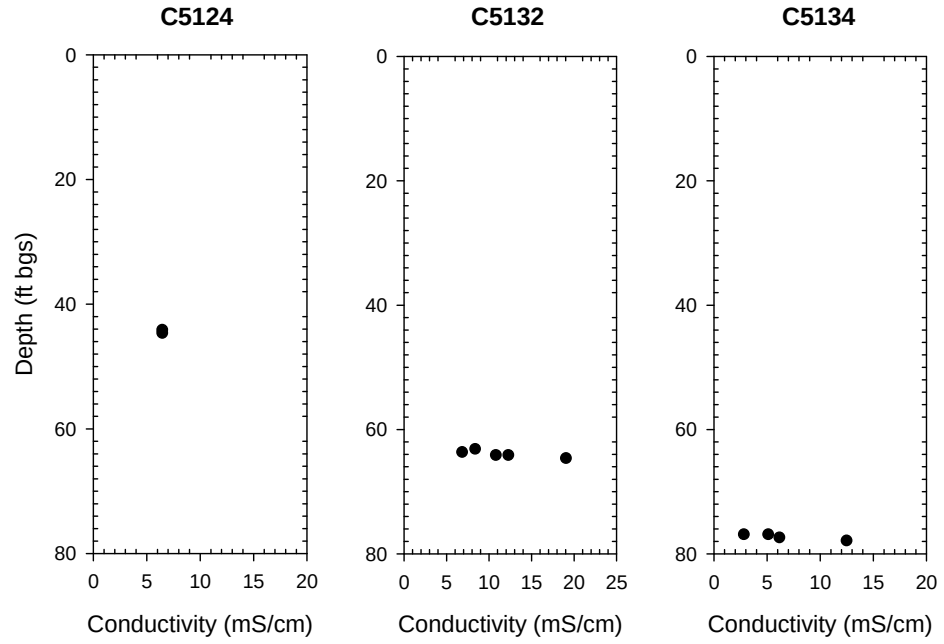

Figure 4.8. 1:1 Sediment:Water Extract Conductivity Data for the 241-BX Farm Direct-Push Samples

4.2.2.2 Composition of 1:1 Sediment:Water Extracts from 241-BX Tank Farm Core and Grab Samples

The concentrations of the major anions, cations, and several trace constituents from the water extract procedure are discussed in this subsection. Anion data are tabulated in Table 4.16 in units of mass per gram of dry sediment. Unfortunately, there was an unidentified chromatographic interference that precluded the quantification of fluoride in all of the direct-push samples collected in the 241-BX Tank Farm. However, the 241-BX-102 leak was not estimated to have contained a measurable amount of fluoride (Knepp 2002). The only anion that was present at elevated concentrations in the 241-BX Farm direct-push samples was phosphate. This finding is consistent with the estimate that the 241-BX-102 leak contained nearly 12,000 kg of phosphate (Jones et al. 2001). Water-extractable phosphate concentrations in the 241-BX direct-push samples ranged from 1.57 to 7.21 μg/g as shown in Figure 4.9. The maximum phosphate concentration measured in the background borehole (C3391) was 0.553 μg/g (Lindenmeier et al. 2003). As well as elevated EC data, sediments retrieved from push hole C5132 contained the highest concentration of water-extractable phosphate. The peak phosphate concentration (7.21 μg/g) was measured in the sample collected from 63.8 ft bgs. The next-deepest sample collected from push hole C5132, while still elevated, contained significantly less water-extractable phosphate (2.14 to 2.57 μg/g at 64.3 ft bgs). Given the limited number of depth-discrete direct-push samples, it is not possible to discuss concentration profiles at this location. However, the elevated phosphate measured in the direct-push samples provide direct evidence that bismuth phosphate-related tank waste has affected the vadose zone at this location.

The 241-BX-102 leak event was reported to have contained in excess of 11,000 kg nitrate (Knepp 2002). Therefore, one might assume that it is surprising that elevated concentrations of nitrate were not

Table 4.16. Water-Extractable Anions in 241-BX Farm Core and Grab Samples (μg/g dry sediment)[(a,b,c,d)]

Sample ID	Probe Hole ID	Mid-Depth (ft bgs)	Fluoride (μg/g)	Chloride (μg/g)	Nitrate (μg/g)	Sulfate (μg/g)	Phosphate (μg/g)
B1JWW6A	C5134	78.0	ND	2.85E-01	1.11E+00	9.09E+00	**3.16E+00**
B1JWW6B	C5134	77.5	ND	3.48E-01	1.74E+00	9.55E+00	**1.63E+00**
B1JWW6C fine	C5134	77.0	ND	1.52E+00	6.64E+00	4.66E+01	<5.15E-01
B1JWW6C coarse	C5134	77.0	ND	4.14E-01	2.05E+00	1.55E+01	<5.21E-01
B1JWW7	C5132	64.8	ND	3.14E-01	8.72E-01	2.02E+00	**1.68E+00**
B1JWW7A	C5132	64.3	ND	3.24E-01	1.14E+00	2.35E+00	**2.57E+00**
B1JWW7A DUP	C5132	64.3	ND	2.82E-01	9.67E-01	2.45E+00	**2.14E+00**
B1JWW7B	C5132	63.8	ND	7.60E-01	3.10E+00	5.30E+00	**7.21E+00**
B1JWW7C	C5132	63.3	ND	7.59E-01	2.33E+00	4.53E+00	**5.46E+00**
B1JWW8A	C5124	44.8	ND	<2.48E-01	2.42E+00	4.08E+00	**1.77E+00**
B1JWW8B	C5124	44.3	ND	4.26E+00	1.85E+00	5.61E+00	**1.57E+00**

(a) Bold values denote concentrations elevated above background.
(b) Less than values indicate the instrument returned a negative value or the reported value is less than the limit of quantification.
(c) ND indicates the analyte was not determined due to chromatographic interference.
(d) Shaded cells indicate grab samples.

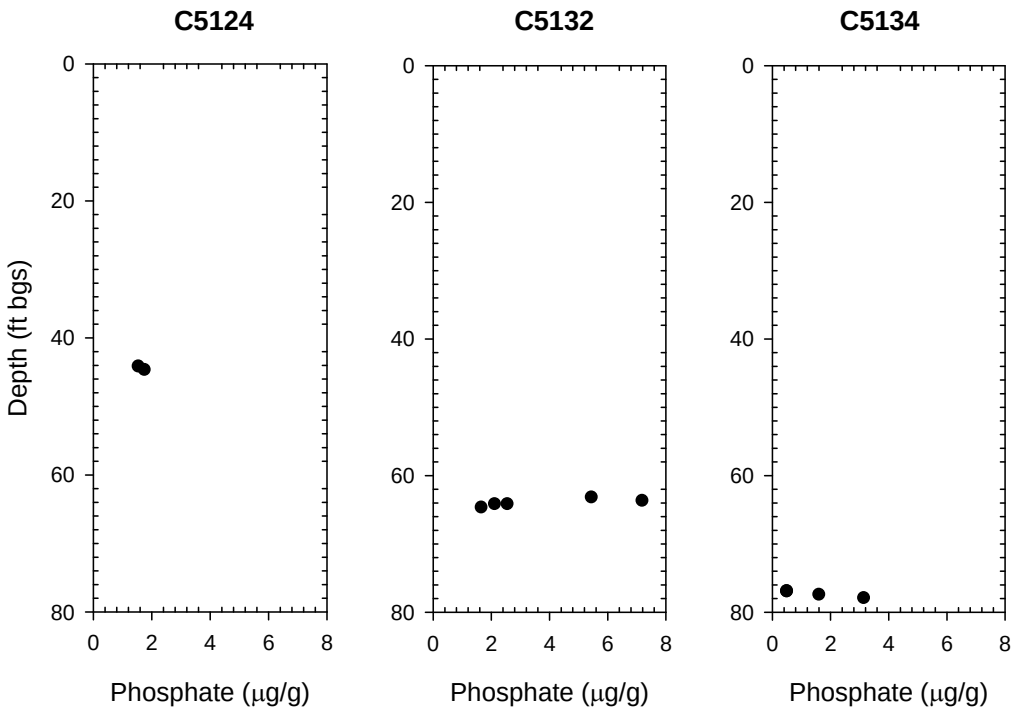

Figure 4.9. 1:1 Sediment:Water Extract Phosphate Data for the 241-BX Farm Direct-Push Samples

observed in any of the direct-push samples analyzed. However, nitrate is a mobile contaminant that has typically been found much deeper (in excess of 120 ft bgs) in the vadose zone at other investigation sites including borehole 299-E33-45 farther northeast of Tank BX-102 (Serne et al. 2002b,e; Brown et al. 2006). Therefore, it appears that the depth sampled via the direct-push technique at these locations was not sufficient to capture the mobile contaminants present in the 241-BX-102 waste stream.

The water-extractable major cations in the 241-BX Tank Farm direct-push sediments are tabulated in Table 4.17 in units of mass per gram of sediment on a dry weight basis; the data for sodium and calcium are shown in Figure 4.10. All of the sediments analyzed contained elevated concentrations of water-extractable sodium. Total water-extractable sodium ranged from a low of 37.7 μg/g in push hole C5134 to a maximum of 149 μg/g in push hole C5132. All of the sediments tested contained sodium as the dominant water-extractable cation; the BX-102 leak event was estimated to have released more than 23,000 kg of sodium to the vadose zone (Rogers and Knepp 2000). In view of these data, it is clear that sodium contained in the BX-102 waste stream leaked into the vadose zone in the vicinity of these push holes and has created an ion exchange front in which sodium has displaced the natural divalent cations from the surface exchange sites in the sediment. Again, because of the lack of depth-discrete samples from the BX direct-push activity, it is not possible to determine the vertical extent of the exchange front; however, it is clear that at least a portion of the waste has migrated to the east/southeast of Tank BX-102.

Table 4.17. Water-Extractable Major Cations in the 241-BX Farm Core and Grab Samples (µg/g dry sediment)[a,b,c,d]

Sample ID	Probe Hole ID	Mid-Depth (ft bgs)	Calcium (µg/g)	Potassium (µg/g)	Magnesium (µg/g)	Strontium (µg/g)	Sodium (µg/g)
B1JWW6A	C5134	78.0	*1.51E+00*	*(1.18E+00)*	7.05E-01	*(1.70E-02)*	**5.89E+01**
B1JWW6B	C5134	77.5	*2.09E+00*	2.12E+00	8.17E-01	*(1.07E-02)*	**4.21E+01**
B1JWW6C fine	C5134	77.0	*1.68E+01*	5.49E+00	*(4.04E-02)*	6.01E-02	**7.26E+01**
B1JWW6C coarse	C5134	77.0	*5.37E+00*	3.10E+00	8.42E-01	*(2.26E-02)*	**3.77E+01**
B1JWW7	C5132	64.8	*4.64E-01*	*(1.13E+00)*	*1.03E-01*	*(2.37E-03)*	**9.80E+01**
B1JWW7A	C5132	64.3	*5.25E-01*	*(1.07E+00)*	*9.12E-02*	*(2.55E-03)*	**1.01E+02**
B1JWW7A DUP	C5132	64.3	*5.17E-01*	*8.75E-01*	*8.18E-02*	*3.13E-03*	**7.96E+01**
B1JWW7B	C5132	63.8	*7.92E-01*	1.43E+00	*6.85E-02*	*(3.49E-03)*	**1.45E+02**
B1JWW7C	C5132	63.3	*4.66E-01*	1.62E+00	*5.47E-02*	*(2.18E-03)*	**1.49E+02**
B1JWW8A	C5124	44.8	*4.40E-01*	1.54E+00	*1.21E-01*	*(2.09E-03)*	**8.11E+01**
B1JWW8B	C5124	44.3	*4.97E-01*	1.55E+00	*9.84E-02*	*(2.74E-03)*	**7.92E+01**

(a) Bold values denote concentrations elevated above background.
(b) Italicized values denote analytically low concentrations.
(c) Parentheses indicate reported value was less than the limit of quantification for the analysis.
(d) Shaded cells indicate grab samples.

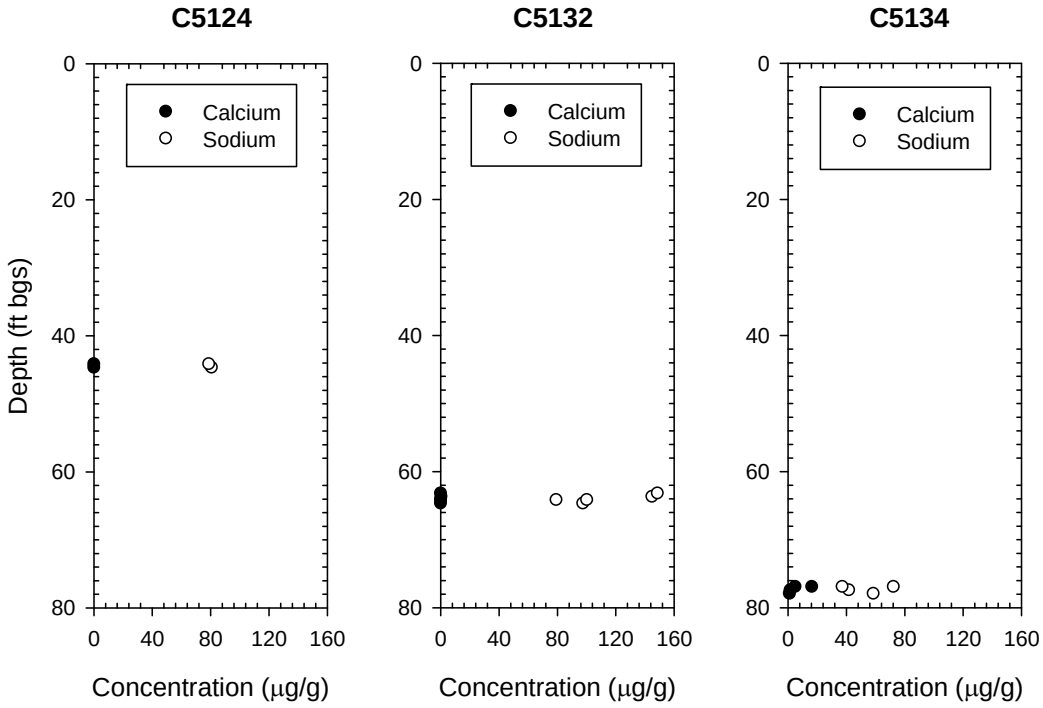

Figure 4.10. 1:1 Sediment:Water Extractable Sodium and Calcium Data from 241-BX Direct-Push Samples

The water-extractable aluminum, iron, sulfur, and phosphorous in the 241-BX farm direct-push sediments are shown in Table 4.18. The sulfur and phosphorous data were converted to water-extractable sulfur as sulfate and phosphorous as phosphate so that the results could be compared to the IC data presented in Table 4.16. Like the samples from the 241-B Tank Farm, the agreement between directly measured sulfate in the water extracts using IC and indirectly by converting the ICP measurements for sulfur to sulfate was poor. Typically, these two analytical methods generate sulfate data with a percent difference of ±10%; however, for the present set of samples, relative percent differences ranged from approximately 18 to 70%. The ICP results, which represent total sulfur in the samples, were always higher than the sulfate data reported via ion chromatography. These data indicate that either there is a non-sulfate source of sulfur in these sediments or one of the data sets is biased. Based on this, only the data acquired via ion chromatographic analysis of the samples should be used to report sulfate concentrations. However, the agreement between directly measured phosphate in the water extracts using IC and indirectly by converting the ICP measurements for phosphorous to phosphate was good. Besides validating the IC data, we can state that the water-extractable phosphorous was in the form of phosphate. Water-soluble aluminum was elevated (above the limit of detection) in most of the 241-BX Farm direct-push sediments. It appears that these elevated concentrations are a result of some chemical reaction, such as dissolution or precipitation, between alkaline tank fluids and native sediments that formed precipitates of amorphous aluminum phases that are more water soluble than aluminum-rich crystalline mineral phases in the pristine sediments.

The water extract data for potentially mobile metals, such as technetium-99, uranium-238, chromium, molybdenum, and ruthenium are shown in Table 4.19. Additionally, the water-extractable uranium-238 is plotted as a function of depth in Figure 4.11. Water-extractable technetium-99 was found in several of the samples from push holes C5124 and C5132. Although only trace amounts of technetium-99 were detected in the sediments (approximately 0.5 pCi/g or less), more than 3 Ci of technetium-99 are estimated to have been lost as part of the 241-BX-102 leak event. Similar to nitrate, the bulk of the

Table 4.18. Water-Extractable Cations in 241-BX Farm Core and Grab Samples (µg/g dry sediment)[(a,b,c)]

Sample ID	Probe Hole ID	Mid-Depth (ft bgs)	Aluminum (µg/g)	Iron (µg/g)	Sulfur as SO_4^{2-} (µg/g)	Phosphorous as PO_4^{3-} (µg/g)
B1JWW6A	C5134	78.0	2.45E-01	1.76E-01	1.16E+01	**3.24E+00**
B1JWW6B	C5134	77.5	(9.84E-02)	7.81E-02	1.29E+01	**1.70E+00**
B1JWW6C fine	C5134	77.0	(5.45E-02)	(3.91E-03)	5.58E+01	(1.89E-01)
B1JWW6C coarse	C5134	77.0	(7.07E-02)	(2.31E-02)	1.95E+01	(4.32E-01)
B1JWW7	C5132	64.8	3.17E-01	2.34E-01	4.19E+00	**1.85E+00**
B1JWW7A	C5132	64.3	3.77E-01	2.07E-01	3.76E+00	**2.67E+00**
B1JWW7A DUP	C5132	64.3	2.74E-01	2.41E-01	3.51E+00	**2.27E+00**
B1JWW7B	C5132	63.8	2.08E-01	1.88E-01	7.38E+00	**7.36E+00**
B1JWW7C	C5132	63.3	2.39E-01	1.00E-01	7.07E+00	**5.91E+00**
B1JWW8A	C5124	44.8	2.47E-01	3.94E-01	5.88E+00	**1.93E+00**
B1JWW8B	C5124	44.3	2.04E-01	2.76E-01	7.96E+00	**1.71E+00**

(a) Bold values denote concentrations elevated above background.
(b) Parentheses indicate reported value was less than the limit of quantification for the analysis.
(c) Shaded cells indicate grab samples.

Table 4.19. Water-Extractable Mobile Metals in the 241-BX Farm Core and Grab Samples (μg/g dry sediment)[a,b,c,d]

Sample ID	Probe Hole ID	Mid-Depth (ft bgs)	^{99}Tc (pCi/g)	^{238}U (μg/g)	^{53}Cr (μg/g)	^{95}Mo (μg/g)	^{101}Ru (μg/g)	^{102}Ru (μg/g)
B1JWW6A	C5134	78.0	(8.31E-02)	**1.85E+00**	3.98E-03	1.64E-02	(4.19E-05)	(2.76E-05)
B1JWW6B	C5134	77.5	(7.63E-02)	**3.59E+00**	3.20E-03	2.14E-02	(8.33E-05)	(3.22E-05)
B1JWW6C fine	C5134	77.0	2.45E-01	**3.80E-02**	7.82E-02	9.70E-02	**2.61E-04**	**1.33E-04**
B1JWW6C coarse	C5134	77.0	(1.40E-01)	**1.77E+00**	7.93E-03	2.80E-02	(1.06E-04)	(4.90E-05)
B1JWW7	C5132	64.8	(8.18E-02)	**2.75E+00**	3.70E-04	1.73E-02	(1.26E-05)	<1.26E-04
B1JWW7A	C5132	64.3	(1.02E-01)	**4.36E+00**	6.14E-04	2.19E-02	(2.58E-06)	(1.03E-06)
B1JWW7A DUP	C5132	64.3	(1.01E-01)	**4.12E+00**	(2.45E-03)	2.18E-02	<5.15E-04	<5.15E-04
B1JWW7B	C5132	63.8	**5.25E-01**	**1.20E+01**	1.02E-03	3.68E-02	(6.81E-05)	(1.55E-05)
B1JWW7C	C5132	63.3	**4.91E-01**	**4.61E+00**	5.46E-04	6.20E-02	(2.28E-05)	(8.61E-06)
B1JWW8A	C5124	44.8	**2.15E-01**	**3.14E-02**	1.54E-02	8.31E-03	(1.41E-04)	(4.83E-05)
B1JWW8B	C5124	44.3	**2.40E-01**	**2.01E-02**	1.06E-02	1.01E-02	(6.40E-05)	(4.25E-05)

(a) Bold values denote concentrations elevated above background.
(b) Parentheses indicate reported value was less than the limit of quantification for the analysis.
(c) Less than values indicate the instrument returned a negative value.
(d) Shaded cells indicate grab samples.

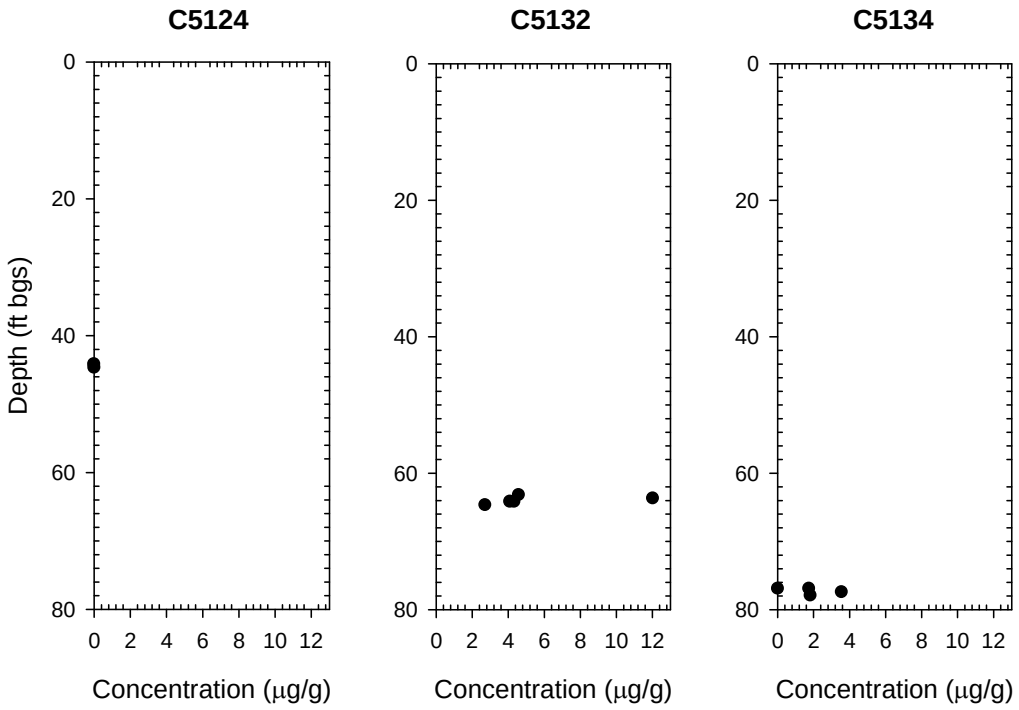

Figure 4.11. 1:1 Sediment:Water Extractable Uranium-238 Data from 241-BX Direct-Push Samples

technetium-99 contamination likely resides much deeper in the vadose zone at these locations. Water-leachable uranium-238 is elevated in all of the BX Tank Farm direct-push samples analyzed. The peak water-extractable uranium-238 concentration measured in the background borehole (C3391) by Lindenmeier et al. (2003) was 1.40E-03 μg/g. Comparing this to the range measured in the 241-BX direct-push samples (2.01E-02 to 1.20E+01 μg/g) confirms the supposition that the 241-BX samples contain Hanford-process uranium. The peak concentration measured in the 241-BX direct-push samples, at 12.0 μg/g, compared well with the peak water-extractable concentration (approximately 22 μg/g) reported by Serne et al. (2002e) for the BX-102 borehole (299-E33-45), which was emplaced deeper and farther north of Tank 241-BX-102 than the direct-push holes.

Measurable concentrations of ruthenium were found in one direct-push sample from push hole C5134 (Table 4.19). The fine-grained material from sample B1JWW6C contained varying concentrations of ruthenium-101 and ruthenium-102. Both of these isotopes of ruthenium are produced as a byproduct of nuclear fission, and their presence in the direct-push samples could potentially be used to constrain contaminant source terms (i.e., determine whether the waste encountered via the direct-push campaign appears to be from a single source, such as Tank BX-102, or multiple sources, such as Tanks BX-101 and BX-102). However, more data are necessary to make a reasonable identification of contaminant source terms (Brown et al. 2007); thus, the source of the contamination can not yet be quantitatively identified.

4.2.3 Vadose Zone Pore Water Chemical Composition

The 1:1 water extract data were processed to derive the pore water composition of the vadose zone sediments so that electrical balances (anions versus cations) of the samples could be evaluated. From

knowledge of the moisture content of the sediment samples taken from the liners of each direct-push sampler and the grab samples, the amount of deionized water that would be needed to make the water extract exactly one part water (total of native pore water and added deionized water) to one part by weight dry sediment was calculated. The ratio of the total volume of water in the extract to the native mass of pore water is the dilution factor. We assumed that the deionized water acted solely as a diluent of the existing pore water and that the deionized water did not dissolve any of the solids in the sediments. Thus, by correcting for dilution, an estimate of the actual chemical composition of the native pore-water in the vadose zone sediments could be derived.

Tables 4.20 and 4.21 show the derived pore water composition of key constituents in meq/L. The highest dissolved salt loads were found in the sediment collected within probe hole C5132, which was the closest sampling push hole to Tank 241-BX-102. The sediment was collected from approximately 64 ft bgs and had high pH and EC values. As a result of the high pH, carbon dioxide was absorbed by the pore water present in the sediment and resulted in the majority of the anionic charge being attributed to alkalinity (215 meq/L). The remainder of the dissolved anionic species in sample B1JWW7 were phosphate (2.66 meq/L), sulfate (2.11 meq/L), nitrate (0.705 meq/L), and chloride (0.443 meq/L), for a total anionic charge of 221 meq/L. The anions in this samples were primarily balanced by sodium (214 meq/L), with trace amounts of calcium (1.16 meq/L) and magnesium (0.426 meq/L). These concentrations are very dilute compared to the peak vadose zone pore water found during the BX-102 borehole campaign (Serne et al 2002e), where the total dissolved salt load was as high as 1,000 meq/L. However, Serne et al. (2002e) found the peak dissolved salt load at approximately 152 ft bgs, which was well beyond the depth presently samples by the direct-push technique.

Table 4.20. Calculated Pore Water Anion Concentrations in 241-BX Farm Core and Grab Samples[(a,b,c)]

Sample ID	Probe Hole ID	Mid-Depth (ft bgs)	Fluoride (meq/L)	Chloride (meq/L)	Nitrate (meq/L)	Sulfate (meq/L)	Phosphate (meq/L)	Alkalinity (meq/L)
B1JWW6A	C5134	78.0	ND	3.87E-01	8.65E-01	9.13E+00	4.82E+00	1.28E+02
B1JWW6B	C5134	77.5	ND	3.05E-01	8.75E-01	6.19E+00	1.60E+00	5.99E+01
B1JWW6C fine	C5134	77.0	ND	3.35E-01	8.38E-01	7.59E+00	<1.27E-01	2.49E+01
B1JWW6C coarse	C5134	77.0	ND	3.05E-01	8.63E-01	8.44E+00	<4.30E-01	5.04E+01
B1JWW7	C5132	64.8	ND	4.43E-01	7.05E-01	2.11E+00	2.66E+00	2.15E+02
B1JWW7A	C5132	64.3	ND	2.91E-01	5.85E-01	1.56E+00	2.58E+00	1.37E+02
B1JWW7A DUP	C5132	64.3	ND	2.53E-01	4.96E-01	1.63E+00	2.14E+00	1.19E+02
B1JWW7B	C5132	63.8	ND	2.72E-01	6.35E-01	1.40E+00	2.90E+00	7.52E+01
B1JWW7C	C5132	63.3	ND	3.34E-01	5.87E-01	1.47E+00	2.69E+00	9.35E+01
B1JWW8A	C5124	44.8	ND	1.41E-01	7.91E-01	1.72E+00	1.13E+00	7.04E+01
B1JWW8B	C5124	44.3	ND	2.41E+00	5.97E-01	2.34E+00	9.92E-01	6.46E+01

(a) Less than values indicate the instrument returned a negative value.
(b) ND indicates the analyte was not determined due to chromatographic interference.
(c) Shaded cells indicate grab samples.

Table 4.21. Calculated Pore Water Cation Concentrations in the 241-BX Tank Farm Direct-Push Core and Grab Samples[a,b]

Sample ID	Probe Hole ID	Mid-Depth (ft bgs)	Calcium (meq/L)	Potassium (meq/L)	Magnesium (meq/L)	Sodium (meq/L)
B1JWW6A	C5134	78.0	3.65E+00	(1.46E-00)	2.80E+00	1.24E+02
B1JWW6B	C5134	77.5	3.25E+00	1.69E+00	2.09E+00	5.70E+01
B1JWW6C fine	C5134	77.0	6.55E+00	1.10E+00	(2.60E-02)	2.47E+01
B1JWW6C coarse	C5134	77.0	7.02E+00	2.08E+00	1.81E+00	4.29E+01
B1JWW7	C5132	64.8	1.16E+00	(1.46E-00)	4.26E-01	2.14E+02
B1JWW7A	C5132	64.3	8.35E-01	(8.70E-01)	2.39E-01	1.39E+02
B1JWW7A DUP	C5132	64.3	8.22E-01	7.14E-01	2.14E-01	1.10E+02
B1JWW7B	C5132	63.8	5.04E-01	4.66E-01	7.17E-02	8.04E+01
B1JWW7C	C5132	63.3	3.64E-01	6.50E-01	7.02E-02	1.01E+02
B1JWW8A	C5124	44.8	4.45E-01	7.98E-01	2.02E-01	7.14E+01
B1JWW8B	C5124	44.3	4.98E-01	7.97E-01	1.62E-01	6.90E+01

(a) Parentheses indicate reported value was less than the limit of quantification for the analysis.
(b) Shaded cells indicate grab samples.

Alkalinity, or bicarbonate/carbonate, was the dominant dissolved anionic constituent in all of the 241-BX Farm direct-push samples (Figure 4.12). The total anion charge attributed to alkalinity in the 241-BX Farm samples ranged from 24.9 to 215 meq/L. In all cases, the alkalinity was primarily balanced by sodium, which had a total charge ranging from 24.7 to 214 meq/L. The presence of sodium as the dominant exchangeable cation is an indicator of the presence of tank waste in the sediments, as discussed above. The source appears to be a moderately concentrated sodium-bearing waste solution that has

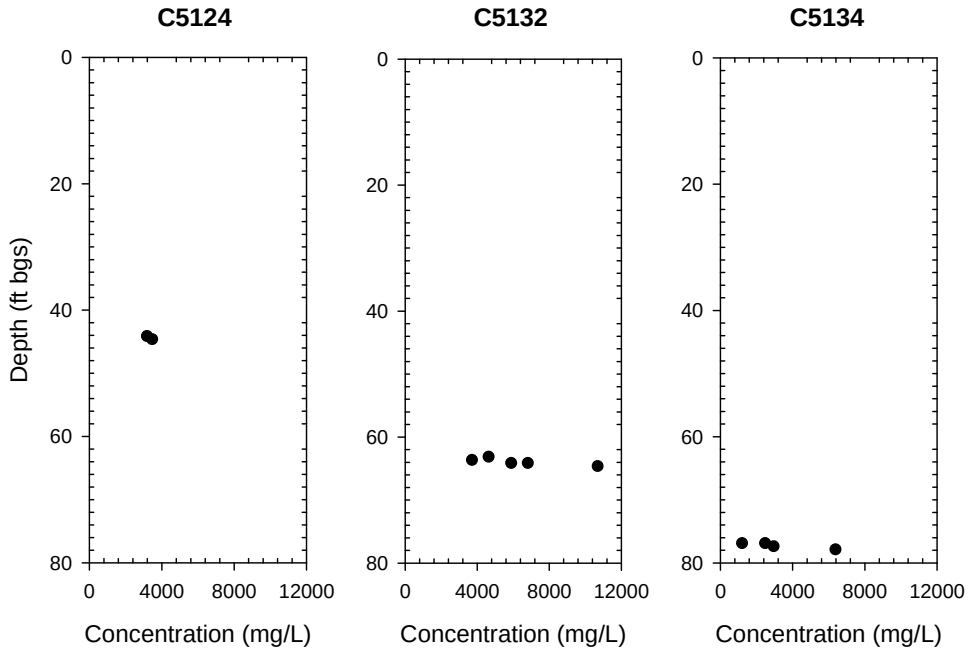

Figure 4.12. Pore Water-Corrected 1:1 Sediment:Water Extractable Alkalinity Data from 241-BX Farm Direct-Push Samples

displaced the natural divalent cations from the exchange sites in the sediments. The total vertical extent of the ion exchange front is unknown due to the lack of sediment samples from deeper in the vadose zone. As mentioned previously, the elevated alkalinity in these samples was correlated with elevated pH.

Overall, the calculated charge balance between cations and anions for all of the samples was quite good; there was less than 10% difference between total dissolved cations and anions for all of the samples analyzed except B1JWW6C coarse, which had a difference of 11.2%. Therefore, it appears that analysis of the 1:1 sediment:water extracts for major cations via ICP-OES and anions via IC resulted in quantification of all the major dissolved constituents in the samples. Note also that the anion content of the solution is dominated by carbonate (in the form of the bicarbonate anion). This is different from many other bore hole samples in which the pore-water solution compositions are dominated by the nitrate anion.

The pore water-corrected concentrations of mobile metals are presented in Table 4.22 in units of pCi/L (for technetium-99) or μg/L (for all other constituents). Pore water-corrected technetium-99 activities ranging from 1,920 to 7,670 pCi/L were measured in several of the samples. In fact, at least one sample retrieved from each push hole contained a measurable activity of technetium-99 in the pore water. The peak pore water activity of technetium-99 (7,670 pCi/L) was measured in sample B1JWW7C, which was collected from approximately 63 ft bgs in push hole C5132. However, given that the peak pore water technetium-99 activity in the 241-BX-102 borehole was approximately 350,000 pCi/L at 160 ft bgs (Serne et al. 2002e), it is appropriate to assume that the majority of the technetium-99 contamination present in this area resides much deeper in the vadose zone.

Elevated pore water-corrected uranium-238 was observed in all of the 241-BX direct-push samples. Pore water concentrations of uranium-238 ranged from 297 μg/L in the fine-grained material from liner B1JWW6C to 153,000 μg/L in sample B1JWW7B. Except for the fine-grained material from liner B1JWW6C, the two samples analyzed from probe hole C5124 were the only ones that contained less than

Table 4.22. Calculated Pore Water Mobile Metal Concentrations of Key Contaminants of Concern in the 241-BX Tank Farm Direct-Push Core and Grab Samples[(a,b,c)]

Sample ID	Probe Hole ID	Mid-Depth (ft bgs)	^{99}Tc (pCi/L)	^{238}U (μg/L)	^{53}Cr (μg/L)	^{95}Mo (μg/L)
B1JWW6A	C5134	78.0	(4.01E+03)	**8.93E+04**	1.92E+02	7.92E+02
B1JWW6B	C5134	77.5	(2.37E+03)	**1.12E+05**	9.95E+01	6.66E+02
B1JWW6C fine	C5134	77.0	**1.92E+03**	**2.97E+02**	6.12E+02	7.59E+02
B1JWW6C coarse	C5134	77.0	(3.66E+03)	**4.63E+04**	2.07E+02	7.32E+02
B1JWW7	C5132	64.8	(4.10E+03)	**1.38E+05**	1.86E+01	8.66E+02
B1JWW7A	C5132	64.3	(3.23E+03)	**1.39E+05**	1.95E+01	6.95E+02
B1JWW7A DUP	C5132	64.3	(3.22E+03)	**1.31E+05**	(7.81E+01)	6.92E+02
B1JWW7B	C5132	63.8	**6.67E+03**	**1.53E+05**	1.30E+01	4.69E+02
B1JWW7C	C5132	63.3	**7.67E+03**	**7.20E+04**	8.52E+00	9.67E+02
B1JWW8A	C5124	44.8	**4.36E+03**	**6.36E+02**	3.12E+02	1.68E+02
B1JWW8B	C5124	44.3	**4.80E+03**	**4.03E+02**	2.13E+02	2.03E+02

(a) Bold values denote elevated concentrations.
(b) Parentheses indicate reported value was less than the limit of quantification for the analysis.
(c) Shaded cells indicate grab samples.

10,000 μg/L uranium-238; sample B1JWW8A contained 636 μg/L uranium-238, and sample B1JWW8B contained 403 μg/L uranium-238. Coincidentally, these samples, which were collected at approximately 45 ft bgs, were the shallowest sediments collected as part of the 241-BX Farm direct-push campaign. Thus the lower pore water-calculated uranium-238 concentrations in these samples are likely a result of their location in the vadose zone (i.e., uranium is considered to be relatively mobile and has likely penetrated deeper into the vadose zone at this location). In support of this hypothesis, Serne et al. (2002e) observed a peak pore water uranium-238 concentration in excess of 500,000 μg/L approximately 133 ft bgs in the 241-BX-102 borehole (299-E33-45). Although the pore water-corrected uranium-238 concentrations significantly exceeded the maximum contamination limit of 30 μg/L, these values represent pore water concentrations and would be diluted significantly should the solutions make it to the water table.

4.2.4 8 M Nitric Acid-Extractable Amounts of Selected Elements in the 241-BX Tank Farm Direct-Push Sediments

The same cores and grab samples that were characterized for water-leachable constituents were also characterized to determine the concentrations of constituents that could be extracted with hot 8 M nitric acid. A comparison of acid extractable with water extractable quantities is an indication of the relative mobility of a constituent and can aid in differentiating anthropogenic from naturally occurring constituents. The acid-extractable concentrations are shown in Tables 4.23 through 4.25. For most of the constituents, there were no significantly elevated acid-extractable concentrations from the 241-BX Tank Farm direct-push sediments except for uranium-238 and possibly sodium. Acid-extractable uranium-238 was elevated in all of the samples except those from direct-push hole C5124. The elevated uranium-238 concentrations ranged from 44.3 μg/g in push hole C5132 to 555 μg/g in push hole C5134. Because Hanford formation sediment contains only 3 to 5 μg/g natural uranium, it is obvious that the samples contain contaminant uranium. As mentioned in subsection 4.2.2.2, the sediments from push holes C5132

Table 4.23. Acid-Extractable Cations in the 241-BX Tank Farm Direct-Push Core and Grab Samples (μg/g dry sediment)[(a,b,c)]

Sample ID	Probe Hole ID	Mid-Depth (ft bgs)	Calcium (μg/g)	Potassium (μg/g)	Magnesium (μg/g)	Sodium (μg/g)	Strontium (μg/g)
B1JWW6A	C5134	78.0	9.92E+03	1.18E+03	5.40E+03	4.86E+02	3.51E+01
B1JWW6B	C5134	77.5	9.06E+03	1.17E+03	5.29E+03	4.60E+02	3.46E+01
B1JWW6C fine	C5134	77.0	1.18E+04	2.12E+03	6.30E+03	4.08E+02	4.51E+01
B1JWW6C coarse	C5134	77.0	8.92E+03	1.12E+03	5.48E+03	3.32E+02	2.97E+01
B1JWW7	C5132	64.8	8.49E+03	1.14E+03	4.81E+03	8.04E+02	3.28E+01
B1JWW7A	C5132	64.3	8.51E+03	1.10E+03	4.86E+03	8.85E+02	3.21E+01
B1JWW7A DUP	C5132	64.3	7.64E+03	8.98E+02	4.74E+03	6.33E+02	2.65E+01
B1JWW7B	C5132	63.8	9.69E+03	1.60E+03	5.43E+03	**1.09E+03**	3.95E+01
B1JWW7C	C5132	63.3	9.87E+03	1.73E+03	5.67E+03	**1.26E+03**	3.84E+01
B1JWW8A	C5124	44.8	9.07E+03	1.20E+03	4.66E+03	7.68E+02	3.36E+01
B1JWW8B	C5124	44.3	7.49E+03	1.06E+03	4.27E+03	6.64E+02	3.20E+01

(a) Bold values denote concentrations elevated above background.
(b) Shaded cells indicate grab samples.
(c) Sodium values are qualitative; results have been corrected for sodium contamination measured in preparation blanks.

Table 4.24. Acid-Leachable Cations in the 241-BX Farm Core and Grab Samples (µg/g dry sediment)[(a)]

Sample ID	Probe Hole ID	Mid-Depth (ft bgs)	Aluminum (µg/g)	Iron (µg/g)	Phosphorus (µg/g)	Chromium (µg/g)
B1JWW6A	C5134	78.0	7.61E+03	1.70E+04	5.43E+02	2.12E+01
B1JWW6B	C5134	77.5	7.69E+03	1.85E+04	7.39E+02	1.91E+01
B1JWW6C fine	C5134	77.0	1.05E+04	1.87E+04	1.10E+03	3.80E+01
B1JWW6C coarse	C5134	77.0	7.17E+03	1.75E+04	7.08E+02	2.90E+01
B1JWW7	C5132	64.8	7.20E+03	1.72E+04	5.47E+02	1.17E+01
B1JWW7A	C5132	64.3	7.21E+03	1.79E+04	6.39E+02	2.26E+01
B1JWW7A DUP	C5132	64.3	5.83E+03	1.60E+04	6.48E+02	1.63E+01
B1JWW7B	C5132	63.8	9.07E+03	1.75E+04	5.75E+02	1.98E+01
B1JWW7C	C5132	63.3	9.78E+03	1.84E+04	5.58E+02	2.53E+01
B1JWW8A	C5124	44.8	7.58E+03	1.69E+04	5.72E+02	1.54E+01
B1JWW8B	C5124	44.3	6.69E+03	1.64E+04	5.60E+02	1.25E+01

(a) Shaded cells indicate grab samples.

Table 4.25. Acid-Leachable Mobile Metals in the 241-BX Farm Core and Grab Samples[(a,b,c,d)]

Sample ID	Probe Hole ID	Mid-Depth (ft bgs)	^{99}Tc (pCi/g)	^{238}U (µg/g)	^{95}Mo (µg/g)	^{101}Ru (µg/g)	^{102}Ru (µg/g)
B1JWW6A	C5134	78.0	(5.89E+00)	**5.55E+02**	4.93E-01	(1.69E-03)	(7.60E-03)
B1JWW6B	C5134	77.5	(5.28E+00)	**1.26E+02**	4.83E-01	(3.58E-03)	(6.43E-03)
B1JWW6C fine	C5134	77.0	(4.68E+00)	**2.75E+02**	1.06E+00	6.48E-02	3.48E-02
B1JWW6C coarse	C5134	77.0	(5.50E+00)	**5.87E+01**	6.79E-01	(7.89E-03)	(7.40E-03)
B1JWW7	C5132	64.8	(4.38E+00)	**2.06E+02**	3.51E-01	<2.58E-02	(6.16E-03)
B1JWW7A	C5132	64.3	(2.45E+00)	**1.31E+02**	4.59E-01	<2.40E-02	(3.37E-03)
B1JWW7A DUP	C5132	64.3	(9.83E+00)	**1.88E+02**	(3.51E-01)	<1.16E+01	(1.32E-02)
B1JWW7B	C5132	63.8	(4.87E+00)	**2.03E+02**	3.36E-01	(2.01E-03)	(7.41E-03)
B1JWW7C	C5132	63.3	(1.64E+01)	**4.43E+01**	7.38E-01	<2.84E-02	(5.34E-03)
B1JWW8A	C5124	44.8	(1.36E+01)	1.81E-01	2.69E-01	(5.22E-03)	(9.07E-03)
B1JWW8B	C5124	44.3	(7.24E+00)	1.35E-01	2.20E-01	(7.47E-04)	(4.11E-03)

(a) Bold values denote concentrations elevated above background.
(b) Parentheses indicate reported value is less than the limit of quantification for the analysis.
(c) Less than symbol indicates the instrument returned a negative value.
(d) Shaded cells indicate grab samples.

and C5134 contained elevated concentrations of water-extractable uranium-238. Some samples contained more than three orders of magnitude more acid-leachable than water-extractable uranium-238 (see Figure 4.13 for acid-leachable uranium-238 concentrations in the BX direct-push sediments).

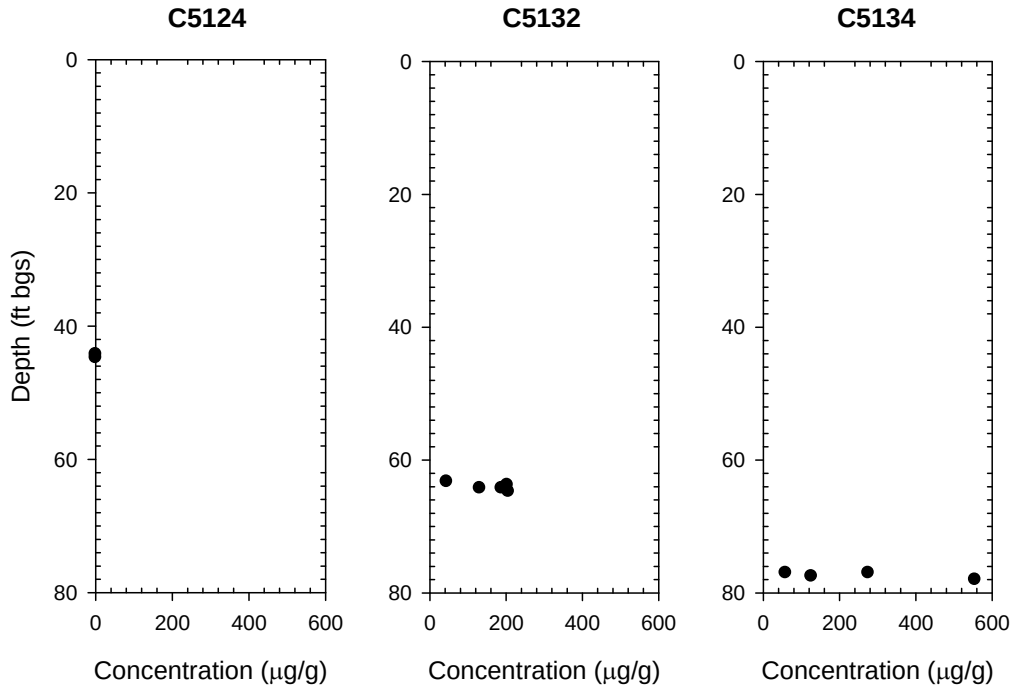

Figure 4.13. Acid-Extractable Uranium-238 Data from the 241-BX Farm Direct-Push Samples

The average acid-leachable sodium content determined in all background borehole (C3391) samples analyzed by Lindenmeier et al. (2003) was 340 μg/g. Comparatively, several of the 241-BX Farm direct-push samples contained in excess of 600 μg/g acid-leachable sodium; therefore, there are indications that a signature associated with tank waste contaminant sodium can be discerned in the acid-leach samples. However, the sodium data reported in Table 4.23 are considered qualitative because they were generated via blank subtraction. The preparation blanks prepared at the time of sediment extraction contained elevated sodium concentrations due to leaching of sodium from the beakers used to process the samples. This background sodium was subtracted from the sample data, and the results were reported as qualitative rather than quantitative. Although the sodium data in Table 4.23 are considered qualitative, a sufficient concentration difference exists between the C3391 sodium data and the 241-BX direct-push data to ascertain that the 241-BX Farm direct-push acid-leach samples contain elevated concentrations of sodium.

Comparison of the water to acid-extractable quantities of each constituent was performed by taking the data in Tables 4.17 through 4.19 and dividing them by the data in Tables 4.23 through 4.25. The data are not presented in this report, but they show that less than 0.1% of the acid-extractable quantities of the following elements were water leachable: aluminum, barium, iron, magnesium, manganese, and titanium. Less than 1% of the acid-extractable quantities of the following elements were water leachable: calcium, chromium, cobalt, nickel, phosphorous as phosphate, potassium, strontium, zinc, and zirconium. Less than 5% of the acid-extractable copper and lead were water extractable. Less than 10% of the acid-extractable molybdenum was water extractable. Last, less than 20% of the acid-extractable sodium and uranium were water extractable. These results are evidence that some of the sediments collected as part of the 241-BX Farm direct-push campaign contain sodium and uranium contamination resulting from Hanford waste processes.

4.2.5 Radionuclide Content in Vadose Zone Sediment from the 241-BX Tank Farm Direct-Push Holes

Data from the GEA of the 241-BX direct-push samples are shown in Table 4.26. The direct measurement of sediment samples for gamma-emitting radionuclides showed that the sediments contained natural potassium-40, the activation product cobalt-60, and the fission product isotopes cesium-137, europium-154, and europium-155. Two of the three sampling push holes emplaced within the 241-BX Tank Farm contained anthropogenic gamma emitting radionuclides. Specifically, both sediment samples retrieved from push hole C5124 contained quantifiable activities of cobalt-60, europium-154, and europium-155. Conversely, the only 241-BX direct-push sample that contained a quantifiable activity of cesium-137 was collected within push hole C5134. For comparison purposes, cobalt-60, cesium-137, europium-154, and europium-155 were not detected by Serne et al. (2002e) in the sediments analyzed from the BX-102 borehole (299-E33-45), which is farther north of BX direct-push holes.

Table 4.26. Gamma Emitting Radionuclides in the 241-BX Tank Farm Direct-Push Sediments[a,b,c,d]

Sample ID	Probe Hole ID	Mid-Depth (ft bgs)	^{40}K (pCi/g)	^{60}Co (pCi/g)	^{137}Cs (pCi/g)	^{154}Eu (pCi/g)	^{155}Eu (pCi/g)	^{238}U[c] (pCi/g)
B1JWW6A	C5134	78.0	2.00E+01	<3.39E-01	<4.13E-01	<9.71E-01	<3.31E+00	2.98E+02
B1JWW6B	C5134	77.5	1.62E+01	<1.76E-01	<2.37E-01	<5.35E-01	<1.08E+00	6.62E+01
B1JWW6C fine	C5134	77.0	2.42E+01	<3.60E-01	**8.11E-01**	<1.03E+00	<2.07E+00	2.37E+02
B1JWW6C coarse	C5134	77.0	1.97E+01	<3.94E-01	<5.04E-01	<9.91E-01	<1.93E+00	<7.66E+01
B1JWW7	C5132	64.8	1.59E+01	<2.00E-01	<2.81E-01	<7.02E-01	<1.96E+00	<5.67E+01
B1JWW7A	C5132	64.3	<4.74E+00	<1.51E-01	<1.87E-01	<5.19E-01	<1.06E+00	<4.69E+01
B1JWW7B	C5132	63.8	1.91E+01	<2.49E-01	<3.29E-01	<7.89E-01	<2.26E+00	1.48E+02
B1JWW7C	C5132	63.3	<5.51E+00	<1.76E-01	<2.19E-01	<5.08E-01	<8.96E-01	<3.75E+01
B1JWW8A	C5124	44.8	1.69E+01	**1.37E+00**	<4.00E-01	**3.73E+00**	**1.72E+00**	<8.95E+01
B1JWW8B	C5124	44.3	1.97E+01	**1.59E+00**	<4.26E-01	**2.18E+00**	**1.27E+00**	<9.94E+01

(a) Shaded cells indicate grab samples.
(b) < indicates the analyte was not detected at the minimum detectable activity reported for the sample.
(c) Uranium-238 was measured as the daughter product ^{234m}Pa at 1001 kev.
(d) Bold values denote concentrations elevated above background.

4.2.6 Total Carbon, Calcium Carbonate, and Organic Carbon Content of Vadose Zone Sediment from the 241-BX Tank Farm Direct-Push Holes

Data from the total carbon, inorganic carbon, and organic carbon (calculated by difference) contents of the 241-BX Tank Farm direct-push sediments are shown in Table 4.27. Inorganic carbon was converted to the equivalent calcium carbonate content. In general, the sediments were low in organic carbon (<0.1% by weight) which is typical of Hanford sediments. Inorganic carbon, as $CaCO_3$, was also present at concentrations that are typical for Hanford formation sediments (1 to 3 wt% as $CaCO_3$) and compare well with other samples collected with the 241-BX Tank Farm (Serne et al. 2002e).

4.3 Tier II Sample Investigations

4.3.1 Background

Tier I characterization data demonstrated that sediment samples from the direct-push BX Tank Farm were contaminated by waste effluent. The evidence for contamination includes relatively high pH (8 to 9) values and salinities as well as elevated sodium concentrations in the pore water solution determined from 1:1 water extractions. These same tests coupled with acid extract results also revealed relatively high extractable uranium concentrations in sediments, which are reflected in high uranium desorption K_d (>1 mL/g) values in several sediment samples. Because the apparent high desorption K_d values were unexpected, and since the Tier I characterization tasks were not aimed at elucidating a detailed understanding of partitioning of uranium between soil and aqueous solution, we conducted additional tests in an attempt to overcome this deficiency. The additional Tier II tests include segregating the various size fractions of soil particles to better understand which size fractions sequester uranium. In many cases, radionuclide elements, such as uranium, will be sequestered in soil particles of a specific size fraction and correlated with the mineralogy of the size fraction (Whicker et al. 2007). In addition, several tests were done on bulk specimens to characterize the mobility of uranium and narrow the list of possible phases that might harbor uranium. Further tests attempted to pinpoint the site of uranium sequestration by performing a micro-examination of select spots in the samples. These tests were carried out using the latest technology such as time resolved laser induced fluorescence (TRLIF), which takes advantage of the fluorescence spectra of uranyl [U(VI)] minerals. In addition, we performed a detailed assay for ^{90}Sr in the sediments and the results revealed high concentrations of this isotope of strontium. Previous gross alpha- beta-counting detected the presence of beta-emitting radionuclide elements, but were incapable of distinguishing which isotope was present. Confirmation of the presence of strontium-90 and uranium in the sediments validates that tank wastes contaminated these samples. These methods and the resulting data are described in Section 4.3.2.

Table 4.27. Carbon Content of the 241-BX Farm Vadose Zone Samples(a)

Sample ID	Probe Hole ID	Mid-Depth (ft bgs)	Total Carbon (%)	Inorganic Carbon (%)	Inorganic Carbon as $CaCO_3$ (%)	Organic Carbon (%)
B1JWW6A	C5134	78.0	0.27	0.23	1.96	0.03
B1JWW6B	C5134	77.5	0.35	0.31	2.61	0.03
B1JWW6C fine	C5134	77.0	0.34	0.32	2.63	0.02
B1JWW6C coarse	C5134	77.0	0.30	0.29	2.45	0.00
B1JWW7	C5132	64.8	0.23	0.21	1.79	0.02
B1JWW7A	C5132	64.3	0.21	0.20	1.64	0.01
B1JWW7B	C5132	63.8	0.25	0.25	2.04	0.00
B1JWW7C	C5132	63.3	0.28	0.28	2.31	0.00
B1JWW8A	C5124	44.8	0.23	0.21	1.76	0.02
B1JWW8B	C5124	44.3	0.22	0.17	1.40	0.05

(a) Shaded cells indicate grab samples.

4.3.2 Results and Discussion

4.3.2.1 Particle-Size Distribution

Particle-size distribution data for two BX-direct-push sediments (B1JWW6C fine and B1JWW6C coarse) are shown in Table 4.28. As described in the previous Tier I characterization results (see Section 4.2), the B1JWW6C fine sample is very fine sand- and clay/silt-dominated sediment with a negligible amount of gravel size fraction (<0.4 wt% for particles larger than 2 mm). Notably, the three finest size fractions (fine sand, very fine sand, and silt and clay) make up nearly 90% of the material in the B1JWW6C fine sample. In contrast, coarse sand and very coarse sand size fractions dominate the B1JWW6C coarse sediment. This distribution of particle sizes in sample B1JWW6C coarse, mainly sand-size with only a minor silt/clay fraction, is typical for the sand-dominated Hanford formation.

Table 4.28. Summary of Particle Size Distributions for Bulk BX Direct-Push Samples

Size Fractions	B1JWW6C Fine (wt%)	B1JWW6C Coarse (wt%)
Gravel (>2.0 mm)	0.38	5.45
Very coarse sand (1.0 mm < size < 2.0 mm)	4.27	40.8
Coarse sand (0.5 mm < size < 1.0 mm)	5.23	29.9
Medium sand (0.25 mm < size < 0.5 mm)	0.90	6.24
Find sand (0.125 mm < size < 0.25 mm)	20.7	9.29
Very fine sand (0.0625 mm< size <0.125 mm)	36.1	4.61
Silt and clay (<0.0625 mm)	32.4	3.70

4.3.2.2 Total U(VI) Concentration by Microwave Digestion

Total uranium, most of which is in the oxidized U(VI) form in Hanford sediments, was determined by the microwave-assisted digestion method. The uranium concentration of bulk sediment of sample B1JWW6C fine was compared with the bulk and various size fractions of sample B1JWW6C coarse. The concentrations of uranium in the bulk samples (fine- and coarse-grained) are 390 and 108 μg/g, respectively. These data indicate that there is a connection between sediment particle size and the amount of uranium present in a sample. This supposition is bolstered by the results for uranium concentrations in the various size fractions split off from bulk B1JWW6C coarse (Table 4.29). Values of total U(VI)

Table 4.29. Total U(VI) Concentration from Microwave Digestion

Size Fractions	B1JWW6C Fine U(μg/g)	B1JWW6C Coarse U(μg/g)
Bulk	390	108
Gravel (> 2.0 mm)		61.3
Very coarse sand (1.0 mm < size < 2.0 mm)		56.9
Coarse sand (0.5 mm < size < 1.0 mm)		49.0
Medium sand (0.25 mm < size < 0.5 mm)		97.3
Find sand (0.125 mm < size < 0.25 mm)		178
Very fine sand (0.0625 mm< size <0.125 mm)		259
Silt and clay (<0.0625 mm)		352

concentrations ranged from 49 to 352 µg/g depending on the size fraction. In general, total U(VI) concentrations increased as the particle size fraction decreased. As Table 4.29 reveals, the highest U(VI) concentration was found in the silt/clay size fraction in the B1JWW6C coarse sediment, although it is not clear from these data alone why this is the case. A detailed reckoning of minerals in each size fraction might lend some important evidence, but this analysis has not yet been performed.

4.3.2.3 X-Ray Diffraction

The mineralogy of two bulk sediment samples (B1JWW6C fine and B1JWW6C coarse) were characterized by XRD. The results indicate that the two sediments had a similar mineralogy. A typical example of an XRD trace of the B1JWW6C fine bulk sample is provided in Figure 4.14 along with the mineral powder diffraction files for comparison. The top figure displays the XRD trace from ~2° to 34° 2θ and the bottom figure exhibits the trace from ~33° to 65° 2θ. The sample was made up primarily of quartz and feldspar, with minor amounts of hornblende and phyllosilicates (chlorite and muscovite). The broad reflection present at 5.9° 2θ is considered to be a combination of smectite clays and chlorite. These mineral compositions are similar to those found in other Hanford formation sediments from the 200-W Area (Um et al. 2007).

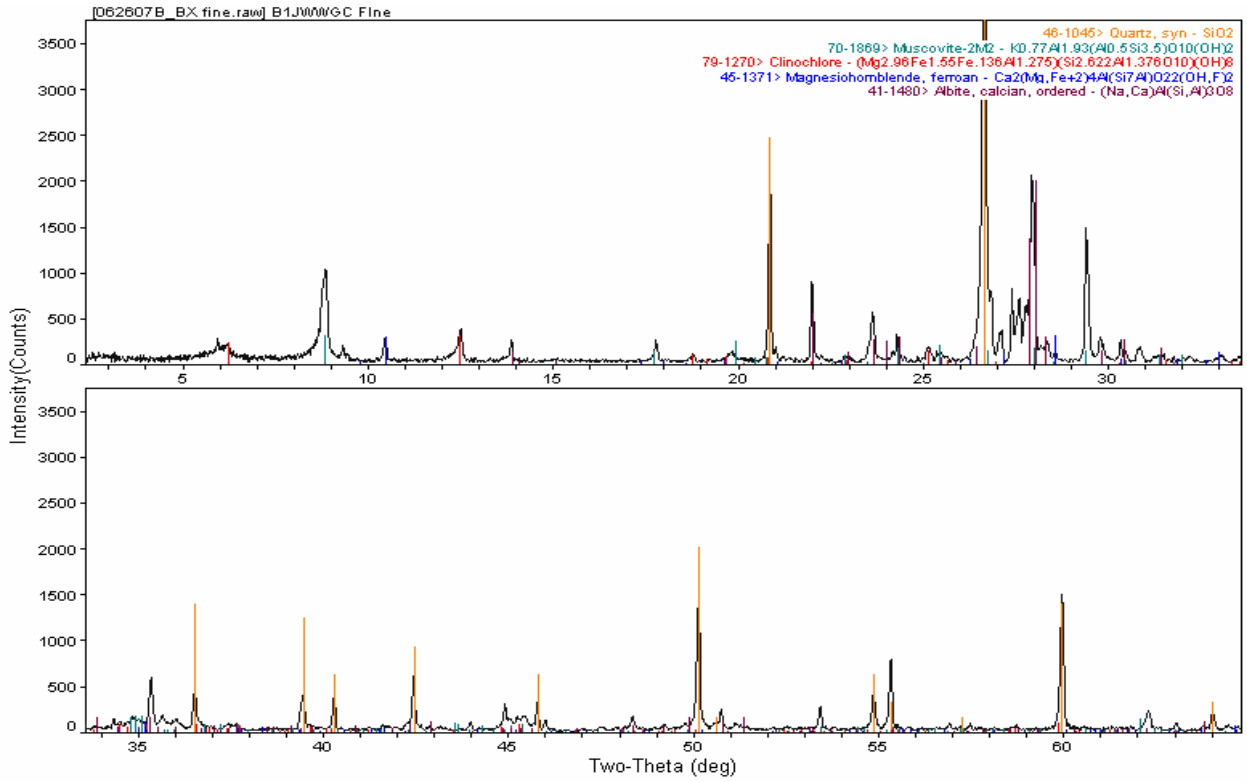

Figure 4.14. Typical XRD Pattern of B1JWW6C Fine Sediment. The top figure displays the XRD trace from ~2° to 34° 2θ, and the bottom figure exhibits the trace from ~33° to 65° 2θ. The analysis shows that the sediment is mainly composed of quartz and feldspar with minor amounts of chlorite, muscovite, and amphibole.

4.3.2.4 (Bi)carbonate Leaching for Labile U(VI)

The concentration of U(VI) leached from the BX direct-push sediments by sodium bicarbonate-carbonate solution (pH ~9.1) reached a steady state after 6 to 7 days reaction. The lack of change in concentration of U(VI) in the fine-grained sample was not significant after the first 7 days, as shown on the left side of Figure 4.15. There was a relatively rapid increase of U(VI) released in the first 5 days for B1JWW6C fine sediment over the B1JWW6C coarse sample, indicating steady-state release occurred earlier in the coarse sediment. A possible explanation is that the coarser-grained sediment contained larger pore spaces, which would facilitate ingress of the bicarbonate-carbonate solution to sites that harbored uranium. In contrast, the fine-grained specimen contains much smaller pore sizes, so transport of dissolved uranium from the sediment into bulk solution may be diffusion limited. Because calcium carbonate (solid) is present in both sediments (2.2 and 2.0 wt% as $CaCO_3$ for fine and coarse, respectively), U(VI) might also be present as a co-precipitate with calcite. However, we think that this is unlikely for two reasons. First, the amount of U(VI) that can be sequestered by calcite is small (Reeder et al. 2000, 2001). Second, because the measured pH showed fairly constant values (Figure 4.15 right), especially for fine sediment, significant calcite dissolution was not likely to have occurred during early reaction times.

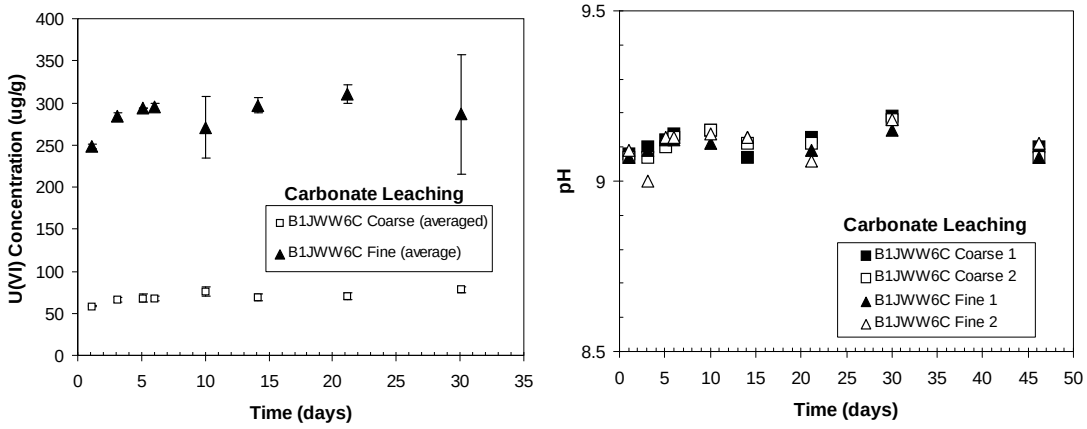

Figure 4.15. U(VI) Leached Concentration as a Function of Time (L) and Measured pH as a Function of Reaction Time (R). Error bars on the U(VI) concentration (L) correspond to 1-σ uncertainties.

As stated, we also measured the concentration of calcium in the leachate solution. Release of calcium can be attributed to several sources, including dissolution of calcium-bearing phases and ion-exchange with Na^+ ions from the leachant solution. Ca^{2+} release is monitored because if uranium release is primarily due to dissolution of the uranyl silicate phase uranophane $[Ca(UO_2)_2(SiO_3OH)_2(H_2O)_5]$, the release of Ca^{2+} will be proportional to that of U(VI). Several investigators have commented on the likelihood of the presence of uranyl silicates in contaminated Hanford sediments (e.g., Liu et al. 2004), and uranophane is the most common uranyl silicate phase in low-temperature aqueous environments (Burns 1999). However, both sediments released approximately the same amount of Ca^{2+} to solution at steady-state times (1.9 mg/L) (data not shown). This is inconsistent with the idea that uranophane dissolution is the *primary* phase releasing both Ca^{2+} and U(VI) to solution because the fine-grained sediment shows a release of uranium that is nearly four times that of the coarse-grained sample. Thus it is likely that other

mechanisms for releasing Ca^{2+} to solution, such as dissolution of a Ca-bearing (not U-bearing) phase or ion exchange, overwhelms the Ca^{2+} signal of a potential uranophane dissolution process.

Labile U(VI) leaching results after 21 days reaction for the two BX Tank Farm sediments tested showed average concentrations of 72.1 and 292 μg U/g for samples B1JWW6C coarse and B1JWW6C fine, respectively (Figure 4.15 left). Based on these labile U(VI) concentrations from carbonate leaching and U(VI) concentrations in pore water calculated from the previous Tier I 1:1 water extracts (297 and 4.63×10^4 μg/L for B1JWW6C fine and B1JWW6C coarse sediments, respectively), calculated U(VI) desorption K_ds are 983 and 1.56 mL/g for the B1JWW6C fine and B1JWW6C coarse sediment, respectively. These apparent K_d values are numerically similar to those measured based on acid extraction and pore water U(VI) concentrations (927 and 1.27 mL/g for B1JWW6C fine and B1JWW6C coarse sediment, respectively) in the previous Tier I analyses. The correlation between sediment particle size and leachable uranium concentrations could be explained by several factors. One possibility is that finer-grained particles are inherently more reactive toward uranium than larger particles. This greater reactivity manifests itself in greater uptake of sorbed uranium onto mineral grains or in faster precipitation kinetics of U-bearing phases mediated by higher surface areas of smaller particles. Thus, the reactivity could be attributed to intrinsic factors such as greater reactive surface area or extrinsic factors such as a different set of minerals that are segregated into the finer-grained fraction of the sediment. Another possibility is that sorption of uranium to sediment particles is time-dependent. As we have previously reported, aqueous solutions tend to accumulate in finer-grained sediments due to differences in water tension between coarse- and fine-grained sediments. Thus, the residence time of aqueous solution containing dissolved uranium is longer in fine-grained sediments and may result in more uranium sorption into these materials. For now, there are insufficient data to distinguish between the possibilities, but all are testable hypotheses that could be pursued in the future. Another feature is that the amount of uranium extracted by the bicarbonate-carbonate leachate (72 and 292 μg/g uranium for coarse- and fine-grained samples, respectively) is roughly the same concentration as that from the microwave-assisted digestion (108 and 390 μg/g U, respectively). This could be interpreted as 67 and 75% of the uranium from the coarse- and fine-grained specimens, respectively, are in a labile form.

4.3.2.5 Isotope Exchange for Quantifying Labile U(VI)

The amount of labile U(VI) was also estimated by the fractional distribution of $^{233}U(VI)$ between the solid and aqueous phases and total dissolved U(VI) concentration within the measured time frame after obtaining isotopic equilibrium. Figure 4.16 shows the activity of $^{233}U(VI)$ tracer, dissolved total U(VI) concentration, and calculated labile U(VI) concentration for the two BX direct-push sediment samples. The sediments were initially pre-equilibrated with synthetic groundwater for 1 day before spiking with the $^{233}U(VI)$ tracer. Although a relatively short time for pre-equilibrium (1 day) was allowed, the two sediments showed that a mostly stable dissolved-U(VI) concentration was acquired before the addition of $^{233}U(VI)$. The coarse sediment sample especially showed almost constant dissolved U(VI) and calculated labile U(VI) concentrations, even after 5 days reaction. This rapidly attained equilibrium was similar to the carbonate leaching result for the coarse sediment. Relatively rapid attainment of equilibrium in the coarse sediment resulted from fast exchange of $^{233}U(VI)$ with adsorbed U(VI) on larger mineral surfaces because the coarse grains have few diffusion barriers to U(VI) exchange on mineral surfaces, suggesting that adsorbed U(VI) phases predominate in the B1JWW6C coarse sediment. However, the dissolved U(VI) concentration of the B1JWW6C fine sediment increased at a relatively fast rate during early reaction time (up to seven days), then slowly increased to reach equilibrium. In addition, because of the

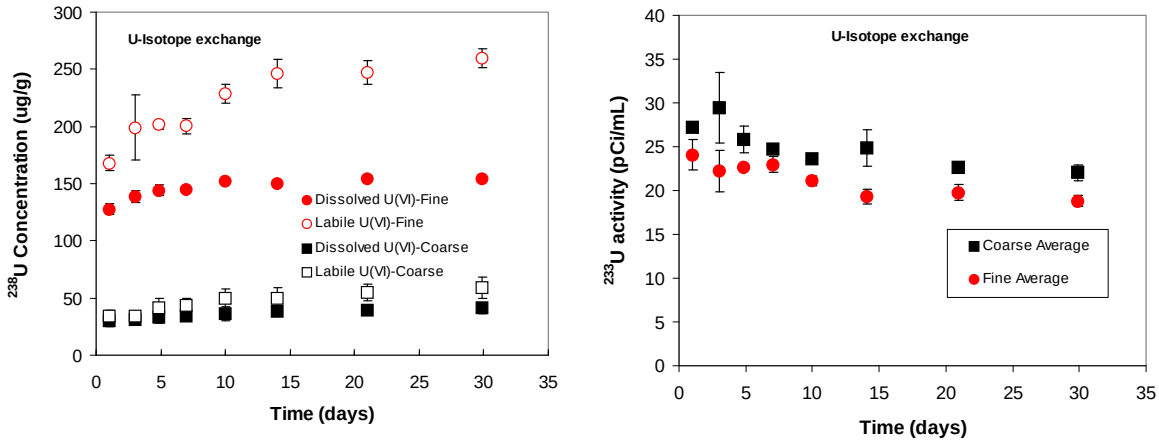

Figure 4.16. Dissolved U(VI) Concentration and Calculated Labile U(VI) Concentration (L) and ^{233}U Activity in Solution as a Function of Reaction Time (R)

slowly decreasing $^{233}U(VI)$ activity, the calculated labile U(VI) concentration in the fine sediment showed a slow, continuous increase after a relatively fast increase up to 14 days. A continuously increasing calculated labile U(VI) concentration and relatively slowly attained isotopic equilibrium in B1JWW6C fine sediment compared to the B1JWW6C coarse sample indicates diffusion-controlled U(VI) desorption/ dissolution is likely occurring. An increase in uranium concentration during the experiment may be due to continuous but slow dissolution of U(VI)-bearing precipitates (or coprecipitates). Though fractional volumes are small, coprecipitated U(VI) phases (uranyl silicates) may be present in addition to an adsorbed U(VI) phase in B1JWW6C, and slow release of uranium from these reservoirs may affect the results of the test.

The concentrations of labile uranium calculated by Eq. (3.1) are 55.1 and 247 µg/g U in the coarse- and fine-grained specimens, respectively. These U(VI) concentrations are 51 and 63% of total U(VI) concentrations (108 and 390 µg/g for coarse and fine sediment, respectively) obtained by microwave digestion (Table 4.29). Compared to the concentrations of labile uranium determined by the bicarbonate-carbonate extract, the values are quite close. The concentrations of labile uranium determined by isotope exchange are 75 and 85% of that determined by the bicarbonate-carbonate leaching method for the coarse- and fine-grained specimens. These values indicate that the bicarbonate-carbonate extract method yields a relatively good estimate of the labile uranium in sediments. This conclusion supports the findings of Kohler et al. (2004), who reported that isotope exchange and bicarbonate-carbonate extraction methods yielded similar results for labile uranium.

Based on the results of 21 days of isotope exchange experiments, U(VI) desorption K_d values were calculated and compared with those calculated using other methods. These include the U(VI) concentrations obtained by the bicarbonate-carbonate extraction, the strong acid extraction, and the microwave-assisted digestion described above. Labile U(VI) concentrations determined from isotope exchange are 247 and 55.1 µg/g for B1JWW6C fine and B1JWW6C coarse samples, respectively. These values translate to U(VI) desorption K_ds of 832 and 1.19 mL/g for B1JWW6C fine and B1JWW6C coarse samples, respectively. These K_d values are lower than those previously computed from bicarbonate-carbonate leaching (983 and 1.56 mL/g) and strong acid extraction (927 and 1.27 mL/g). However, given the large differences in methods and assumptions, the desorption K_d values determined by the three techniques are

remarkably similar. Further, the K_d values computed from the three methods are likely to reside within the uncertainty of measurement. Though we did not attempt to perform a rigorous quantification of the uncertainty, if a reasonable error of 10% were assigned to the K_d values, they are statistically identical. The results do, however, indicate a difference in the K_d values of the fine- and coarse-grained sediments that cannot be attributed to statistical fluctuations. Thus, concentrations of uranium released from the fine-grained sediment are lower and possibly kinetically slower than the coarse-grained specimen.

4.3.2.6 Spectroscopic XRF and XANES Analyses

Even though the macroscopic studies of bulk sediment and size fractions described above provided an estimate of the adsorbed U(VI) concentration, more specific quantitative information is required to understand U(VI) speciation and binding mechanisms on individual sediment grains. The XRF maps of the fine and coarse sediments are shown in Figures 4.17 through 4.24. Each false color map shows the distribution of Ca, Cr, Cu, Fe, Mn, Pb, Sr, Ti, U, and Zn on a 400 × 400 μm area in the sediment particles. Each pixel measures 10 × 15 μm, and the color intensity indicates the qualitative concentration gradient of the metal; blue indicates the lowest relative concentration and white the highest relative concentration.

Interpretation of Figures 4.17 through 4.24 should be tempered with the following caveats. First, although the X-ray peaks are well-resolved and present no problems with overlap, the high "noise" exhibited by the background made a quantitative background subtraction difficult. Thus, it is possible that some of the X-rays picked up by the detector represent background counts, and may not be, therefore, indicative of the presence of certain elements. Therefore, we made every effort to not over-interpret the results shown below until we have a chance to resolve the problem of background correction. Further, note that the "spot" size of the beam that rasters across the specimen is relatively large, such that the excited volume of the beam may enclose several phases simultaneously. Therefore, it is likely that the areas displaying multiple elements may originate from multiple sources. Thus, the association of several metals in the same area does not necessarily indicate that the metals are in the same solid phase.

Figures 4.17 and 4.18 show the elemental distribution of metals in the monolayer preparation of the fine sediment fraction (B1JWW6C fine) at two spots in the sample. Figure 4.17 shows large areas contain Ca, Fe, Mn, Pb, Sr and U, while a smaller area is noted for Cr, Cu, Ti, and Zn. Because of the wide distribution of U in the sample, there is correlation with all of the metals. However, spatial considerations indicate that U correlates mostly with Ca-, Pb-, and Sr-containing phases. Some U correlations were observed for metals with limited distribution, such as Cu, Mn, and Ti. Figure 4.18 shows Ca and Zn are widely distributed in the sample, while Cr, Cu, Fe, Mn, Pb, Sr, Ti, and U are distributed more narrowly. Uranium is present as discrete spots associated with Ca-, Cr-, Fe-, Mn-, and Pb-containing phases. Figure 4.18 illustrates that there is little correlation between U and other metals (Cu, Sr, Ti, and Zn). Micro-XANES analysis of U was done at the pixel in each sample that showed the highest concentration of U (white). Comparison of the XANES analysis of U in the sediment with known U standards showed it to be present as the hexavalent form U(VI) in both BX Tank Farm direct-push sediments (Figure 4.25).

Figures 4.19 and 4.20 show the elemental distribution of metals in the thick (1/16-inch) preparation of the fine sediment fraction at two locations in the sample. Figure 4.19 shows that strontium exhibits the greatest coverage in the sediment, while the other metals are present in discrete areas unevenly distributed throughout. The uranium was associated to the greatest relative extent with areas containing Ca, Cr, Fe, Mn, Pb, and Zn, although at these locations they did not show the highest element concentration.

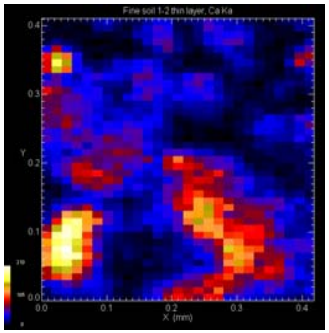

Ca

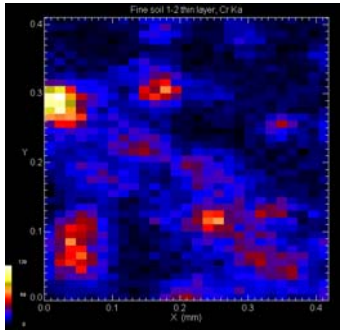

Cr

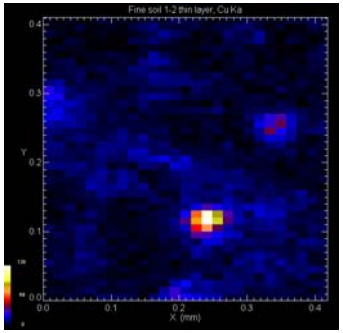

Cu

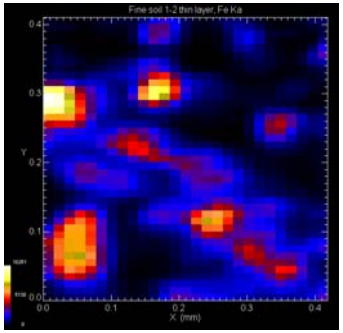

Fe

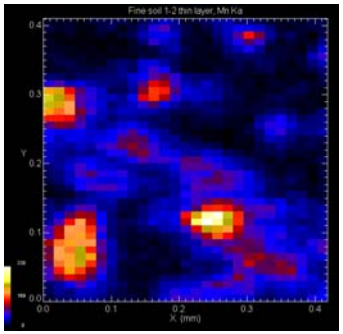

Mn

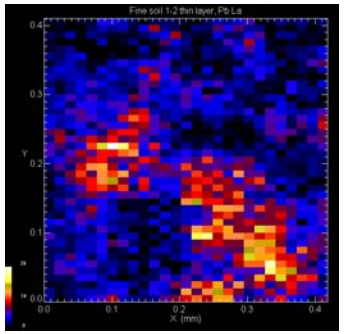

Pb

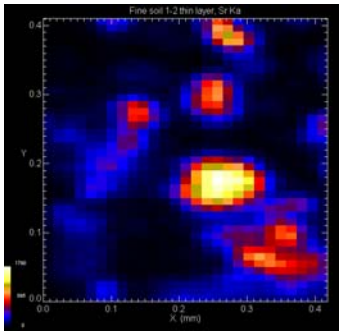

Sr

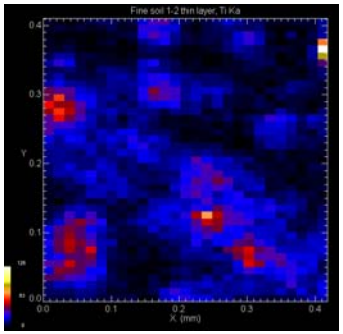

Ti

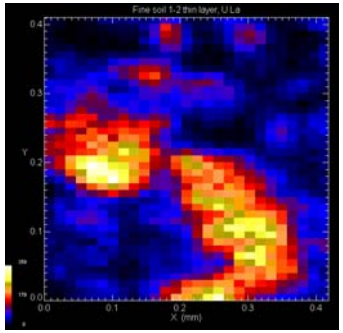

U

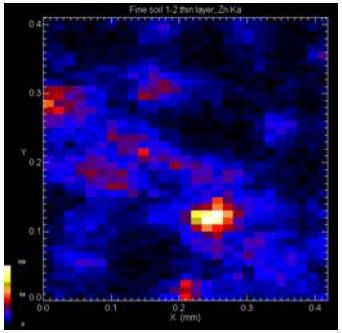

Zn

Figure 4.17. Elemental Map (400 × 400 μm) Showing Spatial Association of Ca, Cr, Cu, Fe, Mn, Pb, Sr, Ti, U, and Zn in B1JWW6C Fine Sediment (Spot 1) Prepared as a Monolayer Sample. The U appears to be associated predominantly with the Ca-, Pb-, and Sr-containing phases. Resolution is 10 μm.

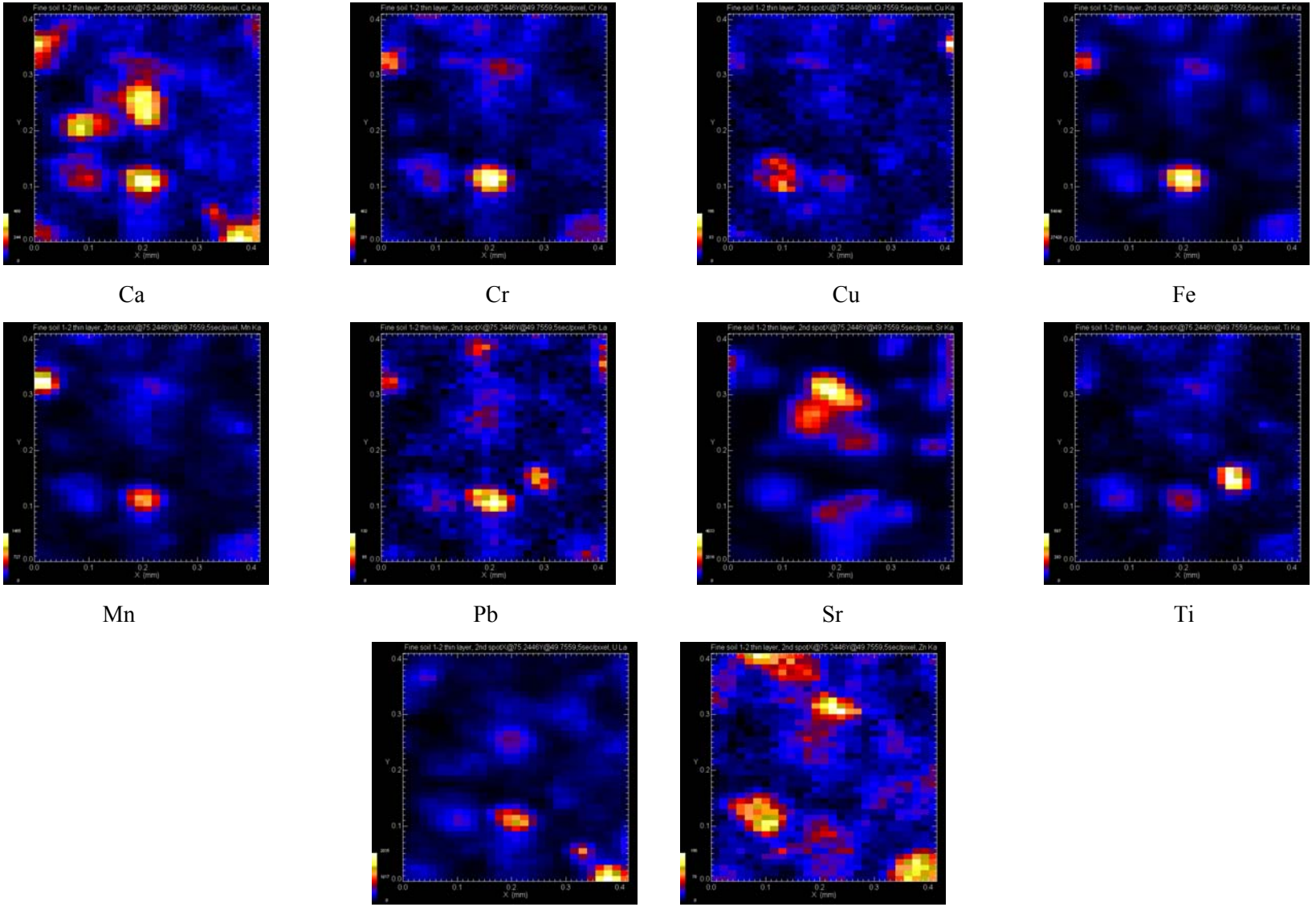

Figure 4.18. Elemental Map (400 × 400 µm) Showing Spatial Association of Ca, Cr, Cu, Fe, Mn, Pb, Sr, Ti, U, and Zn in B1JWW6C Fine Sediment (Spot 2) Prepared as a Monolayer Sample. The U is associated predominantly with the Ca-, Cr-, Fe-, Mn-, and Pb-containing phases. Resolution is 10 µm.

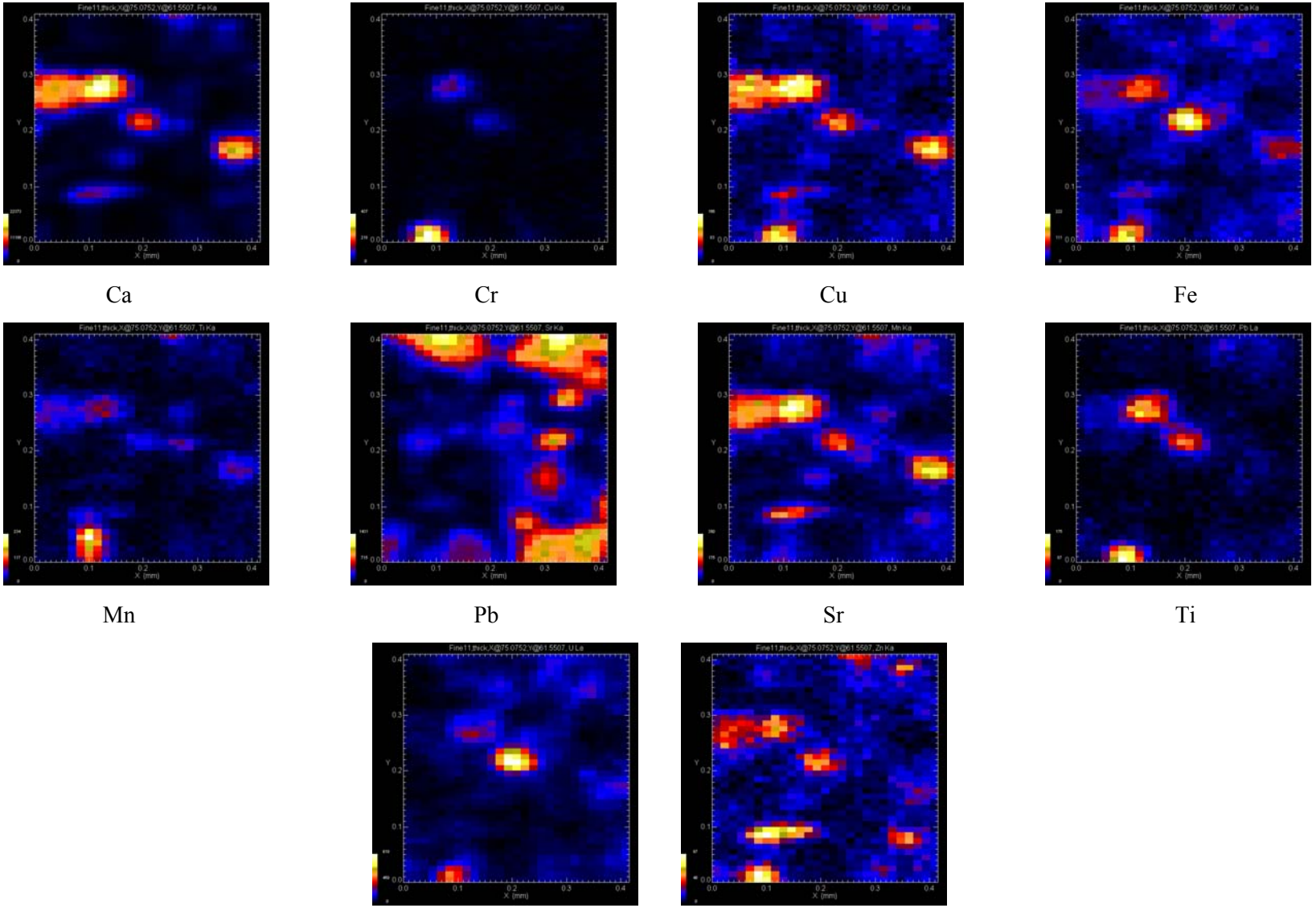

Figure 4.19. Elemental Map (400 × 400 µm) Showing Spatial Association of Ca, Cr, Cu, Fe, Mn, Pb, Sr, Ti, U, and Zn in B1JWW6C Fine Sediment (Spot 1) Prepared as a 1/16-in.-Thick Sample. The U is associated predominantly with the Ca-containing phase. Resolution is 10 µm.

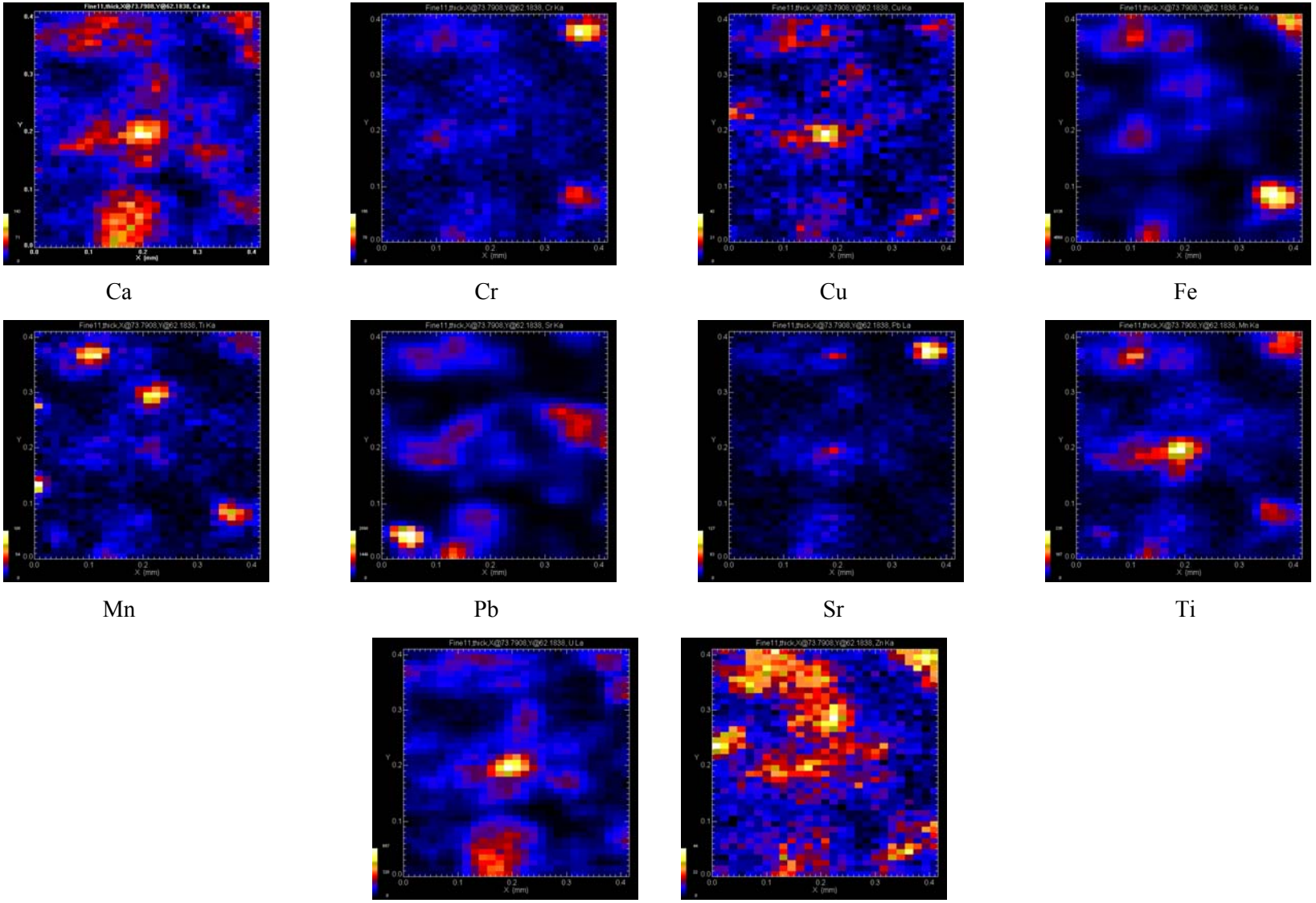

Figure 4.20. Elemental Map (400 × 400 μm) Showing Spatial Association of Ca, Cr, Cu, Fe, Mn, Pb, Sr, Ti, U, and Zn in B1JWW6C Fine Sediment (Spot 2) Prepared as a 1/16-in.-Thick Sample. The U is associated predominantly with the Ca-, Cu-, Mn-, and Zn-containing phases. Resolution is 10 μm.

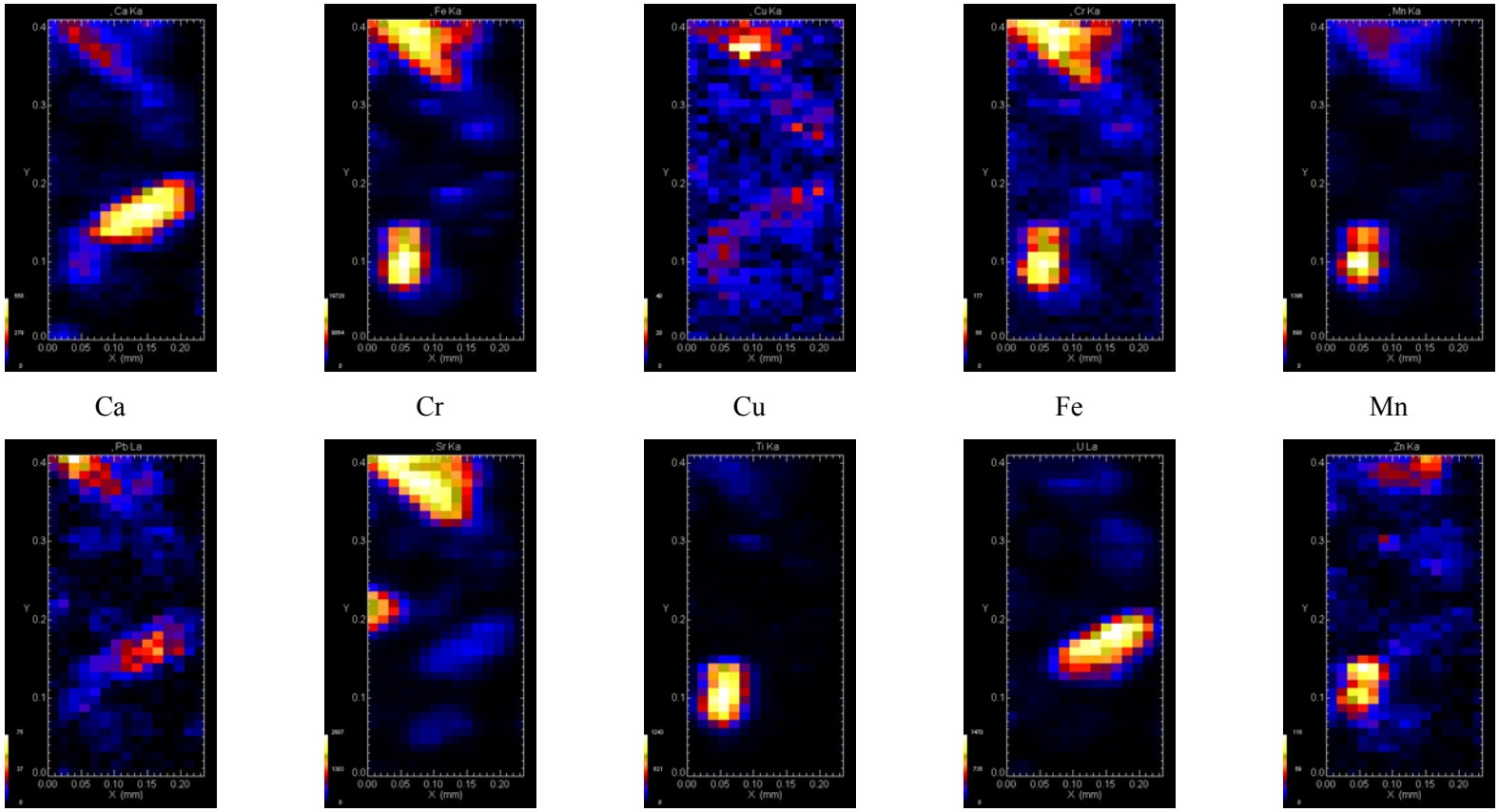

Figure 4.21. Elemental Map (200 × 200 μm) Showing Spatial Association of Ca, Cr, Cu, Fe, Mn, Pb, Sr, Ti, U, and Zn in B1JWW6C Coarse Sediment (Spot 1) Prepared as a Monolayer Sample. The U is associated predominantly with the Ca-containing phase. Resolution is 10 μm.

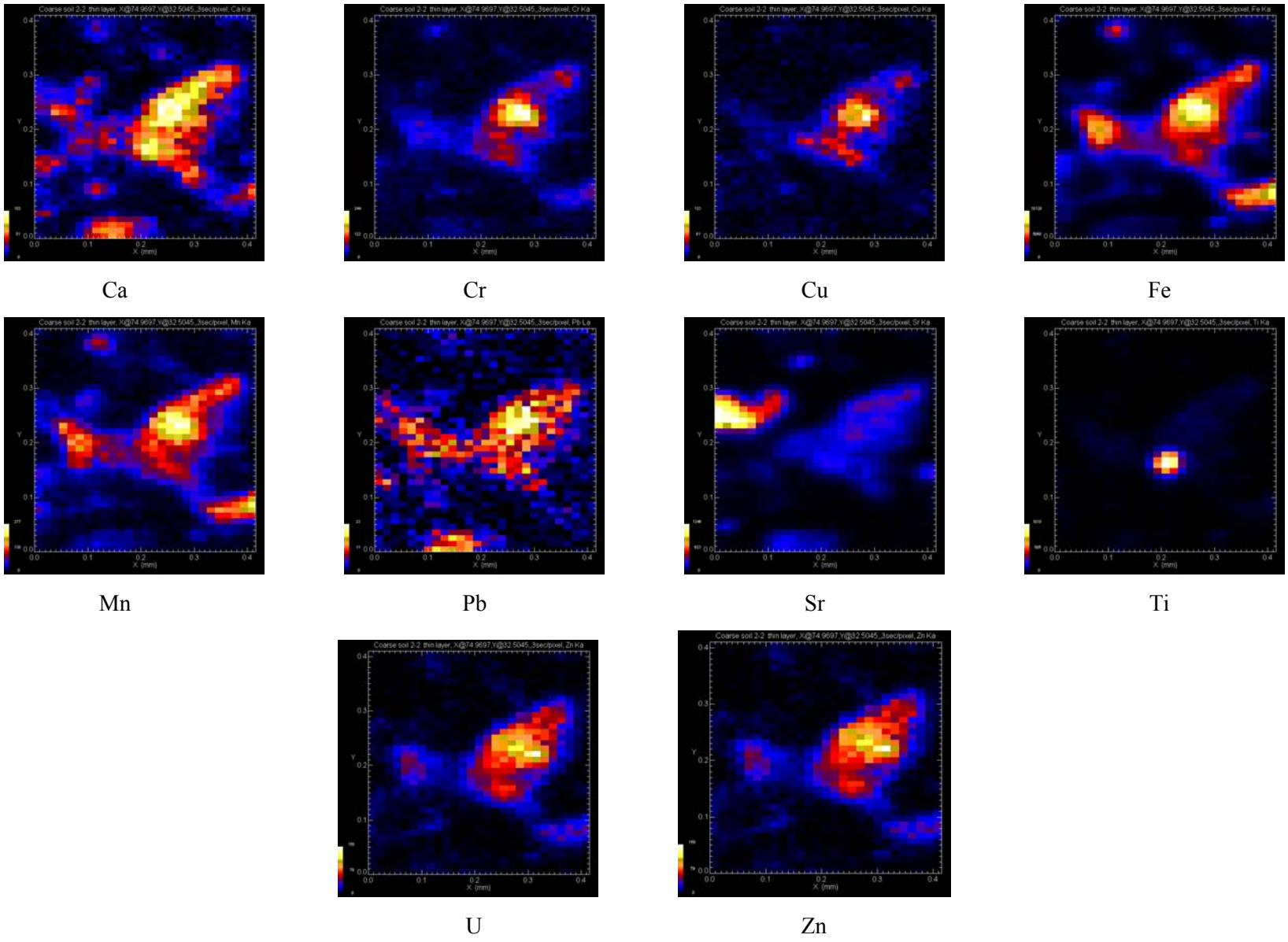

Figure 4.22. Elemental Map (400 × 400 μm) Showing Spatial Association of Ca, Cr, Cu, Fe, Mn, Pb, Sr, Ti, U, and Zn in B1JWW6C Coarse Sediment (Spot 2) Prepared as a Monolayer Sample. The U is associated predominantly with the Ca-, Fe-, Mn-, Pb-, and Zn-containing phases. Resolution is 10 μm.

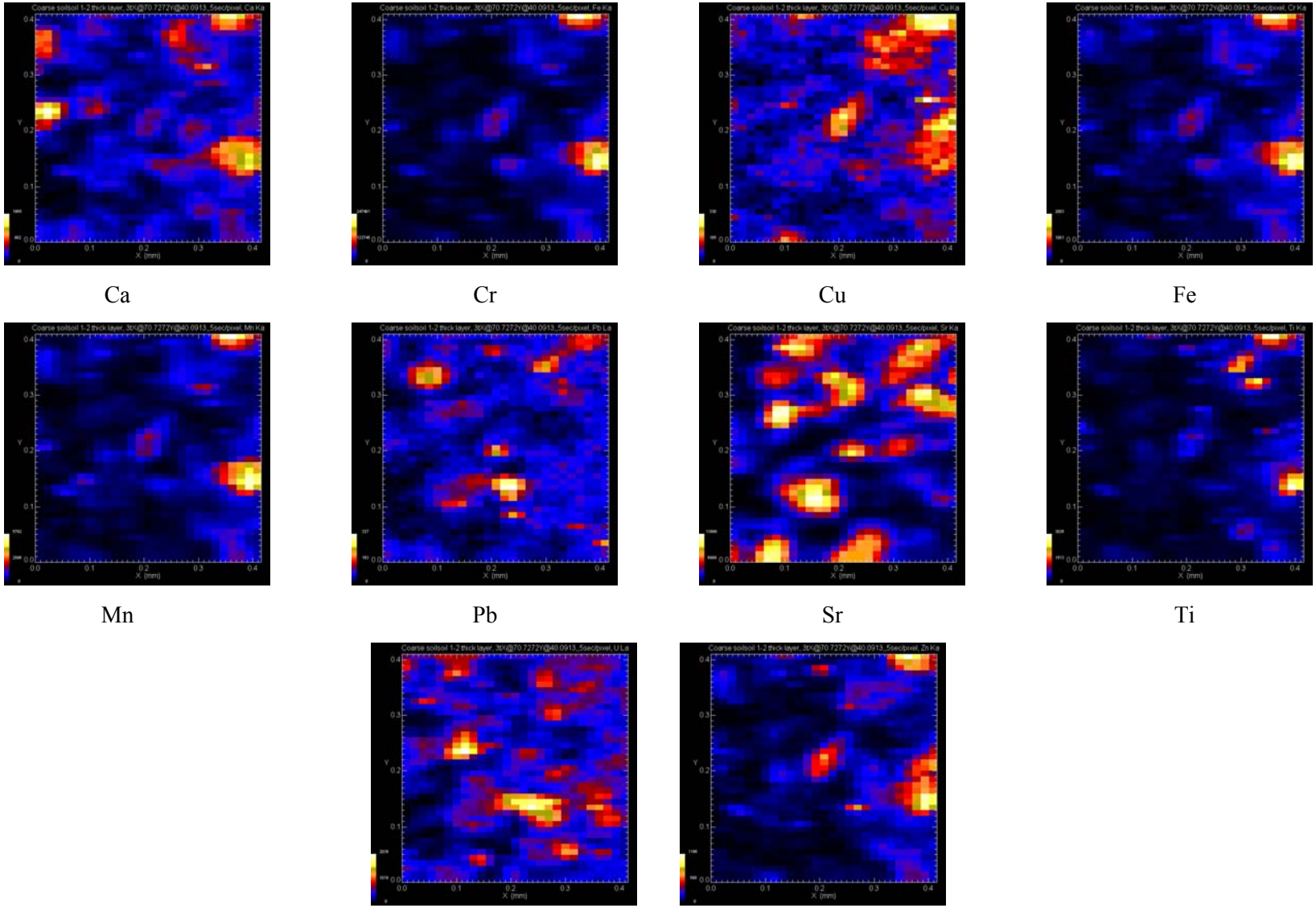

Figure 4.23. Elemental Map (400 × 400 µm) Showing Spatial Association of Ca, Cr, Cu, Fe, Mn, Pb, Sr, Ti, U, and Zn in B1JWW6C Coarse Sediment (Spot 1) Prepared as a 1/16-in.-Thick Sample. The U is associated predominantly with the Pb- and Sr-containing phases. Resolution is 10 µm.

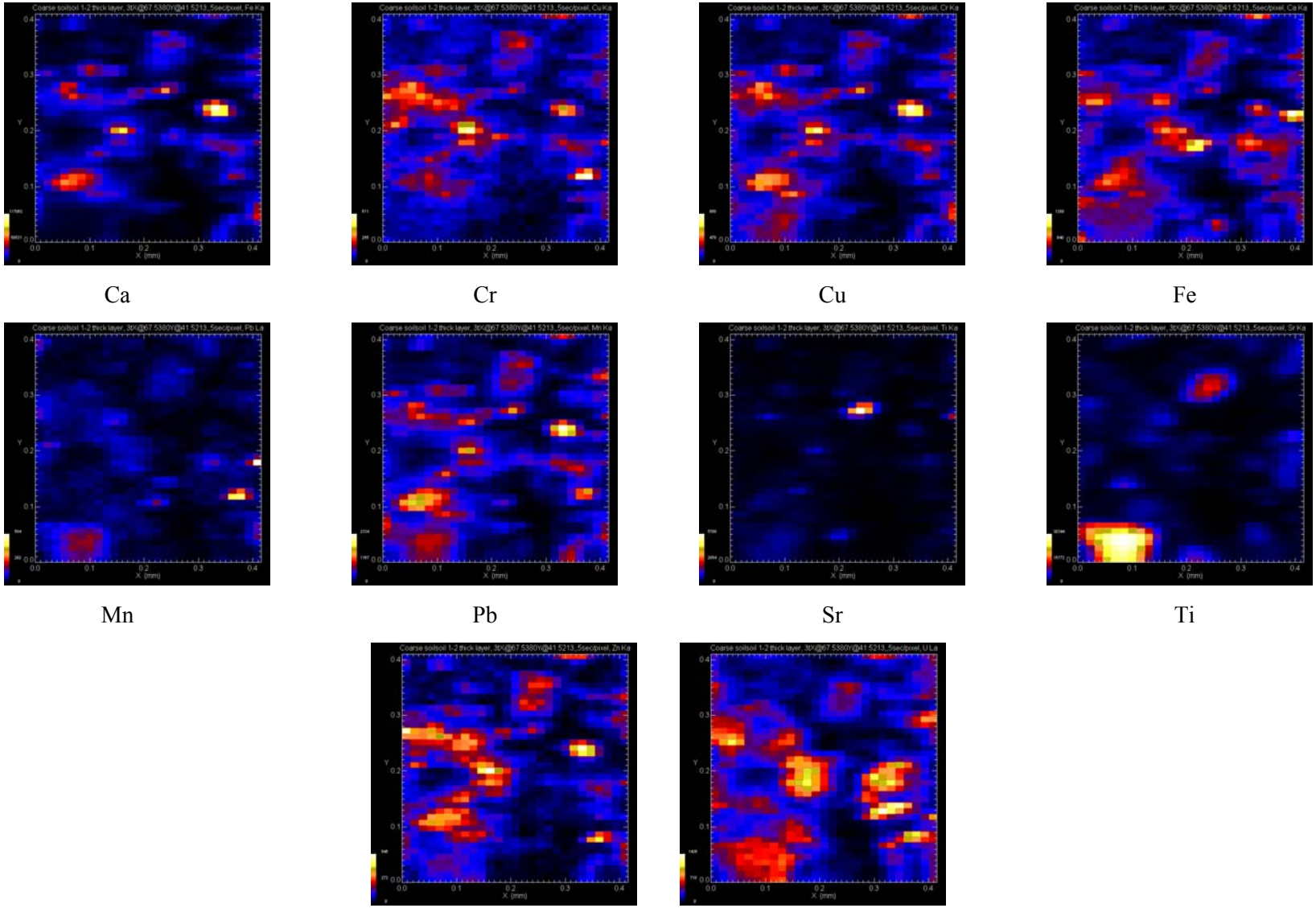

Figure 4.24. Elemental Map (400 × 400 μm) Showing Spatial Association of Ca, Cr, Cu, Fe, Mn, Pb, Sr, Ti, U, and Zn in B1JWW6C Coarse Sediment (Spot 2) Prepared as a 1/16-in.-Thick Sample. The U is associated predominantly with the Ca-, Cr-, Cu-, and Zn-containing phases. Resolution is 10 μm.

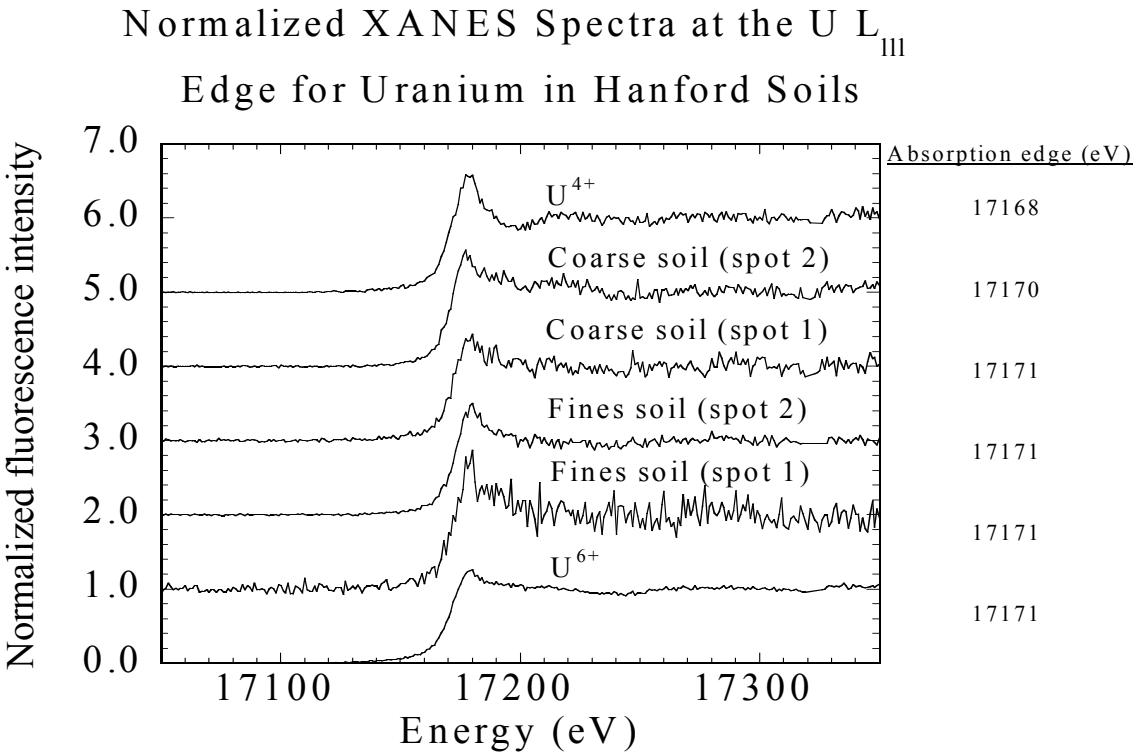

Figure 4.25. Normalized XANES Spectra at t L_{lll} Edge for Fine and Coarse Fractions of B1JWW6C Sediments. The absorption edges for the fine sediment fractions and Spot 1 of the coarse sediment indicate U is in the hexavalent form, while Spot 2 of the coarse sediment indicates a possible mixed oxidation state for U. Spot size is 10 × 15 μm.

Figure 4.20 indicates large regions containing Ca and Zn, while the other elements were scattered throughout the studied area. Uranium showed two areas of relatively high concentration and association with Ca-, Cu-, Mn-, and Zn-containing phases in the sample shown in Figure 4.20. There is little correlation between U and Cr, Fe, Pb, Sr, or Ti in the sample. Analysis of metals in these thick samples may be complicated by their presence in other particles in the sample due to the penetration depth of the high-energy beam (17.4 keV). Micro-XANES analysis was not successful at obtaining definitive oxidation state information on the thick samples because of weak instrument output signals. However, bulk XANES analysis for the fine sediment fraction showed that the uranium absorption edge was at 17171 eV, confirming that uranium was present in the hexavalent form (Figure 4.25).

Figures 4.21 and 4.22 show the spatial association of U with metals in the monolayer preparation of the coarse sediment fraction (B1JWW6C coarse). The sample area in Figure 4.21 is 200 x 200 μm and shows the metals present in large discrete areas of the sediment. It is evident that U is associated predominantly with the Ca-containing phase. Association of the metals Cr, Fe, Mn, Ti, and Zn with each other was also observed. Figure 4.22 exhibits relatively large areas for Ca-, Fe-, Mn-, Pb-, U-, and Zn-containing phases; a smaller distribution was observed for Cr-, Cu-, Sr-, and Ti-containing phases. The shape of the U-containing area correlated well with the spatial distribution of Ca, Fe, Mn, Pb, and Zn. Association of U with Cr and Cu was indicated as well, but there was no association of U with Sr. Micro-XANES analysis of U in the coarse sediment showed its presence in the hexavalent form in Spot 1, while in Spot 2 the absorption edge is shifted to lower energy by 1 eV, indicating that it may be present as a

mixed oxidation state. However, the 1-eV resolution of the energy as well as the shape of the spectrum still suggest that the predominant oxidation state is U(VI) (Figure 4.25).

Figures 4.23 and 4.24 show the spatial association of U with metals in the 1/16-in. preparation of the coarse sediment fraction at two locations. The Ca-, Cu-, Pb-, Sr-, and U-containing phases are widely distributed throughout the sediment sample, as shown in Figure 4.23. Smaller areas are noted for Cr, Fe, Mn, Ti, and Zn. Uranium is correlated predominantly with Pb- and Sr-containing phases in this sample section. Minimal or no association of other metals with U was observed on the grains probed in Figure 4.23. Figure 4.24 shows Ca-, Cr-, Cu-, Fe-, Mn-, U-, and Zn-containing phases were widely distributed in this sample, while Pb, Sr, and Ti were found in a few discrete areas. Uranium was associated predominantly with Ca-, Cr-, Cu-, and Zn-containing phases, while minor association with Fe, Mn, Pb, and Sr was noted. The oxidation state for U using μXANES could not be obtained due to the weak signals. However, bulk XANES analysis for the coarse sediment fraction showed that the U absorption edge was at 17171 eV, which confirmed U was present as the hexavalent form (Figure 4.26).

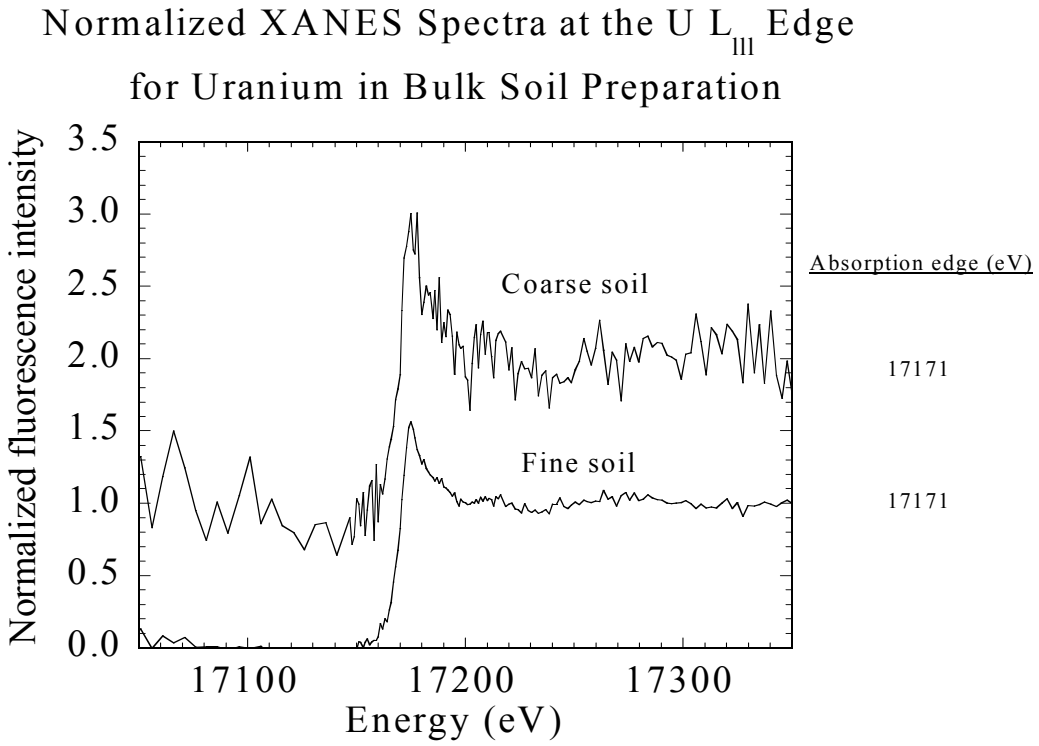

Figure 4.26. Normalized XANES Spectra at the U L_{lll} Edge for Bulk B1JWW6C Fine and Coarse Sediments. The absorption edges for both indicate the average oxidation state for uranium is the hexavalent [U(VI)] form. The spot size is 1 x 15 mm.

Association of U with various elements in the sediment based on duplicate synchrotron μ-XRF analysis is shown in Table 4.30. The predominant association of U in the sample is with the Ca- or Sr-containing phases. Association with other metals is predominantly sample-specific, with Fe and Mn the most frequently observed associations. Micro-XANES analysis confirms that the uranium is present as the hexavalent form in all the BX Tank Farm samples investigated. Analysis of the bulk XANES data also showed that the U is present as the hexavalent form in both the fine and coarse sediment fractions.

Table 4.30. Summary of Apparent Association of U with Selected Metals in BX Tank Farm Sediments

Sample	Major Association	Minor Association
Fine (spot 1) monolayer	Ca, Pb, Sr	Cr, Cu, Fe, Mn, Ti
Fine (spot 2) monolayer	Ca, Cr, Fe, Mn, Pb	Cu, Sr, Ti, Zn
Fine (spot 1) thick	Ca	Cr, Fe, Mn, Pb, Zn
Fine (spot 2) thick	Ca, Cu, Mn, Zn	Cr, Fe, Pb, Sr, Ti
Coarse (spot 1) monolayer	Ca	---
Coarse (spot 2) monolayer	Ca, Fe, Mn, Pb, Zn	Cr, Cu
Coarse (spot 1) thick	Pb, Sr	---
Coarse (spot 2) thick	Ca, Cr, Cu, Zn	Fe, Mn, Pb, Sr

The greater signal intensity of the U in the fine sediment fraction compared to the coarse sediment in both the μ–XANES and bulk XANES data suggests the U is associated predominantly with the fine fraction particles, as was found in microwave digestion of different size fractions. No data for Na or Si could be obtained due to energy limitations of the beam during the analysis. Performing μ-XRD on the individual U-rich grains is strongly recommended to confirm the mineralogical association of U.

4.3.2.7 Time-Resolved Laser-Induced Fluorescence Spectroscopy

At liquid helium temperature, all three sediment samples (B1JWW6C fine, B1JWW6C coarse, and B1JWW6A) displayed the strong fluorescence spectra (Figure 4.27) characteristic of uranyl compounds, with a set of almost evenly spaced vibronic bands ranging from 480 to 600 nm (Wang et al. 2005a). The spectra collected at steady-state conditions at 0 second delay with a gate width of 10 ms showed a broader pattern, especially for B1JWW6C fine and coarse sediments, than time-delayed spectra (1.2-ms delayed

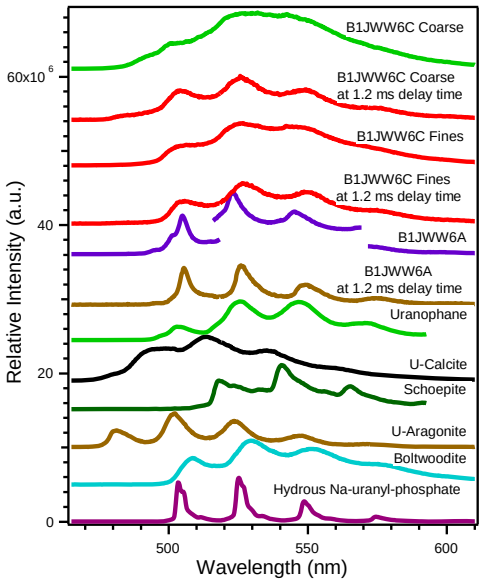

Figure 4.27. Fluorescence Spectra of Sediment Samples and Standard Uranium Natural Minerals at 6 ± 1K; λ_{ex} = 415 nm. Both steady-state (0 delay time at gate width of 10 μs) and time-delayed (1.2 ms) spectra are plotted for 3 samples. All spectra are normalized to the same maximum intensity and offset along the vertical axis.

spectra in Figure 4.27). The spectra varied somewhat among the three samples at different locations within the sample cuvette, indicating that the sediment solids are not homogeneous. However, the major spectral features are consistent in all 3 samples, with band positions at 504, 526, and 550 nm, respectively. Variability was also found in fluorescence spectra of B1JWW6C fine sediment recorded at different delay times after the laser pulse, again indicating that more than one uranyl species was present (Figure 4.28).

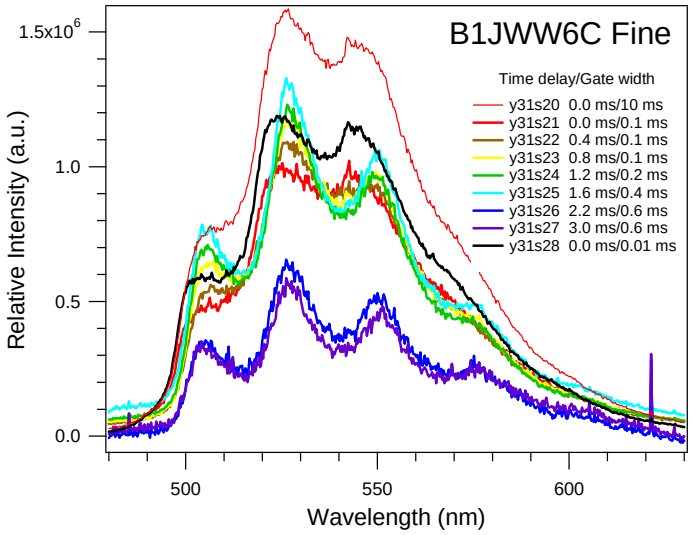

Figure 4.28. Time-Resolved Fluorescence Spectra of B1JWW6C Fine Sediment Sample at 6 ± 1K and λ_{ex} = 415 nm

Qualitatively, the spectra obtained with the 1.2-ms delay showed sharper features than those taken without a delay. The sharper spectra are therefore more useful in identifying the uranyl species that gave rise to the spectra. To identify the uranyl species present in these samples, the spectra were compared with fluorescence spectra of natural uranyl minerals received from the Smithsonian Institution or the American Museum of Natural History and recorded under the same experimental conditions. Within the error of the measurements, the dominant species in the coarse- and fine-grained sediment samples are consistent with uranophane [$Ca(UO_2)_2SiO_3(OH)_2{\cdot}5(H_2O)$] and boltwoodite [$NaUO_2(SiO_3OH)1.5H_2O$]. However, because of close correlation between U(VI) and Ca in previous μ-XRF results, the uranyl species are considered more closely associated with uranophane. Due to significant differences in TRLIF spectra between sediments and U-bearing calcium carbonate minerals (calcite and aragonite), U(VI) was not considered to be harbored by calcium carbonate minerals. This result is also consistent with a previous finding in which the major uranium species from beneath Tank BX-102 at a depth of 61 to 67 ft was a uranophane-type secondary uranyl mineral (Wang et al. 2005a). In contrast, the spectra for B1JWW6A appear to be more consistent with those of uranyl phosphate. Hydrous forms of sodium uranyl phosphate, such as meta-autunite and autunite [$Ca(UO_2)_2(PO_4)_2(H_2O)_{10\text{-}12}$], are common in both naturally weathered uranium deposits and in contaminated sediments (Finch and Murakami 1999). Given the very small K_{sp} value of autunite (Langmuir 1997) and the relatively high phosphate concentration in the BX-102 direct-push sediment water extracts, it should be no surprise if further tests confirmed the presence of this mineral at Hanford.

4.3.2.8 Strontium-90

Results of the strontium analyses (strontium-90) are tabulated in Table 4.31. The data include strontium-85 added as a procedure recovery tracer in the eluent solution and the uncertainty (both in pCi/mL; columns 2 and 3, respectively), the fraction of strontium-85 recovered (column 4), the ^{90}Sr in the eluent and the uncertainty (in pCi/mL; column 5 and 6), and the concentration of strontium-90 normalized to the mass of the sediment sample and the error (pCi/g; columns 7 and 8, shaded). Analysis of the acidic eluent solution shows that strontium-90 is present in every BX direct-push sediment sample collected, except for samples B1M564A, B1M564B, and B1M564C, in which strontium-90 is below the detection level. The strontium-90 values appear to be robust, because tracer recovery is above 90% for all samples. (Small corrections to the ^{90}Sr data were made to account for the amount of ^{85}Sr not recovered and the minimal ingrowth of yttrium-90 that occurred post column separation and prior to sample analysis.) A duplicate analysis of sample B1LTY5B yielded the same strontium-90 concentration within analytical uncertainty. Blank and matrix spikes showed the analytical procedure could account for 100 and 98% of the strontium, respectively. Analyses of blank samples yielded counts at the analytical detection limit.

In general, the concentrations of strontium-90 recovered from the sediment samples are in the nanocurie per gram range. These concentrations are indicative of contamination by waste fluids. Another feature of note is that the second highest concentration of strontium-90 is in a sample identified as part of a fine-grained lens. This observation is consistent with others that indicate greater contaminant concentrations in finer-grained materials, but it is difficult to generalize on this further on the basis of the small number of samples analyzed.

Table 4.31. Concentrations of Strontium-85 (tracer) and Strontium-90 (contaminant) in Hanford Soils. Soil mass-corrected strontium-90 concentrations and associated analytical uncertainties are shown in shaded columns[(a,b,c)]. Recovery of a high (>0.90) fraction of strontium-85 (fourth column) indicates successful separation and recovery of strontium-90 from the sediments.

Sample ID	^{85}Sr Tracer (pCi/mL)	^{85}Sr Error (pCi/mL)	^{85}Sr Tracer Recovery	$^{90}Sr^{(a)}$ (pCi/mL)	^{90}Sr Error (pCi/mL)	$^{90}Sr^{(b)}$ (pCi/g)	^{90}Sr Error (pCi/g)
B1LTY5C	1.99E+03	3.26E+01	0.93	5.07E+02	2.06E+01	2.81E+03	1.14E+02
B1LTY5B	1.92E+03	3.22E+01	0.94	1.69E+02	1.58E+01	1.01E+03	9.44E+01
B1LTY5B Duplicate	1.97E+03	3.25E+01	0.93	1.49E+02	1.54E+01	8.54E+02	8.80E+01
B1LTY5A	1.90E+03	3.20E+01	0.94	1.02E+02	1.46E+01	6.06E+02	8.67E+01
B1M564C	1.92E+03	3.19E+01	0.92	<1.14E+01	1.26E+01	*<6.43E+01*	
B1M564B	1.94E+03	3.21E+01	0.92	<1.14E+01	1.26E+01	*<6.00E+01*	
B1M564A	1.92E+03	3.19E+01	0.92	<1.15E+01	1.27E+01	*<6.32E+01*	
B1M565C Fine Sand	1.94E+03	3.23E+01	0.93	1.16E+02	1.48E+01	6.75E+02	8.64E+01
B1M565C Fine Lens	1.95E+03	3.29E+01	0.96	4.95E+02	2.07E+01	3.34E+03	1.40E+02
B1M565B	1.96E+03	3.29E+01	0.96	5.74E+02	2.17E+01	3.31E+03	1.25E+02
B1M565A	1.99E+03	3.29E+01	0.95	8.54E+02	2.49E+01	4.74E+03	1.38E+02

(a) Denotes values that were not corrected for soil sample mass.
(b) Denotes values that were corrected for soil sample mass.
(c) < indicates the analyte was not detected at the minimum detectable activity reported for the sample.

5.0 Summary and Observations

In this section, summary information about the interpretation of the 241-B and -BX Farms direct-push sediment characterization data is presented. Interpretation of the data has been included to aid in making decisions on what interim actions and future studies are needed to make sound remediation decisions in the B-BX-BY WMA.

The data retrieved from the 241-B and -BX Farms direct-push sediment characterization efforts continue to demonstrate the vertical and lateral effects of tank waste interaction with the vadose zone sediments. We used a wide-ranging suite of tests to characterize the physical and chemical attributes of the sediments recovered from the direct-push activities and to determine the extent of interaction between accidentally released liquid waste and pristine sediment. The lithologic makeup of the recovered sediments showed a wide range of particle size, from cobbles to clay. In some of the sediment samples was a wide distribution of particle sizes, while in others, fine-grained well-sorted material dominated. Abrupt changes in particle size distribution and sorting patterns reflect fluctuations in the energy of the environment of deposition. As a general rule, the finer-grained lithologies contained the highest soil moisture content, which has important consequences for flow and transport of pore fluids and for the distribution of contaminant species. The clay, silt, and fine sand lithologies are interpreted as fine-grained lenticular bodies irregularly distributed throughout the formation typically made up of sand-sized particles.

We were unable to retrieve pore fluids by ultracentrifugation of the sediments because of the limited sample size afforded by the direct-push technology, so we resorted to 1:1 water extracts to estimate the pore water chemistry. These tests revealed relatively high concentrations of sodium, high electrical conductivity, and elevated solution pH values. The data can be construed to signify the interaction of a sodium-rich, saline, and high-pH solution, like that of liquid tank waste, with the sediments. The lack of divalent cations (e.g., Ca^{2+}, Mg^{2+}) compared to Na^{+} in the 1:1 water extract solutions is interpreted as a manifestation of a sodium-rich plume front that swept through the sediments, displacing divalent cations from their sorption sites. However, the accuracy of estimating pore fluid compositions from 1:1 water extracts depends on the degree of contamination by tank waste, and it is possible that the extract solutions are more saline than actual pore water. Nevertheless, the 1:1 water extract data are consistent with the interpretation of contamination by tank waste fluids. The soundness of this interpretation is amplified by the presence of relatively elevated concentrations of aluminum, iron, and phosphorous in the water extracts. We speculate that the unusually high concentrations of aluminum and iron are the result of the interaction between a caustic fluid and the sediment minerals. Partial dissolution of aluminum- and iron-bearing minerals was followed by re-precipitation as the contaminant front moved through. Precipitation from solution is a kinetically driven process that favors the formation of amorphous phases that are more soluble than their crystalline counterparts. Thus, the water-extract solution may have dissolved and mobilized higher than usual concentrations of aluminum and iron. The unusually high concentrations of phosphate, on the other hand, may reflect the signature of high-phosphate waste derived from the bismuth phosphate separation process.

The estimated pore water composition for the shallow direct-push sediments from the three locations east of diversion box 241-B-153 and the three locations around tanks BX-101 and BX-102 should be added to the data set being used to compare/correlate or “ground truth” the field electrical resistivity measurements made recently in the B-BX-BY region by hydroGEOPHYSICS, Inc. We recognize that the

six data sets are for rather shallow depths and as a whole represent two small geographic regions. One interesting fact to note is that the estimated pore waters are dominated by sodium and bicarbonate and not nitrate as is often the case in the other data that has been used to correlate the measured pore waters with the field resistivity data. Whoever uses these direct-push pore water data should keep this difference in dominant anion in mind.

Direct confirmation of contamination in the BX samples can be seen in uranium concentrations in acid extract solutions that are well above the natural crustal abundances. The amount of uranium present as labile, easily removed uranium, is interpreted as ~30% of the total uranium. Further evidence for contamination includes detection of the presence of anthropogenic radionuclide elements (cobalt-60, cesium-137, and europium-154, -155) by gamma-emission analysis (GEA) of the sediments. Confirmation of the presence of radionuclide elements in the sediments illustrates that even simple geochemical tests, such as the 1:1 water extracts, can rapidly reveal evidence for contamination as manifested by elevated concentrations of sodium and relatively high electrical conductivities and pH. However, the presence of mobile anthropogenic radionuclide elements such as technetium-99 was not detected in most of the sediments. We infer that this is because mobile elements were not retained by the sediment grains as the contaminant front swept through. Presumably, the mobile elements are distributed along a narrow front marked by sharp concentration gradients (Wan et al. 2004), and it is perhaps no surprise that the sediments recovered from the direct-push boreholes did not intercept this limited distribution of mobile elements at the front. It is plausible that such a front exists below the depth sampled using the direct-push method. The mobile contaminants at nearby borehole 299-E33-45 were found considerably deeper in the vadose zone. The geochemical fractionation of mobile from immobile radionuclide elements hampers efforts to uniquely fingerprint sources of contamination based upon parent-daughter isotopic ratios. The power to distinguish between different reservoirs of waste (individual tanks versus waste in pipelines) based on such unique isotopic signatures will not be apprehended until more data are collected.

Having made the case for broad contamination of sediments in the 241-B and -BX Farms, we focused our efforts on a sediment sample from BX probe hole C5314, which we subdivided into sub-samples B1JWW6C fine and B1JWW6C coarse. We chose to subject these materials to closer scrutiny because the sharp transition from relatively coarse- to fine-grained sediments is typically associated with large differences in the distribution of moisture and elements, with uranium preferentially harbored by the finer-grained material. The mineralogy of the fine- and coarse-grained samples, determined by quantitative XRD, was similar and showed a predominance of quartz and feldspar, but the particle size difference between the samples was large. The particle size distribution of the fine-grained sediment was skewed toward smaller sizes, with nearly 90% of the particle sizes in the three finest categories. In contrast, the coarse-grained sample showed a more even distribution of particle sizes with the majority of the grains in the coarse sand fraction. Bulk samples were completely dissolved in an acid mixture, and the process was expedited using a microwave-assisted procedure; the resulting solution was assayed for uranium. The analyses revealed that there is almost four times more uranium in the fine-grained sediment compared to the bulk coarse-grained sample (390 versus 108 μg/g U). In addition, the various size fractions separated from the coarse-grained specimen were dissolved by the microwave-assisted digestion method, and analyses of the solutions showed that most of the uranium resides in the finest-grained fractions of the sediment. These data point to a number of possible scenarios for the retention of uranium in finer-grained sediments. It is possible that phases which selectively sorb uranium may be segregated into the finer-grained sediments or that the higher surface area of the smaller particles catalyzes the precipitation of fine grains of uranyl minerals. Another scenario is that the smaller inter-granular pore

spaces in the fine-grained sediment retain contaminated solution by virtue of water tension more effectively than the larger pore spaces in the coarse-grained sediment. Further tests, in which the detailed mineralogical and physical properties of the fine-grained sediment will be determined, are needed.

With the total amount of uranium residing in the sediments determined, we next estimated the amount of mobile (or labile) uranium present in the samples. The fraction of labile uranium was estimated in two ways: 1) using a bicarbonate-carbonate leach solution and 2) using an isotope-exchange method. The slightly alkaline bicarbonate-carbonate extracting solution was used because it minimized dissolution of potentially U-bearing phases. The isotope exchange method entailed equilibration of the sediment sample with synthetic groundwater followed by spiking the solution with uranium-233, which could be easily distinguished analytically from common uranium (U-238). The system was allowed to come to equilibrium, and the uptake of uranium-233 by the sediment was measured. The bicarbonate-carbonate leaching and the uranium-233 uptake experiments yielded similar estimates of the labile fraction of uranium. In the fine-grained specimen, ~65 to 75% of the uranium is labile, whereas ~50 to 65% of the uranium in the coarse-grained specimen is labile. This indicates that an important reservoir of uranium is likely retained in a solid dissolution-resistant phase or phases.

We attempted to identify the phase(s) that sequester(s) uranium by subjecting the samples to a set of analytical procedures designed to pinpoint the location and to identify the metals with which uranium is associated. Small areas (400 × 400 μm) were analyzed by μ-XRF techniques, and spots in which relatively high concentrations of uranium was present were identified. False-color X-ray micrographs illustrated the distribution of U within the analyzed area and showed the distribution of other metals (Cr, Cu, Fe, Mn, Pb, Sr, Ti, and Zn) as well. In some cases, the relative concentration of the cation may have been overestimated due to inappropriate background subtraction; we are investigating the accuracy of the results. However, it does seem clear that there is an association between U and Ca that suggests the presence of a calcium uranyl silicate, such as uranophane [$Ca(UO_2)_2(SiO_3OH)_2(H_2O)_5$]. Uranophane-group minerals such as boltwoodite [$K(UO_2)(SiO_3OH)(H_2O)_{1.5}$] and sodium boltwoodite [$Na(UO_2)(SiO_3OH)(H_2O)_{1.5}$] are common uranyl silicates in nature and have been identified as a secondary mineral product on the surface of corroded UO_2 in silica-rich solutions (Wronkiewicz et al. 1992). A relatively new technique, TRLIF, was brought to bear on the uranium "hot spots" in an attempt to determine the identity of the uranium phase. The advantage of TRLIF is that very small spots (10 × 15 μm) containing low concentrations of the target element can be analyzed. Typically, TRLIF can determine trace quantities of an element that are beyond the resolving power of other spectroscopic techniques, such as Raman or NMR. The fluorescence signal from the target can be enhanced by performing the analysis at cryogenic temperatures (6±1K). Because the emitted signal persists over a time interval, collecting the signal at different time intervals may also result in greater resolution of the spectrum. The results obtained from these samples indicated the possibility of more than one uranium phase, but the spectra were consistent with that of uranophane in both the fine- and coarse-grained sample. A third sediment sample, B1JWW6A, used for internal comparison, revealed the likely presence of a uranyl phosphate phase rather than uranyl silicate. Examination of the uranium "hot spots" using micro-XANES showed that most, if not all, of the uranium is in the uranyl [U(VI)] form.

Passage of a contaminant plume through the Hanford formation left an indelible mark on the sediment samples collected for this study. Simple tests, such as the 1:1 water extract, can provide rapid evidence for the interaction of the plume with sediments and can be used to quickly delineate the affected zone. An exact estimate of the mass of contaminants that leaked into the sediments cannot be ascertained by this

study, nor can we definitively say if the waste was leaked from a tank, a fluid transfer line, or a distribution box based on the isotopic signature left behind. Part of the problem is that the sediments obtained by the direct-push technology did not retain the more mobile elements, so fractionation likely occurred between parent-daughter isotope pairs. However, the manifestation of uranium has wide-ranging implications for understanding contaminant transport at Hanford. Previous investigations by Liu et al. (2004) emphasize the presence of uranium as uranyl silicate micro-precipitates in lithic fragments of granite. If these micro-precipitates represent the major fraction of contaminant uranium in the sediments, then modeling the release of uranium from the lithic fragments would go a long way toward understanding the movement of uranium. The data from this report show, however, that a relatively recalcitrant phase or phases harbor uranium and reside in the finer-grained fraction of the sediment. Besides the uranium trapped as micro-precipitates in lithic fragments, our work shows that the finer-grained materials also sequester uranium, especially where there is a sharp contrast in hydraulic properties between fine- and coarse-grained sediments. Therefore, this report can be seen as an extension of the earlier uranium micro-precipitate studies. The key to understanding contaminant migration and pore water transport at Hanford may lie in understanding the behavior of aqueous solutions at the interface between coarse- and fine-grained components of the sediment.

6.0 References

American Society for Testing and Materials (ASTM). 1986. *Standard Test Method for Particle Size Analysis of Soils.* ASTM-D422-86, American Society for Testing and Materials, West Conshohocken, Pennsylvania.

American Society for Testing and Materials (ASTM). 1998. *Test Method for Laboratory Determination of Water (Moisture) Content of Soil and Rock by Mass.* ASTM-D2216-98, American Society for Testing and Materials, West Conshohocken, Pennsylvania.

American Society for Testing and Materials (ASTM). 1993. *Standard Practice for Description and Identification of Soils (Visual-Manual Procedure).* ASTM-D2488-93, American Society for Testing and Materials, West Conshohocken, Pennsylvania.

American Society of Agronomy (ASA). 1996. *Methods of Soil Analysis-Part 3, Chemical Methods.* SSSA Book Series 5, DL Sparks (ed.). Soil Science Society of America, Madison, Wisconsin.

Bjornstad BN. 2006. *On the Trail of the Ice Age Floods: A Geological Field Guide to the Mid-Columbia Basin*. Keokee Publishing, Inc., Sandpoint, Idaho.

Brown CF, RJ Serne, BN Bjornstad, DG Horton, and DC Lanigan. 2006. *Characterization of Vadose Zone Sediments Below the C Tank Farm: Borehole C4297 and RCRA Borehole 299-E27-22*. PNNL-15503, Pacific Northwest National Laboratory, Richland, Washington.

Brown CF, RJ Serne, BN Bjornstad, MM Valenta, DC Lanigan, TS Vickerman, RE Clayton, KN Geiszler, C Iovin, ET Clayton, IV Kutnyakov, SR Baum, MJ Lindberg, and RD Orr. 2007. *Characterization of Vadose Zone Sediments from C Waste Management Area: Investigation of the C-152 Transfer Line Leak*. PNNL-15617, Pacific Northwest National Laboratory, Richland, Washington.

Burns PC. 1999. "Crystal Chemistry of Uranium." In *Uranium: Mineralogy, Geochemistry and the Environment. Reviews in Mineralogy*, Vol. 38, pp. 23-90. Mineralogical Society of America, Washington, D.C.

Caggiano JA. 1996. *Assessment Groundwater Monitoring Plan for Single Shell Tank Waste Management Area B-BX-BY*. WHC-SD-ENV-AP-002, Westinghouse Hanford Company, Richland, Washington.

Christensen JN, PE Dresel, ME Conrad, K Maher, and DJ DePaolo. 2004. "Identifying the Sources of Subsurface Contamination at the Hanford Site in Washington Using High-Precision Uranium Isotopic Measurements." *Environ. Sci. & Technol*. 38(12):3330-3337.

DOE. 1988. *Consultation Draft Site Characterization Plan*. DOE/RL-0164, 9 volumes, U.S. Department of Energy Richland Operations Office, Richland, Washington.

DOE. 1999. *Phase 1 RCRA Facility Investigation/Corrective Measures Study Work Plan for the SST Waste Management Areas*. DOE/RL-99-36, Rev. 0, U.S. Department of Energy, Richland Operations Office, Richland, Washington.

DOE. 2002. *Standardized Stratigraphic Nomenclature for Post-Ringold-Formation Sediments Within the Pasco Basin.* DOE/RL-2002-39, U.S. Department of Energy Richland Operations Office, Richland, Washington.

EPA. 1984. *Test Method for the Determination of Inorganic Anions in Water by Ion Chromatography.* EPA-600/4-84-017, Method 300.0A, U.S. Environmental Protection Agency, Washington, D.C.

EPA. 2000a. "Acid Digestion of Sediments, Sludges, and Soils." *Test Methods for Evaluating Solid Waste, Physical/Chemical Methods*. EPA Publication SW-846, Method 3050B. Available at http://www.epa.gov/epaoswer/hazwaste/test/sw846.htm.

EPA. 2000b. "Inductively Coupled Plasma-Atomic Emission Spectrometry." *Test Methods for Evaluating Solid Waste, Physical/Chemical Methods*. EPA Publication SW-846, Method 6010B. Available at http://www.epa.gov/epaoswer/hazwaste/test/sw846.htm.

EPA. 2000c. "Inductively Coupled Plasma-Mass Spectrometry." *Test Methods for Evaluating Solid Waste, Physical/Chemical Methods*. EPA Publication SW-846, Method 6020. Available at http://www.epa.gov/epaoswer/hazwaste/test/sw846.htm.

Finch RJ and T Murakami. 1999. "Systematics and Paragenesis of Uranium Minerals." *Uranium: Mineralogy, Geochemistry and the Environment. Reviews in Mineralogy*, Vol. 38, pp. 91-180. Mineralogical Society of America, Washington, D.C.

Folk RL. 1968. *Petrology of Sedimentary Rocks.* Hemphill, Austin, Texas.

Ilton ES, CX Liu, W Yantasee, ZM Wang, DA Moore, A Felmy, and JM Zachara. 2006. "The dissolution of synthetic Na-boltwoodite in sodium carbonate solutions." *Geochimica et Cosmochimica Acta* 70(19):4836-4849.

Jones, TE., BC Simpson, MI Wood, and RA Corbin. 2001. *Preliminary Inventory Estimates for Single-Shell Tank Leaks in B, BX, and BY Tank Farms*. RPP-7389, Rev. 0, CH2M HILL Hanford Group, Inc., Richland, Washington.

Knepp AJ. 2002. *Field Investigation Report for Waste Management Area B-BX-BY*. RPP-10098, CH2M Hill Hanford Group, Inc., Richland, Washington.

Kohler M, GP Curtis, DE Meece, and JA Davis. 2004. "Methods for estimating absorbed uranium(VI) and distribution coefficients of contaminated sediments." *Environmental Science & Technology* 38:240-247.

Langmuir D. 1997. *Aqueous Environmental Geochemistry*. Prentice Hall, Upper Saddle, New Jersey, p. 549.

Last GV, BN Bjornstad, MP Bergeron, DW Wallace, DR Newcomer, JA Schramke, MA Chamness, CS Cline, SP Airhart, and JS Wilbur. 1989. *Hydrogeology of the 200 Areas Low-Level Burial Grounds - An Interim Report.* PNL-6820, Pacific Northwest Laboratory, Richland, Washington.

Lindenmeier CW, RJ Serne, BN Bjornstad, GW Gee, HT Schaef, DC Lanigan, MJ Lindberg, RE Clayton, VL LeGore, IV Kutnyakov, SR Baum, KN Geiszler, CF Brown, MM Valenta, TS Vickerman, and LJ Royack. 2003. *Characterization of Vadose Zone Sediment: RCRA Borehole 299-E33-338 Located Near the B-BX-BY Waste Management Area*. PNNL-14121, Pacific Northwest National Laboratory, Richland, Washington.

Lindsey KA, BN Bjornstad, JW Lindberg, and KM Hoffman. 1992. *Geologic Setting of the 200 East Area – An Update.* WHC-SD-EN-TI-012, Westinghouse Hanford Company, Richland, Washington.

Lindsey KA, SP Reidel, KR Fecht, JL Slate, AG Law, and AM Tallman. 1994. "Geohydrologic Setting of the Hanford Site, South-Central Washington." In *Geologic Field Trips in the Pacific Northwest*, DA Swanson and RA Hagerud (eds.), pp. 1C-1 to 1C-16. Geological Society of America Meeting, Geological Society of America, Boulder, Colorado.

Lindsey KA, KD Reynolds, and VM Johnson. 2004. *241-C Tank Farm Geologic and Stratigraphic Analysis.* RPP-18290, Rev. 1, CH2M HILL Hanford Group, Inc., Richland, Washington.

Liu C, JM Zachara, OS Qafoku, JP McKinley, SM Heald, and Z Wang. 2004. "Dissolution of uranyl microprecipitates in subsurface sediments at Hanford Site, USA." *Geochimica et Cosmochimica Acta* 68(22):4519-4537.

Liu CX, JM Zachara, W Yantasee, PD Majors, and JP McKinley. 2006. "Microscopic reactive diffusion of uranium in the contaminated sediments at Hanford, United States." *Water Resources Research* Vol. 42, No. 12.

McKinley JP, JM Zachara, CX Liu, SC Heald, BI Prenitzer, and BW Kempshall. 2006. "Microscale controls on the fate of contaminant uranium in the vadose zone, Hanford Site, Washington." *Geochimica et Cosmochimica Acta* 70:1873-1887.

Narbutovskih SM. 1998. *Results of Phase I Groundwater Quality Assessment for Single Shell Tank Waste Management Areas B-BX-BY as the Hanford Site*. PNNL-11826, Pacific Northwest National Laboratory, Richland, Washington.

Pluhar CJ, BN Bjornstad, SP Reidel, RS Coe, and PB Nelson. 2006. "Magnetostratigraphic evidence from the Cold Creek bar for onset of ice-age cataclysmic floods in eastern Washington during the Early Pleistocene." *Quaternary Research* 65:123-135.

Price WH and KR Fecht. 1976. *Geology of the 241-BX Tank Farm*. ARH-LD-130, Atlantic Richfield Hanford Company, Richland, Washington.

Qafoku NP, JM Zachara, CX Liu, PL Gassman, OS Qafoku, and SC Smith. 2005. "Kinetic desorption and sorption of U(VI) during reactive transport in a contaminated Hanford sediment." *Environmental Science and Technology* 39:3157-3165.

Reeder RJ, M Nugent, GM Lamble, CD Tait, and DE Morris. 2000. "Uranyl incorporation into calcite and aragonite: XAFS and luminescence studies." *Environmental Science and Technology* 34:638-644.

Reeder RJ, M Nugent, CD Tait, DE Morris, SM Heald, KM Beck, WP Hess, and A Lanzirotti. 2001. "Coprecipitation of uranium(VI) with calcite: XAFS, micro-XAS, and luminescence characterization." *Geochimica et Cosmochimica Acta* 65(20):3491-3503.

Reidel SP and KR Fecht. 1994. *Geologic Map of the Priest Rapids 1:100,000 Quadrangle, Washington.* Open-File Report 94-13, Washington Division of Geology and Earth Resources.

Rhoades JD. 1996. "Salinity: Electrical Conductivity and Total Dissolved Solids." In *Methods of Soil Analysis Part 3*, JM Bigham (ed.). American Society of Agronomy, Madison, Wisconsin, pp. 417-435.

Rogers PM and AJ Knepp. 2000. *Site-Specific SST Phase 1 RFI/CMS Work Plan Addendum for WMA B-BX-BY*. RPP-6072, Rev. 1, CH2M Hill Hanford Group, Inc., Richland, Washington.

Serne RJ, HT Schaef, BN Bjornstad, BA Williams, DC Lanigan, DG Horton, RE Clayton, VL LeGore, MJ O'Hara, CF Brown, KE Parker, IV Kutnyakov, JN Serne, AV Mitroshkov, GV Last, SC Smith, CW Lindenmeier, JM Zachara, and DS Burke. 2002a. *Characterization of Vadose Zone Sediment: Uncontaminated RCRA Borehole Core Samples and Composite Samples.* PNNL-13757-1, Pacific Northwest National Laboratory, Richland, Washington.

Serne RJ, HT Schaef, BN Bjornstad, DC Lanigan, GW Gee, CW Lindenmeier, RE Clayton, VL LeGore, MJ O'Hara, CF Brown, RD Orr, GV Last, IV Kutnyakov, DS Burke, TC Wilson, and BA Williams. 2002b. *Characterization of Vadose Zone Sediment: Borehole 299-W23-19 [SX-115] in the S-SX Waste Management Area.* PNNL-13757-2, Pacific Northwest National Laboratory, Richland, Washington.

Serne RJ, GV Last, HT Schaef, DC Lanigan, CW Lindenmeier, CC Ainsworth, RE Clayton, VL LeGore, MJ O'Hara, CF Brown, RD Orr, IV Kutnyakov, TC Wilson, KB Wagnon, BA Williams, and DB Burke. 2002c. *Characterization of Vadose Zone Sediment, Part 4: Slant Borehole SX-108 in the S-SX Waste Management Area.* PNNL-13757-4, Pacific Northwest National Laboratory, Richland, Washington.

Serne RJ, GV Last, GW Gee, HT Schaef, DC Lanigan, CW Lindenmeier, RE Clayton, VL LeGore, RD Orr, MJ O'Hara, CF Brown, DS Burke, AT Owen, IV Kutnyakov, and TC Wilson. 2002d. *Characterization of Vadose Zone Sediment: Borehole 41-09-39 in the S-SX Waste Management Area.* PNNL-13757-3, Pacific Northwest National Laboratory, Richland, Washington.

Serne RJ, GV Last, GW Gee, HT Schaef, DC Lanigan, CW Lindenmeier, MJ Lindberg, RE Clayton, VL LeGore, RD Orr, IV Kutnyakov, SR Baum, KN Geiszler, CF Brown, MM Valenta, and TS Vickerman. 2002e. *Characterization of Vadose Zone Sediment: Borehole 299-E33-45 Near BX-102 in the B-BX-BY Waste Management Area.* PNNL-14083, Pacific Northwest National Laboratory, Richland, Washington.

Serne RJ, BN Bjornstad, GW Gee, HT Schaef, DC Lanigan, CW Lindenmeier, RD Orr, VL LeGore, RE Clayton, MJ Lindberg, IV Kutnyakov, SR Baum, KN Geiszler, MM Valenta, TS Vickerman, and LJ Royack. 2002f. *Characterization of Vadose Zone Sediment: Borehole 299-E33-46 near B-110 in the B-BX-BY Waste Management Area.* PNNL-14119, Pacific Northwest National Laboratory, Richland, Washington.

Serne RJ, BN Bjornstad, DG Horton, DC Lanigan, CW Lindenmeier, MJ Lindberg, RE Clayton, VL LeGore, RD Orr, IV Kutnyakov, SR Baum, KN Geiszler, MM Valenta, and TS Vickerman. 2004a. *Characterization of Vadose Zone Sediments Below the TX Tank Farm: Boreholes C3830, C3831, C3832 and RCRA Borehole 299-W10-27*. PNNL-14594, Pacific Northwest National Laboratory, Richland, Washington.

Serne RJ, BN Bjornstad, DG Horton, DC Lanigan, HT Schaef, CW Lindenmeier, MJ Lindberg, RE Clayton, VL LeGore, KN Geiszler, SR Baum, MM Valenta, IV Kutnyakov, TS Vickerman, RD Orr, and CF Brown. 2004b. *Characterization of Vadose Zone Sediments Below the T Tank Farm: Boreholes C4104, C4105, 299-W10-196, and RCRA Borehole 299-W11-39.* PNNL-14849, Pacific Northwest National Laboratory, Richland, Washington.

Serne, RJ, MJ Lindberg, TE Jones, HT Schaef, and KM Krupka. 2007. *Laboratory-Scale Bismuth Phosphate Extraction Process Simulation to Track Fate of Fission Products.* PNNL-14120, Pacific Northwest National Laboratory, Richland, Washington.

Slate JL. 1996. "Buried carbonate paleosols developed in Pliocene-Pleistocene deposits of the Pasco Basin, South-Central Washington." *USA: Quaternary International* 34-36:191-196.

Slate JL. 2000. *Nature and Variability of the Plio-Pleistocene Unit in the 200 West Area of the Hanford Site*. BHI-01203, Rev. 0, Bechtel Hanford, Inc., Richland, Washington.

Tallman AM, KR Fecht, MJ Marratt, and GV Last. 1979. *Geology of the Separation Areas, Hanford Site, South-Central Washington.* RHO-ST-23, Rockwell Hanford Operations, Richland, Washington.

Taylor SR. 1964. "The abundance of chemical elements in the continental crust—a new table." *Geochimica Cosmochimica Acta* 28:1273-1285.

Um W, RJ Serne, and KM Krupka. 2007. "Surface complexation modeling of U(VI) sorption to Hanford sediment with varying geochemical conditions." *Environmental Science and Technology* 41:3587-3592.

USGS. 2001. "Alkalinity and Acid Neutralizing Capacity." *National Field Manual for Collection of Water-Quality Data*, 2nd ed., SA Rounds and FD Wilde (eds.). U.S. Geological Survey. Available at http://water.usgs.gov/owq/FieldManual/Chapter6/section6.6/html/section6.6.htm.

Wan J, TK Tokunaga, E Saiz, JT Larsen, Z Zheng, and RA Couture. 2004. "Colloid formation at waste plume fronts." *Environmental Science and Technology* 38(22):6066-6073.

Wang Z, JM Zachara, Y Wassana, PL Gassman, C Liu, and AG Joly. 2004. "Cryogenic laser induced fluorescence characterization of U(VI) in Hanford vadose zone pore waters." *Environmental Science and Technology* 38(21):5591-5597.

Wang Z, JM Zachara, PL Gassman, C Liu, O Qafoku, W Yantasee, and JG Catalano. 2005a. "Fluorescence spectroscopy of U(VI)-silicates and U(VI)-contaminated Hanford sediment." *Geochimica et Cosmochimica Acta* 69:1391-1403.

Wang Z, JM Zachara, JP McKinley, and SC Smith. 2005b. "Cryogenic laser induced U(VI) fluorescence studies of a U(VI) substituted natural calcite: Implications to U(VI) speciation in contaminated Hanford sediments." *Environmental Science and Technology* 38(8):2651-2659.

Wentworth CK. 1922. "A Grade Scale and Class Terms for Clastic Sediments." *Journal of Geology* 30:377-392.

Whicker JJ, JE Pinder III, SA Ibrahim, JM Stone, DD Breshears, and KN Baker. 2007. "Uranium partition coefficients (K_d) in forest surface soil reveal long equilibrium times and vary by site and soil size fraction." *Health Physics* 93(1):36-46.

Wood MI, TE Jones, R Schalla, BN Bjornstad, and SM Narbutovskih. 2000. *Subsurface Conditions Description of the B-BX-BY Waste Management Area.* HNF-5507, Rev. 0, CH2M HILL Hanford Group, Inc., Richland, Washington.

Wronkiewicz DJ, JK Bates, TJ Gerding, E Veleckis, and BS Tani. 1992. "Uranium release and secondary phase formation during unsaturated testing of UO_2 at 90°C." *Journal of Nuclear Materials* 190:107-127.

Appendix A

Photographs of Core and Grab Samples from the Direct-Push Boreholes near the 241-B Tank Farm

Appendix A – Photographs of Core and Grab Samples from the Direct-Push Boreholes near the 241-B Tank Farm

Figure A.1. Sample B1M564C from Direct-Push Borehole C5164A

Figure A.2. Sample B1M564B from Direct-Push Borehole C5164A

Figure A.3. Sample B1M564A from Direct-Push Borehole C5164A

Figure A.4. Sample B1LTY5C from Direct-Push Borehole C5164B

Figure A.5. Sample B1LTY5B from Direct-Push Borehole C5164B

Figure A.6. Sample B1LTY5A from Direct-Push Borehole C5164B

Figure A.7. Sample B1LTY5 from Direct-Push Borehole C5164B

Figure A.8. Sample B1M565C from Direct-Push Borehole C5168

Figure A.9. Sample B1M565B from Direct-Push Borehole C5168

Figure A.10. Sample B1M565A from Direct-Push Borehole C5168

Figure A.11. Sample B1M565 from Direct-Push Borehole C5168

Figure A.12. Sample B1LTY4 from Direct-Push Borehole C5170

Appendix B

Logs of Core and Grab Samples from the Direct-Push Boreholes near the 241-B Tank Farm

Appendix B – Logs of Core and Grab Samples from Direct-Push Boreholes near 241-B Tank Farm

Pacific Northwest National Laboratory

DAILY BOREHOLE LOG

Boring/Well No C5164A Depth _____ Date 3/15/07 Sheet 1 of 1

Location B tank farm direct push Project _____

Logged by Dreama Horton (Print) (Sign) (Print) (Sign)

Reviewed by _____ (Print) (Sign) Date _____

Lithologic Class. Scheme _____ Procedure _____ Rev ____

Steel Tape/E-Tape _____ / _____ Field Indicator Equip. 1) _____ 2) _____

Drilling Contractor _____

Driller _____

Rig/Method _____

Depth Control Point _____

DEPTH (Ft)	TIME	SAMPLES TYPE	SAMPLES ID NUMBER	CONTAMINATION INSTR.	CONTAMINATION READING	MOISTURE	GRAPHIC LOG C	Z	S	G	LITHOLOGIC DESCRIPTION (particle size distribution, sorting, mineralogy, roundness, color, reaction to HCl, etc.)	H_2O ADDED	CASING	DRILLING COMMENTS (drilling rate, down time, blow counts, water level, drill fluid, etc.)
17			B1M564C			D					17.0 – 17.5. SG 65% gravel up to ~3 cm, 85% basaltic 15% felsic. Subrounded where not broken by sampling method 35% med to coarse sand, Sand is SA, (2.5Y 7/1) light gray v. slight rxn w/ HCl			Samples are 1000 g stainless steel liner 6" long & 1" dia Unless otherwise noted All samples extruded w/ chisel. unless noted otherwise
17.5'			B1M564B			D					17.5-18' SG 70% gravel, subround up to about 3 cm in size & >95% basaltic 30% fine to coarse sand (2.5Y 7/1) light gray Sand is mostly basaltic & SA weak rxn w/ HCl			
			B1M564A			D					18.0 -18.5' SG 75% gravel up to 3 cm 85% basaltic 25% med to coarse sand, SA no rxn w/ HCl			

W = Wet, M = Moist, D = Dry

1998/DCL/PROC/DBL/001

Figure B.1. Core Log for Direct-Push Borehole C5164A

Pacific Northwest National Laboratory

DAILY BOREHOLE LOG

Boring/Well No C5164B Depth _____ Date 2/15/07 Sheet 1 of 2

Location B Tank Farm direct push Project _____

Logged by Duane Horton / _____

Reviewed by _____ / _____ Date _____

Lithologic Class. Scheme _____ Procedure _____ Rev ____

Steel Tape/E-Tape _____ / _____ Field Indicator Equip. 1) _____ 2) _____

Drilling Contractor _____

Driller _____

Rig/Method _____

Depth Control Point _____

DEPTH (ft)	TIME	SAMPLES TYPE	SAMPLES ID NUMBER	CONTAMINATION INSTR.	CONTAMINATION READING	MOISTURE	GRAPHIC LOG C	Z	S	G	LITHOLOGIC DESCRIPTION (particle size distribution, sorting, mineralogy, roundness, color, reaction to HCl, etc.)	H_2O ADDED	CASING	DRILLING COMMENTS (drilling rate, down time, blow counts, water level, drill fluid, etc.)
														All samples 1000g stainless
21'			B1LTY5C								21.0 -21.5' extremely compacted could not extrude, had to chisted sp.; sample out of liner			steel liner unless specified otherwise 6" long 1" dia
											20% gravel 80% fine to med sand			
											95 gravel is mostly basalt w/ ≥ 20-25% felsic. where not broken by direct push, gravel is subrounded to round. sand is			
											(2.5Y 6/2) light brown gray very slight rxn w/ HCl			
											gravel is pebbles up to > 2 cm			
21.5'			B1LTY5B								21.5 -22', sample was not extruded extremely compacted			but was chisted out of liners
											10YR 4/1 dark gray			
											95% sand <5% pebbles			
											pebbles are basaltic & rounded to subrounded and up to ~2cm but broken			
											sand is fine to med gr. basalt > felsic			
											slight rxn w/ HCl			

W = Wet, M = Moist, D = Dry

1998/DCL/PROC/DRLL001

Figure B.2. Core Log for Direct-Push Borehole C5164B

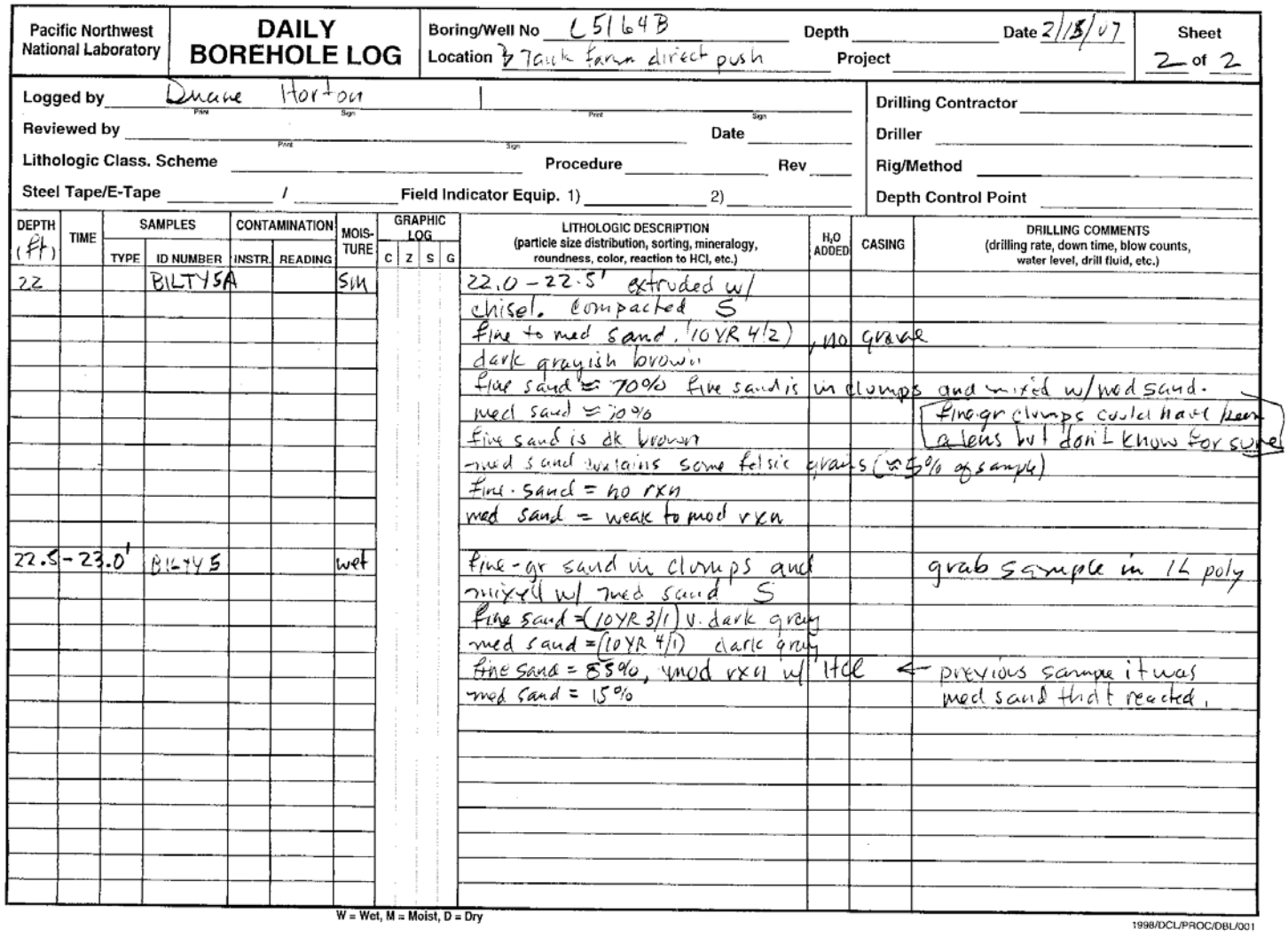

Pacific Northwest National Laboratory

DAILY BOREHOLE LOG

Boring/Well No C5164B Depth _____ Date 2/15/07 Sheet 2 of 2

Location Tank farm direct push Project _____

Logged by Duane Horton (Print / Sign) _____ (Print / Sign)

Reviewed by _____ (Print / Sign) Date _____

Lithologic Class. Scheme _____ Procedure _____ Rev ____

Steel Tape/E-Tape ____ / ____ Field Indicator Equip. 1) ____ 2) ____

Drilling Contractor _____

Driller _____

Rig/Method _____

Depth Control Point _____

DEPTH (Ft)	TIME	SAMPLES TYPE	SAMPLES ID NUMBER	CONTAMINATION INSTR.	CONTAMINATION READING	MOISTURE	GRAPHIC LOG C	Z	S	G	LITHOLOGIC DESCRIPTION (particle size distribution, sorting, mineralogy, roundness, color, reaction to HCl, etc.)	H_2O ADDED	CASING	DRILLING COMMENTS (drilling rate, down time, blow counts, water level, drill fluid, etc.)
22			BILTY5A			SM					22.0 – 22.5' extruded w/ chisel. compacted S			
											fine to med sand. (10YR 4/2) dark grayish brown	no	gravel	
											fine sand = 70% fine sand is in clumps and mixed w/ med sand.			fine gr clumps could have been a lens but don't know for sure
											med sand = 30%			
											fine sand is dk brown			
											med sand contains some felsic grains (≈5% of sample)			
											fine sand = no rxn			
											med sand = weak to mod rxn			
22.5 – 23.0'			BILTY5			wet					fine-gr sand in clumps and mixed w/ med sand S			grab sample in 1L poly
											fine sand = (10YR 3/1) v. dark gray			
											med sand = (10YR 4/1) dark gray			
											fine sand = 85%, mod rxn w/ HCl			← previous sample it was med sand that reacted.
											med sand = 15%			

W = Wet, M = Moist, D = Dry

1998/DCL/PROC/DBL/001

Figure B.3. Core Log for Direct-Push Borehole C5164B

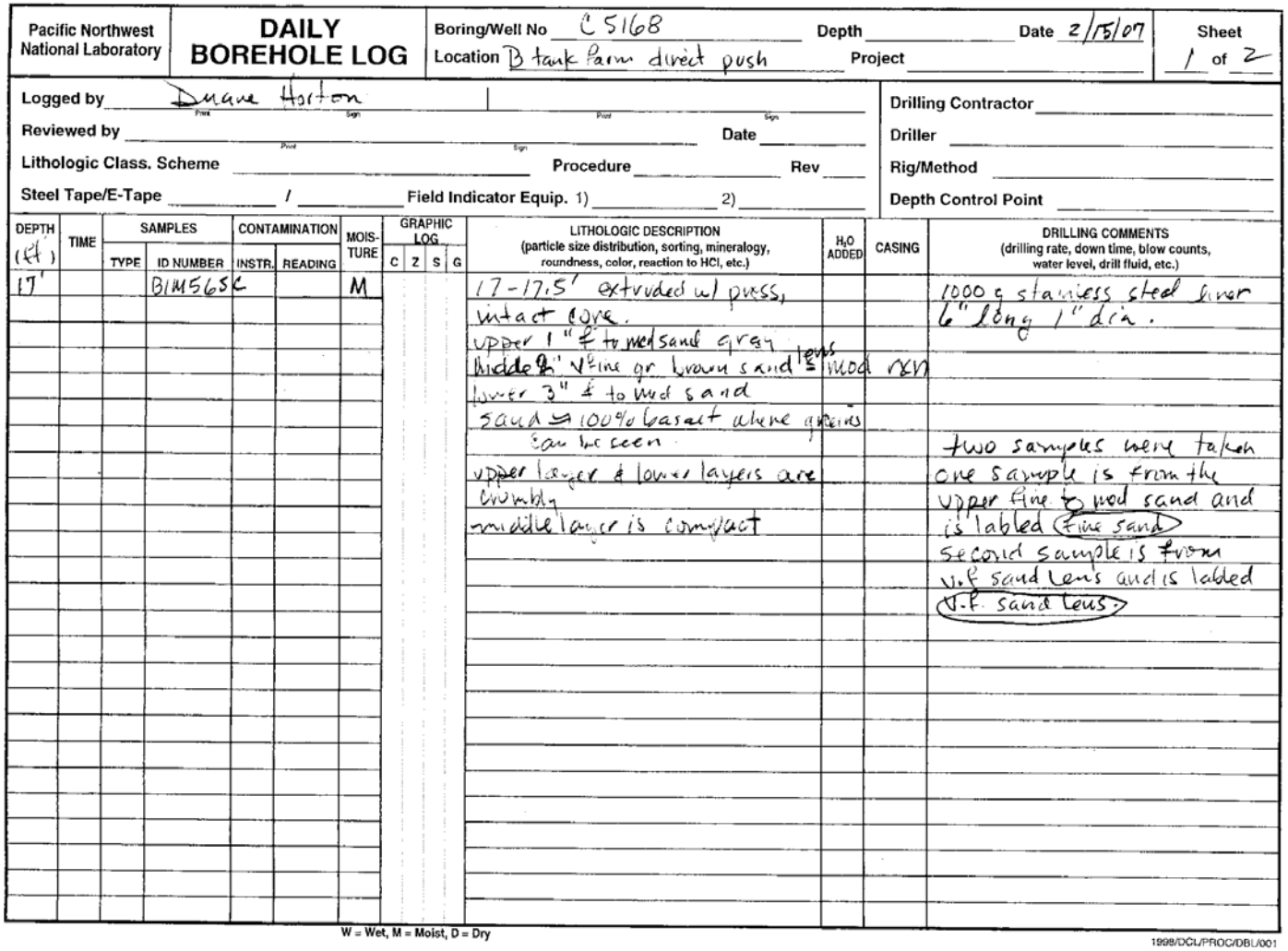

Pacific Northwest National Laboratory

DAILY BOREHOLE LOG

Boring/Well No C5168 Depth _____ Date 2/15/07 Sheet 1 of 2

Location B tank farm direct push Project _____

Logged by Duane Horton (Print / Sign) _____ (Print / Sign)

Reviewed by _____ (Print / Sign) Date _____

Lithologic Class. Scheme _____ Procedure _____ Rev _____

Steel Tape/E-Tape _____ / _____ Field Indicator Equip. 1) _____ 2) _____

Drilling Contractor _____

Driller _____

Rig/Method _____

Depth Control Point _____

DEPTH (ft)	TIME	SAMPLES TYPE	SAMPLES ID NUMBER	CONTAMINATION INSTR.	CONTAMINATION READING	MOISTURE	GRAPHIC LOG C	Z	S	G	LITHOLOGIC DESCRIPTION (particle size distribution, sorting, mineralogy, roundness, color, reaction to HCl, etc.)	H_2O ADDED	CASING	DRILLING COMMENTS (drilling rate, down time, blow counts, water level, drill fluid, etc.)
17'			B1M565C			M					17-17.5' extruded w/ press, intact core. upper 1" f to med sand gray middle 4" v f to f sand gr brown sand lens mod rxn lower 3" f to med sand sand ≥ 100% basalt where grains can be seen upper layer & lower layers are crumbly middle layer is compact			1000 g stainless steel liner 6" long 1" dia. two samples were taken one sample is from the upper fine to med sand and is labled (fine sand) second sample is from v.f sand lens and is labled (V.f. sand lens)

W = Wet, M = Moist, D = Dry

1998/DCL/PROC/DBL/001

Figure B.4. Core Log for Direct-Push Borehole C5168

Pacific Northwest National Laboratory

DAILY BOREHOLE LOG

Boring/Well No C5168 Depth ____ Date ____ Sheet 2 of 2

Location B tank farm direct push Project ____

Logged by Duane Horton (Print / Sign) | ____ (Print / Sign)

Reviewed by ____ (Print / Sign) Date ____

Lithologic Class. Scheme ____ Procedure ____ Rev ____

Steel Tape/E-Tape ____ / ____ Field Indicator Equip. 1) ____ 2) ____

Drilling Contractor ____

Driller ____

Rig/Method ____

Depth Control Point ____

DEPTH (Ft)	TIME	SAMPLES TYPE	SAMPLES ID NUMBER	CONTAMINATION INSTR.	CONTAMINATION READING	MOISTURE	GRAPHIC LOG C	Z	S	G	LITHOLOGIC DESCRIPTION (particle size distribution, sorting, mineralogy, roundness, color, reaction to HCl, etc.)	H_2O ADDED	CASING	DRILLING COMMENTS (drilling rate, down time, blow counts, water level, drill fluid, etc.)
			B1M565	B		SM					17.5 to 18.0' sample was extruded as core			
											fine to med basalt sand			
											slightly compacted, massive			
											(5Y4/2) olive gray			
											only minor felsic grains when			
											grains can be seen			
											weak rxn w/ HCl			
			B1M565A			SM					18.0 to 18.5' (2.5Y 4/2) dark			
											grayish brown sample			
											extracted as core			
											Massive v.f to fine sand, minor med sand			
											slight compaction			
											basaltic sand.			
											no rxn w/ HCl			
			B1M565			SM					18.5-19' S slightly compacted clumps			grab sample 1000 ml
											85% f. sand			poss. in Tth
											15% m. sand = SA			
											>90% basaltic			
											(2.5Y 4/2) dark grayish brown			
											v. slight rxn w/ HCl			

W = Wet, M = Moist, D = Dry

1998/DCL/PROC/DBL/001

Figure B.5. Core Log for Direct-Push Borehole C5168

Pacific Northwest National Laboratory

DAILY BOREHOLE LOG

Boring/Well No C5170 Depth _____ Date 2/15/07 Sheet 1 of 1

Location B tank farm direct push Project _____

Logged by Duane Hurton / _____ _____

Reviewed by _____ Date _____

Lithologic Class. Scheme _____ Procedure _____ Rev ____

Steel Tape/E-Tape ____ / ____ Field Indicator Equip. 1) _____ 2) _____

Drilling Contractor _____

Driller _____

Rig/Method _____

Depth Control Point _____

DEPTH (ft)	TIME	SAMPLES TYPE	SAMPLES ID NUMBER	CONTAMINATION INSTR.	CONTAMINATION READING	MOISTURE	GRAPHIC LOG C	Z	S	G	LITHOLOGIC DESCRIPTION (particle size distribution, sorting, mineralogy, roundness, color, reaction to HCl, etc.)	H_2O ADDED	CASING	DRILLING COMMENTS (drilling rate, down time, blow counts, water level, drill fluid, etc.)
			B1LTY4			D					19.5 - 21.5'			1000-ml poly bottle
											silt			
											(2.5Y 7/1) light gray			
											sample is loose powder except			
											for ½" that is very			
											compact and 1" dia (core)			
											slight rxn w/ HCl			

W = Wet, M = Moist, D = Dry

Figure B.6. Core Log for Direct-Push Borehole C5170

Appendix C

Photographs of Core and Grab Samples from the Direct-Push Boreholes near the 241-BX Tank Farm

Appendix C – Photographs of Core and Grab Samples from Direct-Push Boreholes near 241-BX Tank Farm

Figure C.1. Sample B1JWW8B from Direct-Push Borehole C5124

Figure C.2. Sample B1JWW8A from Direct-Push Borehole C5124

Figure C.3. Sample B1JWW7C from Direct-Push Borehole C5132

Figure C.4. Sample B1JWW7B from Direct-Push Borehole C5132

Figure C.5. Sample B1JWW7A from Direct-Push Borehole C5132

Figure C.6. Sample B1JWW7 from Direct-Push Borehole C5132

Figure C.7. Sample B1JWW6C from Direct-Push Borehole C5134

Figure C.8. Sample B1JWW6B from Direct-Push Borehole C5134

Figure C.9. Sample B1JWW6B from Direct-Push Borehole C5134

Appendix D

Logs of Core and Grab Samples from the Direct-Push Boreholes near the 241-BX Tank Farm

Appendix D – Logs of Core and Grab Samples from Direct-Push Boreholes near 241-BX Tank Farm

Pacific Northwest National Laboratory

CORE LOG

Boring/Well No C5124 Depth 44-45' Date 9-11-06 Sheet 1 of 1

Location BX Tank Farm Project Vadose Zone

Logged by B N Bjornstad (Print / Sign)

Reviewed by _____ (Print / Sign) Date _____

Lithologic Class. Scheme Folk-Wentworth Procedure _____ Rev _____

Drilling Contractor _____

Driller _____

Drill Method Direct Push

DEPTH (ft)	SAMPLES TYPE	SAMPLES ID NUMBER	MOISTURE	GRAPHIC LOG C Z S G	LITHOLOGIC DESCRIPTION (particle size distribution, sorting, mineralogy, roundness, color, reaction to HCl, maximum grain size, consolidation, structure, etc.)	COMMENTS
44.5	core	B1J4W8B	SM		S, crs-v crs sand, 2.5Y5/2 (grayish brn), loose, 50-60% basalt, sl. cohesive, mod. sorted, max. particle size = v crs sand, massive, 50% vcs, 30% crs sand, 10% md S, 10% fn S wk rxn w/ HCl	Samples in stainless steel liners 1.5" diameter, 6" long
45.0		B1J4W8A				

W = Wet, M = Moist, SM = Slightly Moist, D = Dry

2006/DCL/FORMS/CoreLog/001 (006/09)

Figure D.1. Core Log for Direct-Push Borehole C5124

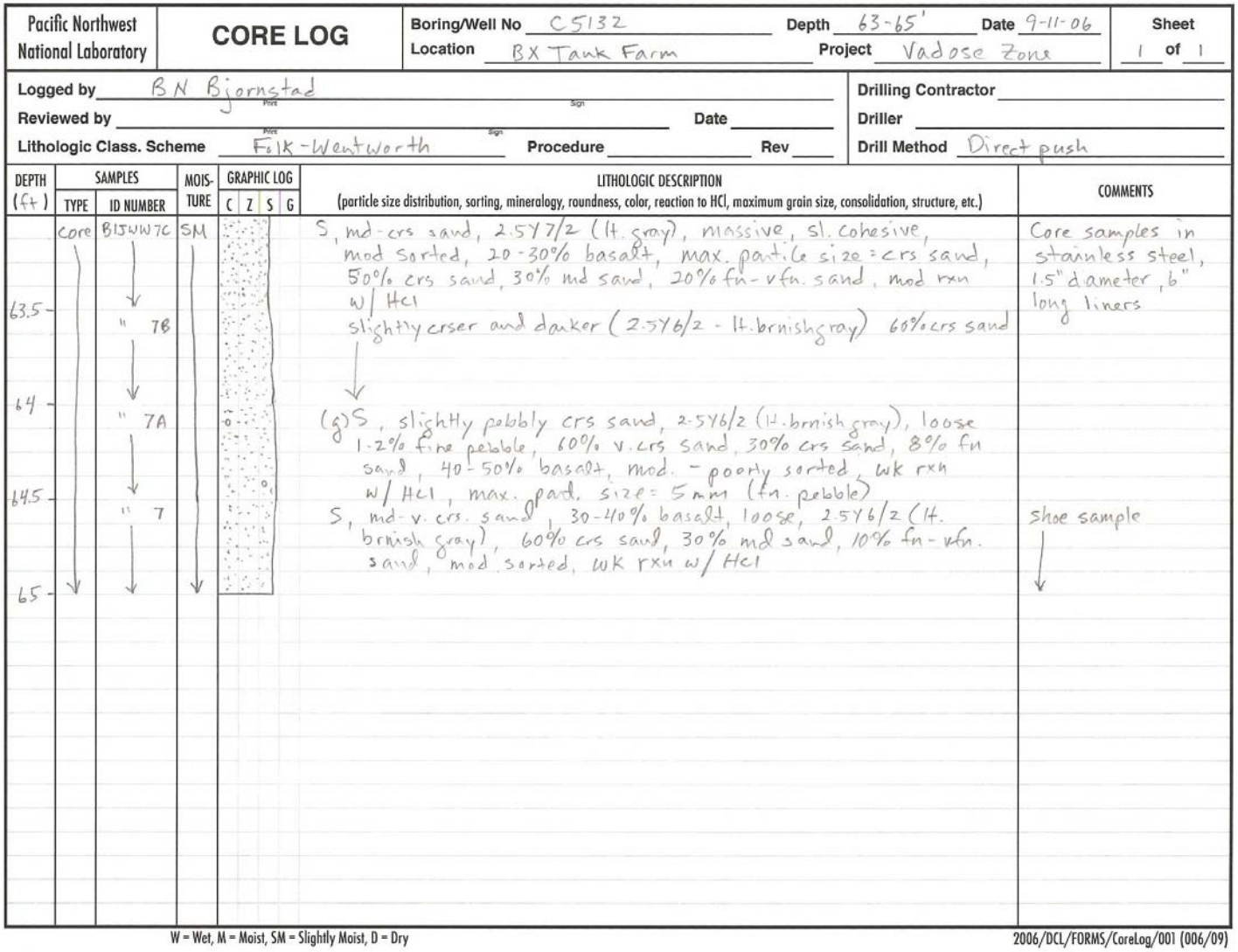

Pacific Northwest National Laboratory

CORE LOG

Boring/Well No C5132 Depth 63-65' Date 9-11-06 Sheet 1 of 1

Location BX Tank Farm Project Vadose Zone

Logged by BN Bjornstad (Print / Sign)

Reviewed by _____ Date _____

Lithologic Class. Scheme Folk-Wentworth Procedure _____ Rev _____

Drilling Contractor _____

Driller _____

Drill Method Direct push

DEPTH (ft)	SAMPLES TYPE	SAMPLES ID NUMBER	MOISTURE	GRAPHIC LOG C Z S G	LITHOLOGIC DESCRIPTION (particle size distribution, sorting, mineralogy, roundness, color, reaction to HCl, maximum grain size, consolidation, structure, etc.)	COMMENTS
	core	B1JWW7C	SM		S, md-crs sand, 2.5Y7/2 (lt. gray), massive, sl. cohesive, mod sorted, 20-30% basalt, max. particle size = crs sand, 50% crs sand, 30% md sand, 20% fn-vfn. sand, mod rxn w/ HCl	Core samples in stainless steel, 1.5" diameter, 6" long liners
63.5		" 7B			slightly crser and darker (2.5Y6/2 - lt. brnish gray) 60% crs sand	
64		" 7A			(g)S, slightly pebbly crs sand, 2.5Y6/2 (lt. brnish gray), loose 1-2% fine pebble, 60% v. crs sand, 30% crs sand, 8% fn sand, 40-50% basalt, mod.-poorly sorted, wk rxn w/ HCl, max. pebble size = 5 mm (fn. pebble)	
64.5		" 7			S, md-v. crs. sand, 30-40% basalt, loose, 2.5Y6/2 (lt. brnish gray), 60% crs sand, 30% md sand, 10% fn-vfn. sand, mod. sorted, wk rxn w/ HCl	shoe sample
65						

W = Wet, M = Moist, SM = Slightly Moist, D = Dry

2006/DCL/FORMS/CoreLog/001 (006/09)

Figure D.2. Core Log for Direct-Push Borehole C5132

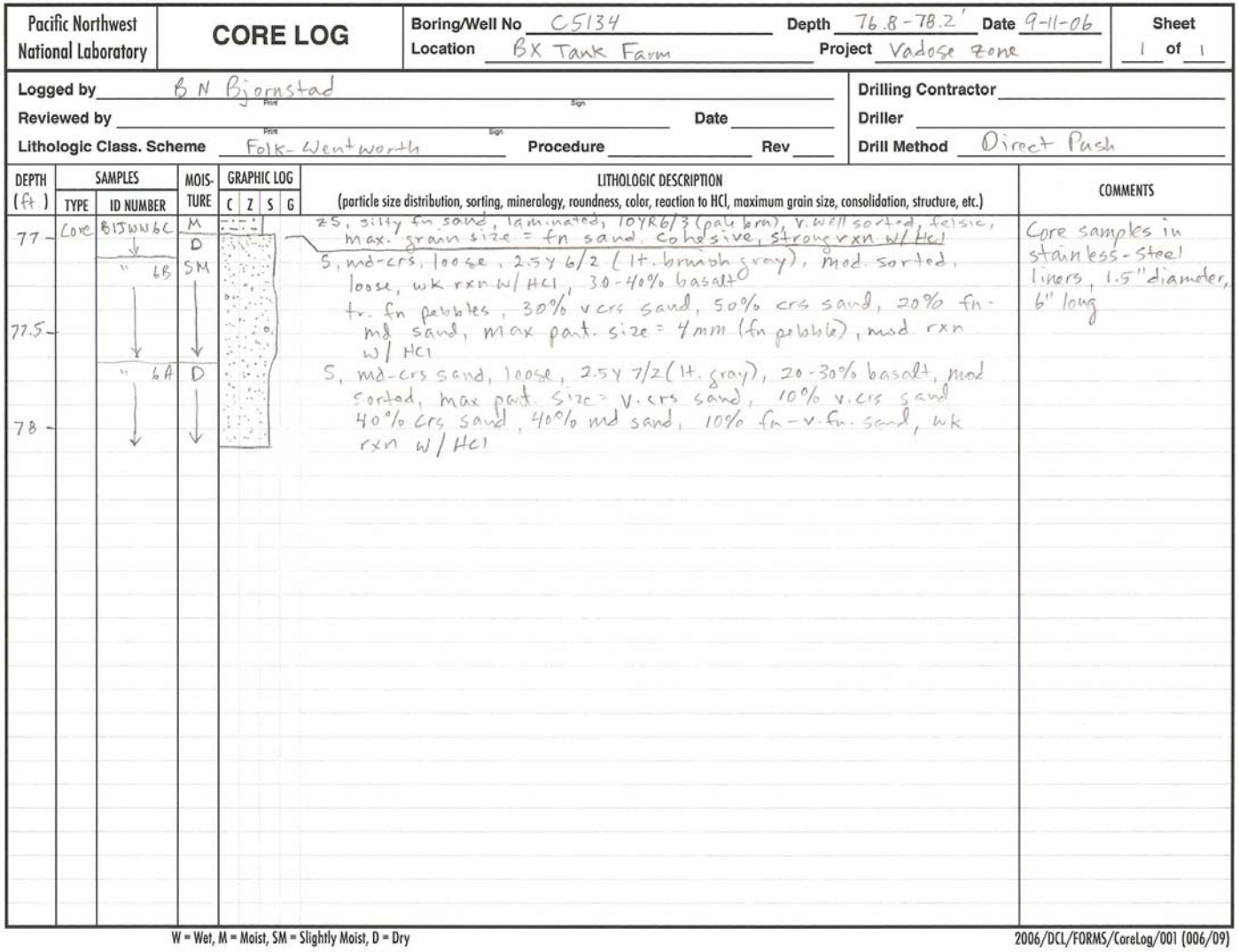

Figure D.3. Core Log for Direct-Push Borehole C5134

Distribution

No. of Copies

OFFSITE

Dr. Harry Babad
2540 Cordoba Court
Richland, WA 99352-1609

Dirk A. Dunning
Oregon Office of Energy
625 Marion Street NE
Salem, OR 97301-3742

Dr. Daniel I. Kaplan
Westinghouse Savannah River Company
Building 774-43A, Room 215
Aiken, SC 29808

Phil Reed
U.S. Nuclear Regulatory Commission
Office of Nuclear Regulatory Research
Division of Systems Analysis and Regulatory Effectiveness
Radiation Protection, Environmental Risk, and Waste Management Branch
Mail Stop: T9-F31
Washington, DC 20555-0001

Tom Stoops, LPG
Oregon Office of Energy
Nuclear Safety Division
625 Marion Street NE
Salem, OR 97303

Mr. Ronald G. Wilhelm
Office of Radiation and Indoor Air
401 M Street, S.W.
Mail Code 6603J
Washington, DC 20460

No. of Copies

W. Alexander Williams
U.S. Department of Energy
Office of Environmental Restoration
EM-33
19901 Germantown Road
Germantown, MD 20874-1290

ONSITE

8 **DOE Richland Operations Office**

B. L. Foley	A6-38
J. P. Hanson	A5-13
R. D. Hildebrand	A6-38
K. A. Kapsi	A5-13
J. G. Morse	A6-38
K. M. Thompson	A6-38
DOE Public Reading Room (2)	H2-53

2 **DOE Office of River Protection**

R. W. Lober	H6-60
S. A. Wiegman	H6-60

15 **CH2M HILL Hanford Group, Inc.**

R. Calmus	S7-75
M. P. Connelly	H6-03
J. G. Field	H6-03
M. Jaraysi	H6-03
J. G. Kristofzski	H6-03
F. M. Mann (5)	H6-03
W. J. McMahon	H6-03
D. A. Myers	H6-03
G. Parsons	T6-04
H. A. Sydnor	H6-03
D. J. Watson	H6-03

No. of Copies

Fluor Federal Services

R. Khaleel	E6-17

12 **Fluor Hanford, Inc.**

M. W. Benecke	E6-44
T. W. Fogwell	E6-35
B. H. Ford	E6-44
J. G. Hogan	S0-01
D. G. Horton	E6-35
S. M. Narbutovskih	E6-44
V. J. Rohay	E6-44
L. C. Swanson	E6-35
G. S. Thomas	E6-44
B. A. Williams	E6-44
M. I. Wood	H8-44
C. Wright	E6-35

S.M. Stoller

R. G. McCain	B2-62

3 **U.S. Environmental Protection Agency**

N. Ceto	B1-46
D. A. Faulk	B1-46
R. Lobos	B1-46

7 **Washington State Department of Ecology**

S. Dahl-Crumpler	H0-57
J. A. Caggiano	H0-57
J.A. Hedges	H0-57
J. Lyon	H0-57
B. Rochette	H0-57
J. Yokel	H0-57
D. Goswami	H0-57

No. of Copies

43 **Pacific Northwest National Laboratory**

S. R. Baum	P7-22
B. N. Bjornstad	K6-81
C. A. Brandt	K9-04
T. M. Brouns	K9-69
C. F. Brown (10)	P7-22
K. J. Cantrell	K6-81
E. T. Clayton	P7-22
D. D. Dauble	K6-84
W. J. Deutsch	SEQUIM
P. E. Dresel	K6-96
K. N. Geiszler	P7-22
M. J. Fayer	K9-33
M. D. Freshley	K9-33
J. S. Fruchter	K6-96
J. P. Icenhower	K6-81
C. Iovin	P7-22
J. M. Keller	BPO
K. M. Krupka	K6-81
I. V. Kutnyakov	P7-22
D. C. Lanigan	K6-75
G. V. Last	K6-81
M. J. Lindberg	P7-22
P. E. Long	K9-33
W. J. Martin	K6-81
C. J. Murray	K6-81
E. M. Pierce	K3-62
N. Qafoku	P7-54
R. J. Serne	P7-22
M. B. Triplett	K6-52
W. Um	P7-22
M. M. Valenta	P7-22
J. M. Zachara	K8-96
Hanford Technical Library (2)	P8-55